U.S. Department of Energy
FreedomCAR and Vehicle Technologies, EE-2G
1000 Independence Avenue, S.W.
Washington, D.C. 20585-0121

FY 2006

Evaluation of 2004 Toyota Prius Hybrid Electric Drive System

Prepared by:

Oak Ridge National Laboratory
Mitch Olszewski, Program Manager

Submitted to:

Energy Efficiency and Renewable Energy
FreedomCAR and Vehicle Technologies
Vehicle Systems Team

Susan A. Rogers, Technology Development Manager

May 2005

OAK RIDGE
NATIONAL LABORATORY
MANAGED BY UT-BATTELLE
FOR THE DEPARTMENT OF ENERGY

ORNL/TM-2006/423

Engineering Science and Technology Division

Evaluation of 2004 Toyota Prius Hybrid Electric Drive System

R. H. Staunton
C. W. Ayers
L. D. Marlino

J. N. Chiasson
University of Tennessee-Knoxville

T. A. Burress
Oak Ridge Institute for Science and Education

Publication Date: May 2006

Prepared by the
OAK RIDGE NATIONAL LABORATORY
Oak Ridge, Tennessee 37831
managed by
UT-BATTELLE, LLC
for the
U.S. DEPARTMENT OF ENERGY
Under contract DE-AC05-00OR22725

UT-BATTELLE
ORNL-27 (4-00)

TABLE OF CONTENTS

Page

LIST OF FIGURES v

LIST OF TABLES vii

ACRONYMS AND ABBREVIATIONS viii

1. INTRODUCTION 1
   1.1 PROGRAM OVERVIEW 1
   1.2 TESTING FACILITIES 2
   1.3 SCOPE AND OBJECTIVE 2
   1.4 APPROACH 3

2. HYBRID ELECTRIC DRIVE SYSTEM DESCRIPTION 4
   2.1 DESIGN REQUIREMENTS 7
   2.2 SYSTEM SUBASSEMBLIES 7
      2.2.1 Engine 8
      2.2.2 Power-Split Device 8
      2.2.3 Generator 10
      2.2.4 Motor 10
      2.2.5 Inverter 10
      2.2.6 Battery 11

3. LABORATORY TESTING 12
   3.1 ANL VEHICLE -EVEL PERFORMANCE TESTS 12
      3.1.1 Initial Performance Testing at ANL 12
      3.1.2 Vehicle Data Characterizing Boost-Converter Operation 14
   3.2 ORNL SUBSYSTEM-LEVEL PERFORMANCE AND VALIDATION TESTS 18
      3.2.1 Locked Rotor Tests 19
      3.2.2 Back-emf Tests 21
         3.2.2.1 Motor tests 21
         3.2.2.2 Generator tests 22
      3.2.3 Hybrid Drive System Loss Tests 23
   3.3 HEV SYSTEM TESTING OVER THE FULL DESIGN RANGE 28
      3.3.1 Test Configuration 29
      3.3.2 General Test Plan and Data Verification 30
      3.3.3 Motor/Inverter Test Data and Efficiency Maps 33
      3.3.4 Buck/Boost-Converter Test Data and Efficiency Maps 36

4. INVERTER, CONTROLLER, AND Z-SOURCE ACTIVITIES 40
   4.1 INVERTER ARCHITECTURE OVERVIEW 40
   4.2 INVERTER MODIFICATIONS 40
   4.3 CONTROLLER DEVELOPMENT 41
      4.3.1 Establishing the Need for Field Weakening 42
      4.3.2 Controller Software 43
      4.3.3 Controller Hardware 44

4.4 COMPARISION OF PRIUS INVERTER AND Z-SOURCE INVERTER..... 47

TABLE OF CONTENTS (cont'd)

Page

5. HEV SYSTEM MANUFACTURING AND PACKAGING 49
5.1 PMSM 49
5.2 INVERTER/CONVERTER 50
5.3 CONVERTER COMPONENTS 56

6. SUMMARY AND CONCLUSIONS 60
6.1 FINDINGS AND OBSERVATIONS 60
6.2 NEEDED RESEARCH AND DEVELOPMENT 63

REFERENCES 64

APPENDIX A – DRIVE-CYCLE PLOTS SHOWING CONVERTER OPERATION 65

APPENDIX B – PRIUS PERFORMANCE-MAPPING DATA 69

LIST OF FIGURES

Figure		Page
1.1	Predominant project challenge represented by a highly integrated vehicle control system.	3
2.1	Subassembly arrangement for the THS II	5
2.2	2004 Prius engine and hybrid drive assembly	5
2.3	Heat removal and lubrication scheme for the 2004 Prius	6
2.4	Diagram of the 2004 Prius power-split device	8
2.5	Diagram of the 2004 Prius gear train between the motor and wheels	9
2.6	2004 Prius gears with number of gear teeth shown	9
2.7	2004 Prius generator rotor	10
2.8	2004 Prius motor rotor and stator	11
2.9	2004 Prius inverter and voltage converter unit	11
3.1	Instrumentation locations for ANL testing	13
3.2	Sample power measurements under varying speed conditions	13
3.3	Sample power measurements under controlled speed conditions	14
3.4	Extrapolation of generator back-emf data for generator speeds up to 10,000 rpm	15
3.5	Drive-cycle data from ANL showing voltage-boost converter response	16
3.6	Second drive-cycle data set from ANL showing voltage-boost converter response	16
3.7	Third drive-cycle data set from ANL showing voltage-boost converter response	17
3.8	Drive-cycle data set showing voltage boost at high speeds	17
3.9	Motor-shaft angle vs. torque (rotor locked)	19
3.10	Locked rotor peak torque as a function of current	20
3.11	Motor back-emf voltage vs. motor-shaft speed	22
3.12	Generator back-emf voltage vs. generator shaft speed	23
3.13	Hybrid electric drive system and component/subassembly losses at 25°C	24
3.14	Configuration B losses as a function of oil temperature	28
3.15	The test configuration for Prius performance characterization tests.	29
3.16	The test hardware for Prius performance characterization tests.	29
3.17	Maximum torque-speed performance specifications for the 2004 Prius	31
3.18	2004 Prius motor efficiency contour map.	34
3.19	2004 Prius inverter efficiency contour map	35
3.20	2004 Prius combined motor/inverter efficiency contour map	35
3.21	Boost-converter efficiency vs. output power.	36
3.22	Boost-converter efficiency vs. output current	37
4.1	TC placement at IPEM area of cold plate	41
4.2	Limitations in operation of PMSM where field weakening is not used	43
4.3	Upper-level flow diagram of Prius controller system	46
4.4	Configurations for (a) conventional boosted inverter and (b) new Z-source inverter	7
4.5	Efficiency comparisons of inverter topologies and inverter/motor systems	48
5.1	Casing of the 2004 Prius PMSM with dimensions and volume calculations	50
5.2	Overall subsystem packaging in the 2004 Prius inverter/converter	51
5.3	Overview of packaging in an opened 2004 Prius inverter/converter	51
5.4	Overview of packaging in a 2004 Prius inverter/converter with capacitor module removed	52
5.5	Empty inverter/converter housing showing cold plate surfaces	53
5.6	Power module 18-pack dye array in a 2004 Prius inverter	53

LIST OF FIGURES (cont'd)

Figure		Page
5.7	Close-up of a IGBT/diode pair in the 2004 Prius inverter	54
5.8	Packaging of the 2004 Prius compressor inverter and dc-to-dc converter circuit	54
5.9	Overall volume and mass of the 2004 Prius inverter/converter	55
5.10	Radiator for Prius engine (upper) and hybrid subsystems (lower)	56
5.11	General circuit schematic of the Prius inverter	56
5.12	Disassembly of the converter power module	57
5.13	Close-up of converter IGBTs and diodes	57
5.14	Voltage-boost converter auto-transformer	58
5.15	Conceptual change to inverter/converter casing for excluding the buck/boost converter	58
6.1	Prius combined efficiency contour maps	62
A.1	Drive-cycle plot chosen to illustrate a rapid acceleration	65
A.2	Second drive-cycle plot chosen to illustrate a rapid acceleration	66
A.3	Drive-cycle plot chosen to illustrate a fluctuating boosted voltage	66
A.4	Drive-cycle plot chosen to illustrate a gradual acceleration	67
A.5	Consideration of curve smoothening on the boosted voltage plot	67
A.6	Drive-cycle plot chosen to illustrate a high level of change for each parameter	68
A.7	Drive-cycle plot chosen to illustrate a 70 mph sustained speed	68
B.1	Speed-torque combinations at which data sets were obtained	69

LIST OF TABLES

Table		Page
2.1	Specification for THS II subassemblies	7
3.1	Measurement variables for ANL testing program	12
3.2	Motor torque vs. motor-shaft angle	20
3.3	Test conditions for back-emf voltage measurements	21
3.4	Back-emf voltage measurements for the 2004 Prius motor	21
3.5	Back-emf voltage measurements for the 2004 Prius generator	22
3.6	Subassembly configurations for loss determinations	23
3.7	Summary of hybrid drive system losses	24
3.8	Configuration B losses at a nominal oil temperature of 28°C	25
3.9	Configuration B losses at a nominal oil temperature of 40°C	25
3.10	Configuration B losses at a nominal oil temperature of 50°C	26
3.11	Configuration B losses at a nominal oil temperature of 60°C	26
3.12	Configuration B losses at a nominal oil temperature of 70°C	27
3.13	Configuration B losses at a nominal oil temperature of 80°C	27
3.14	Cooling and coolant temperature and flow limits	31
3.15	Boost-converter test data including efficiency, motor load, and electrical parameters	38
4.1	Efficiency comparisons of inverter topologies and inverter/motor systems	48
5.1	Physical characterization of the PMSM, inverter, converter, and cooling system	59
6.1	Summary of gear-train losses at 25°C	60
6.2	Summary of back-emf test results	61
6.3	Summary of motor current and torque test results	61
B-1	Mechanical, operational, electrical, and thermal data from the Prius performance-mapping test	70

ACRONYMS AND ABBREVIATIONS

ac	alternating current
ANL	Argonne National Laboratory
APRF	Advanced Powertrain Research Facility
ATPZEV	advanced technology partial zero emission vehicle
CAFE	Corporate Average Fuel Economy
CPSR	constant power speed ratio
CT	current transformer
DAS	data acquisition system
dc	direct current
DOE	U.S. Department of Energy
ECU	electronic-control unit
EERE	Energy Efficiency and Renewable Energy
emf	electromotive force (measured in volts)
EMI	electromagnetic interference
FCVT	FreedomCAR and Vehicle Technologies
FEA	finite-element analysis
GMR	Giant Magneto Resistive
HEV	hybrid electric vehicle
i_d	direct-axis current
i_q	quadrature-axis current
IGBT	insulated-gate bipolar transistor
I/O	input/output
IPEM	integrated power electronics module (inverter)
IPM	integrated power module (converter)
IR	International Rectifier
km/h	kilometers per hour
kW	kilowatt
mph	miles per hour
NTRC	National Transportation Research Center
Nm	Newton meter
OEM	original equipment manufacturer
ORNL	Oak Ridge National Laboratory
PEEMRC	Power Electronics and Electric Machinery Research Center
PI	proportional integral
PM	permanent magnet
PMSM	permanent magnet synchronous motor
PWM	pulse-width modulation
SDP	switching device power
SUV	sport utility vehicle
rms	root mean square
rpm	revolutions per minute
TC	thermocouple
THS II	Toyota Hybrid System (second generation)
V	volts
W	watts

1. INTRODUCTION

The 2004 Toyota Prius is a hybrid automobile equipped with a gasoline engine and a battery- and generator-powered electric motor. Both of these motive-power sources are capable of providing mechanical-drive power for the vehicle. The engine can deliver a peak-power output of 57 kilowatts (kW) at 5000 revolutions per minute (rpm) while the motor can deliver a peak-power output of 50 kW over the speed range of 1200–1540 rpm. Together, this engine-motor combination has a specified peak-power output of 82 kW at a vehicle speed of 85 kilometers per hour (km/h). In operation, the 2004 Prius exhibits superior fuel economy compared to conventionally powered automobiles.

To acquire knowledge and thereby improve understanding of the propulsion technology used in the 2004 Prius, a full range of design characterization studies were conducted to evaluate the electrical and mechanical characteristics of the 2004 Prius and its hybrid electric drive system. These characterization studies included (1) a design review, (2) a packaging and fabrication assessment, (3) bench-top electrical tests, (4) back-electromotive force (emf) and locked rotor tests, (5) loss tests, (6) thermal tests at elevated temperatures, and most recently (7) full-design-range performance testing in a controlled laboratory environment. This final test effectively mapped the electrical and thermal results for motor/inverter operation over the full range of speeds and shaft loads that these assemblies are designed for in the Prius vehicle operations.

This testing was undertaken by the Oak Ridge National Laboratory (ORNL) as part of the U.S. Department of Energy (DOE) – Energy Efficiency and Renewable Energy (EERE) FreedomCAR and Vehicle Technologies (FCVT) program through its vehicle systems technologies subprogram.

The thermal tests at elevated temperatures were conducted late in 2004, and this report does not discuss this testing in detail. The thermal tests explored the derating of the Prius motor design if operated at temperatures as high as is normally encountered in a vehicle engine. The continuous ratings at base speed (1200 rpm) with different coolant temperatures are projected from test data at 900 rpm. A separate, comprehensive report on this thermal control study is available [1].

1.1 PROGRAM OVERVIEW

The hybrid electric vehicle (HEV) program officially began in 1993 as a five-year cost-shared partnership between DOE and American auto manufacturers: General Motors, Ford, and DaimlerChrysler. Currently, HEV research and development is conducted by DOE through its FCVT program. The mission of the FCVT program is to develop more energy efficient and environmentally friendly highway transportation technologies. Program activities include research, development, demonstration, testing, technology validation, and technology transfer. These activities are aimed at developing technologies that can be domestically produced in a clean and cost-competitive manner.

The vehicle systems technologies subprogram is one of four subprograms under the FCVT program which supports the efforts of FCVT through a three-phase approach intended to:

- Identify overall propulsion and vehicle-related needs by analyzing programmatic goals and reviewing industry's recommendations and requirements then develop the appropriate technical targets for systems, subsystems, and component research and development activities;
- Develop and validate individual subsystems and components including electric motors, emission-control devices, battery systems, power electronics, accessories, and devices to reduce parasitic losses; and

- Determine how well the components and subassemblies work together in a vehicle environment or as a complete propulsion system and whether the efficiency and performance targets at the vehicle level have been achieved.

Source: http://www.eere.energy.gov/vehiclesandfuels/technologies/systems/index.shtml

The research performed under the vehicle systems subprogram will help remove technical and cost barriers to enable technology for use in such advanced vehicles as hybrid and fuel-cell-powered vehicles.

1.2 TESTING FACILITIES

Evaluation of the 2004 Prius and its hybrid electric drive system involved both vehicle-level and subassembly-level performance testing. Vehicle-level testing is being conducted at the Advanced Powertrain Research Facility (APRF) located at the Argonne National Laboratory (ANL), in Argonne, Illinois. The APRF is a multi-dynamometer vehicle test facility capable of testing conventional and hybrid vehicle propulsion systems and vehicles. Subassembly-level testing is being conducted by ORNL at its Power Electronics and Electric Machinery Research Center (PEEMRC). The PEEMRC is a broad-based research center for power electronic inverters and electric machinery (motor) development. Located in the recently constructed national user facility known as the National Transportation Research Center (NTRC), the PEEMRC has more than 9000 square feet of space for developing and building the next generation prototypes of inverters, rectifiers, and electric machine technology.

1.3 SCOPE AND OBJECTIVE

This report summarizes vehicle-level and subsystem-level test results obtained for the 2004 Prius and various electrical and mechanical subassemblies of its hybrid electric drive system. The primary objective of these tests was to (1) characterize the electrical and mechanical performance of the 2004 Prius, and (2) map the performance of the inverter/motor system over the full design speed and load ranges.

Information about the 2004 Prius and its technical design features is presented in Section 2 to serve as a foundation for subsequent discussions about the various subassemblies of the hybrid electric drive system that were tested. Laboratory test results are summarized in Section 3. They include electrical and mechanical data that have been acquired to date at ANL and ORNL. The objectives of these tests were to characterize the functional performance of the hybrid electric drive system and to understand the design methodology used in the construction of the various system subassemblies — specifically the generator, traction motor, and inverters.

Information about the inverters and converter is presented in Section 4. This information includes discussions about the functional characteristics and control development for the motor inverter and converter and a description of inverter modifications that will provide a way to measure current and voltage values at specific locations. Packaging and volume/weight data is provided in Section 5. This information includes the derivation of peak-power-to-volume and -weight ratios which are related to key FCVT design targets. Preliminary conclusions and findings based on the acquired test data along with areas of needed research and development are presented in Section 6.

1.4 APPROACH

Complementary electrical and mechanical data from vehicle-level and subsystem-level tests were acquired to gain a full understanding of the 2004 Prius performance. These data were then used to determine back-emf voltage and energy loss values over the specified operating range of the vehicle.

Vehicle-level tests were performed at the APRF with the electrical and mechanical systems installed in the original factory configuration. The inverter, motor, generator, axles, and related subassemblies are instrumented to acquire power-flow data needed to characterize vehicle performance.

Subsystem-level tests were performed at the NTRC by removing the hybrid electric drive system and inverter from the vehicle and mechanically connecting the shaft to a dynamometer. This arrangement required a reconfiguration of the inverter so that it will operate outside the vehicle (see below). Using this approach makes it possible to separately evaluate the performance of each power-related subsystem of the hybrid electric drive system. Subsystem-level test results provide data needed to characterize the overall performance of the 2004 Prius HEV system.

Operating the permanent magnet synchronous motor (PMSM) and inverter systems outside the vehicle represents a considerable challenge. Figure 1.1 shows a partial diagram of the electronic-control unit (ECU) and some of the many interconnected vehicle systems. The ECU is the "brain" of the highly integrated vehicle electrical system. In order to operate the inverter and PMSM outside the vehicle, it was necessary to sever the many interconnecting lines between the inverter/PMSM/boost-converter system and the ECU (many more lines exist than are shown in the simplified schematic). Extracting and operating the ECU *with* the subassemblies of interest would have meant attending to the hundreds of signals it must have to operate (an option that was not chosen). Therefore, to accomplish out-of-vehicle operation, ORNL was forced to replace the ECU with a sophisticated and versatile inverter controller capable of providing complex control features such as a high-speed control loop and field weakening.

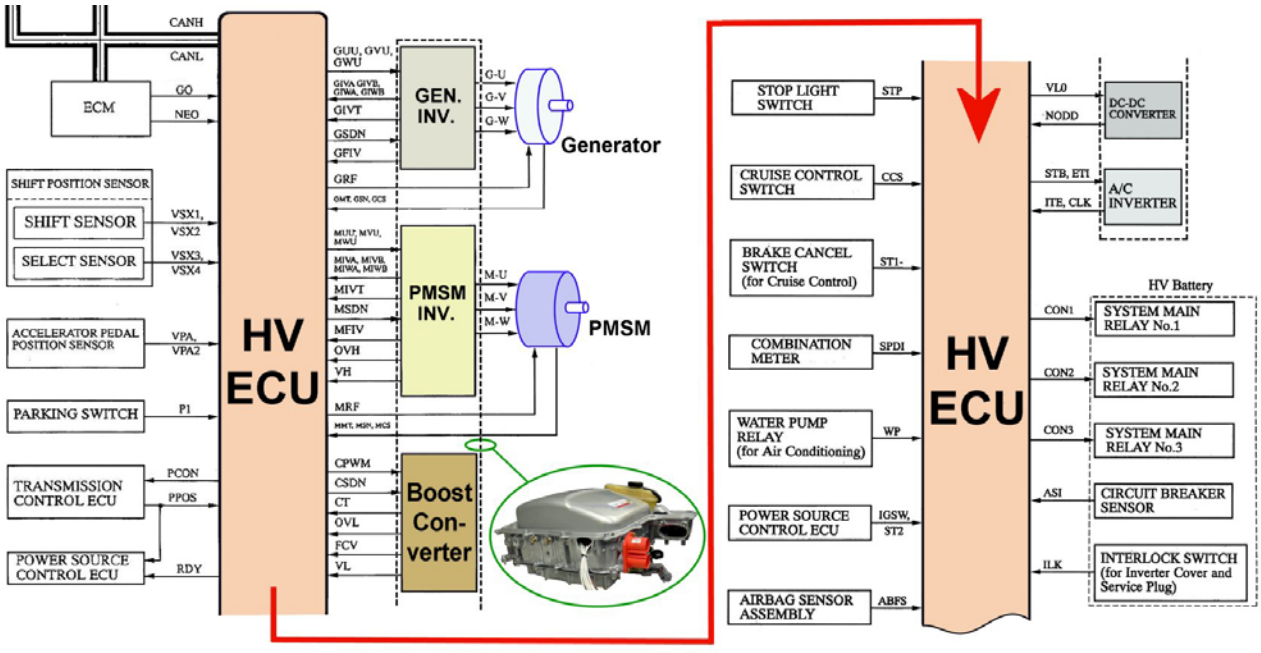

Fig. 1.1. Predominant project challenge represented by a highly integrated vehicle control system.

2. HYBRID ELECTRIC DRIVE SYSTEM DESCRIPTION

The 2004 Prius is a new-generation hybrid automobile that was introduced into the market in September 2003 by the Toyota Motor Corporation. As a hybrid vehicle, the 2004 Prius uses both a gasoline-powered internal combustion engine capable of delivering a peak-power output of 57 kW and a battery-powered electric motor capable of delivering a peak-power output of 50 kW as motive power sources. Combining these two-motive power sources results in improved fuel efficiency and reduced emissions compared to traditional automobiles and provides the 2004 Prius with the following energy-saving characteristics.

- Energy-loss reduction is achieved by automatically stopping the engine when idling.
- Energy is recovered and reused by capturing kinetic energy that is normally wasted as heat during deceleration and braking. The starter and electric motor then convert this energy to electricity for use.
- Engine is able to operate at peak-efficiency speed a high percentage of the time.
- Supplementary power is provided by the electric motor during acceleration when engine efficiency is low.
- Optimal vehicle efficiency is realized by using the electric motor to run the vehicle under operating conditions when engine efficiency is low and by generating electricity when engine efficiency is high.

Enhanced performance of the 2004 Prius is attributed to the new-generation Toyota Hybrid System (THS II). This system is a power train consisting of a high-power motor, generator, and a battery of relatively low power. Major subassemblies of the THS II are shown in Fig. 2.1. As this figure indicates, a mechanical subassembly referred to as a power-split device (planetary-gear set) separates power supplied by the gasoline engine into two paths. In the mechanical path, engine power is transmitted to the vehicle's wheels directly through the transmission. In the electrical path, a generator converts mechanical energy from the engine into electrical energy. Electricity produced by the generator is then available for either supplementing the battery power to the electric motor or charging the battery, or both. By using energy in this manner, the 2004 Prius requires no external power source for battery charging. The power-split device allows the engine to function at or near its optimal operating speed, regardless of vehicle speed, while still being able to efficiently add power to the wheels and simultaneously drive the generator. A photograph of the engine and hybrid drive assembly after removal from the car is shown in Fig. 2.2.

In operation, the 2004 Prius is capable of functioning in the following modes:

- When engine efficiency is low, such as during start-up and mid-range speeds, motive power is provided by the motor alone using energy stored in the battery.
- Under normal driving conditions, overall efficiency is optimized by controlling the power allocation so that some of the engine power is used for turning the generator to supply electricity for the motor while the remaining power is used for turning the wheels.
- During periods of acceleration when extra power is needed, the generator supplements the electricity being drawn from the battery so the motor is supplied with the required level of electrical energy.

- While decelerating and braking, the motor acts as a generator that is driven by the wheels thus allowing the recovery of kinetic energy. The recovered kinetic energy is converted to electrical energy that is stored in the battery.
- When necessary, the generator recharges the battery to maintain sufficient reserves.
- At times when the vehicle is not moving and when the engine moves outside of certain speed and load conditions, the engine stops automatically.

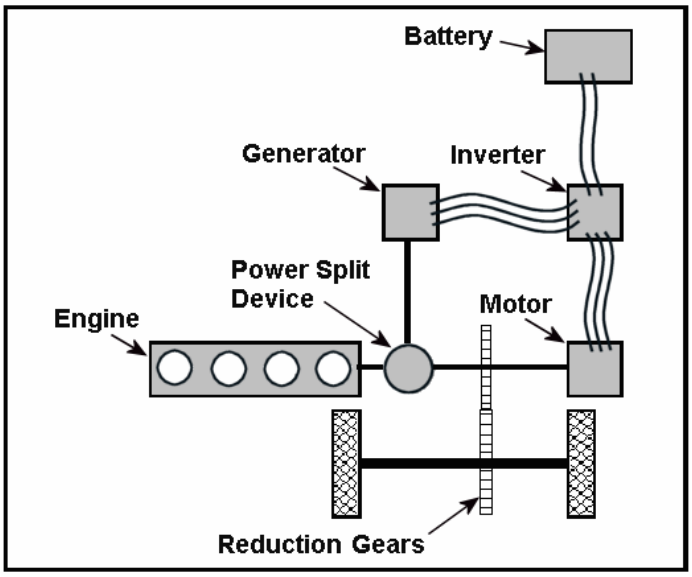

Fig. 2.1. Subassembly arrangement for the THS II.

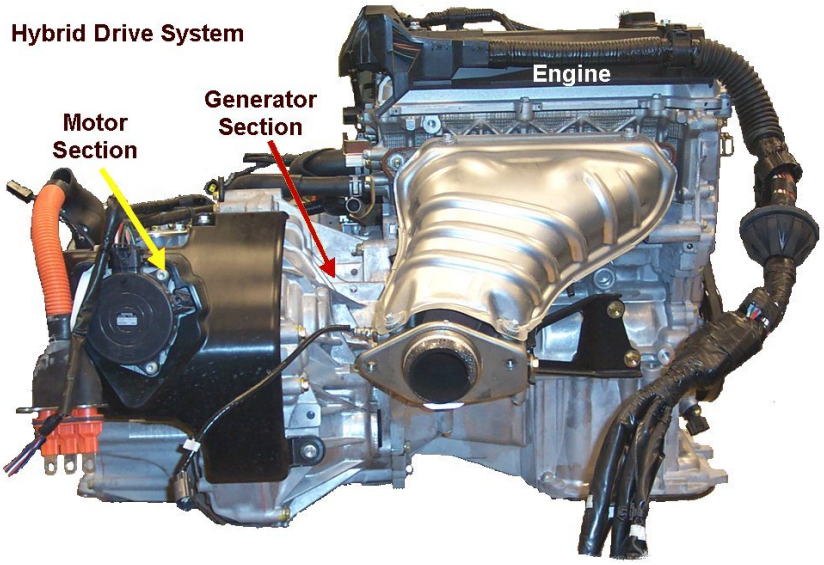

Fig. 2.2. 2004 Prius engine and hybrid drive assembly.

Additional information about the capabilities and properties of the 2004 Prius are presented in a separate ORNL report [2].

To maintain the operating temperature of the various system components within an acceptable range, the 2004 Prius has two separate ethylene glycol based coolant systems. The arrangement of these coolant systems and a brief description of their functional characteristics are presented in Fig. 2.3.

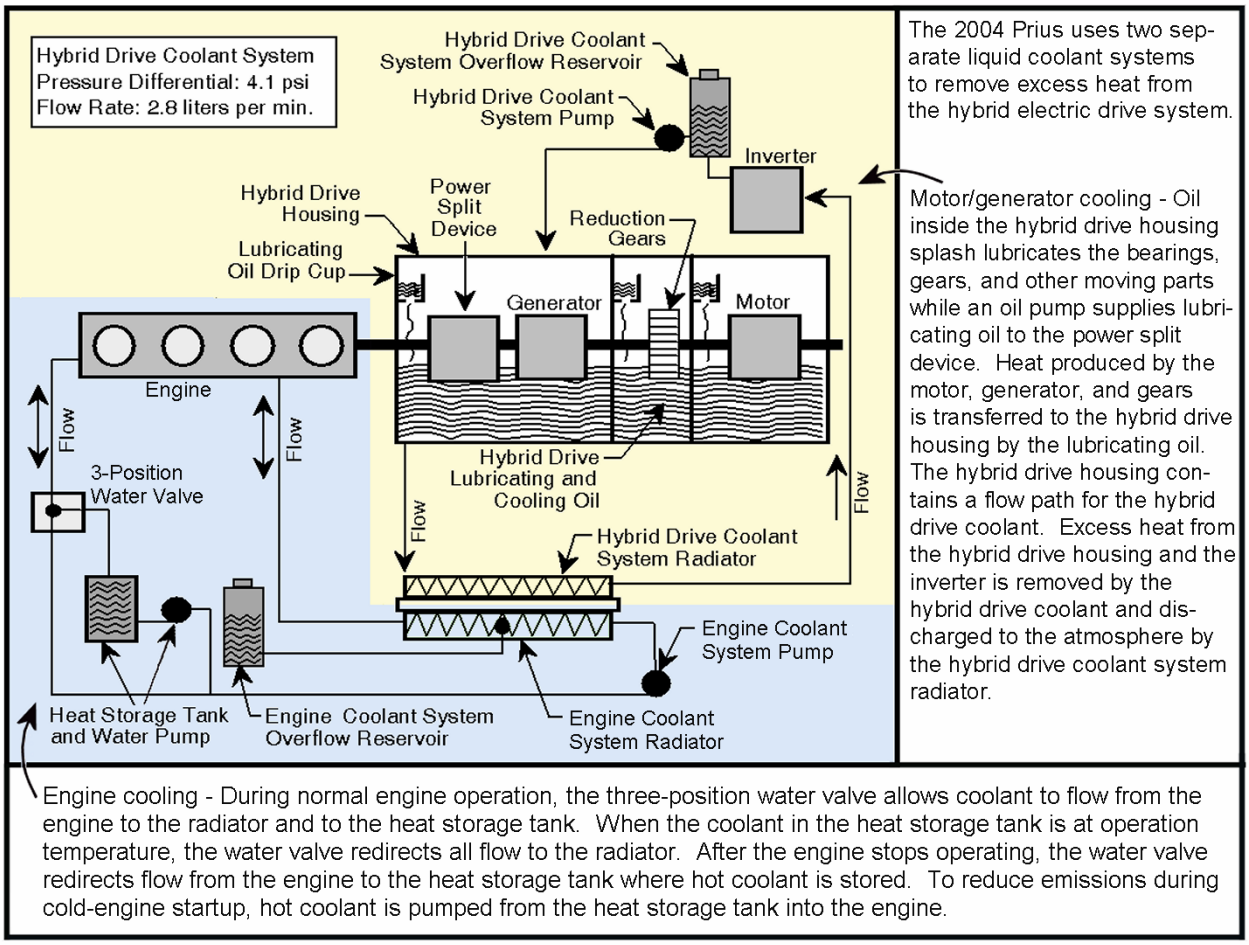

Fig. 2.3. Heat removal and lubrication scheme for the 2004 Prius.

The engine-coolant system is similar to the coolant system in a traditional automobile. Its purpose is to circulate a liquid coolant through the engine to remove excess thermal energy generated by fuel combustion. A pump forces the coolant to flow from the engine to a radiator where the waste heat is dumped. To keep the coolant from escaping, the coolant is confined in a closed loop that is protected from over pressurization by a self-closing pressure relief valve (radiator cap). This valve vents at a pressure that is slightly above atmospheric pressure thereby allowing the coolant to remain liquid at a temperature slightly above the boiling point of water. To accommodate changes in coolant volume caused by temperature and pressure fluctuations, the system includes a tank that functions as an overflow reservoir. The engine-coolant system also includes an insulated coolant storage bottle that stores hot coolant during shutdown and makes it available when the engine is restarted. Using hot coolant in this way reduces exhaust-gas emissions produced during cold-engine startup.

The hybrid-drive-coolant system is separate from the engine-coolant system because the two systems operate at different temperatures[1]. Powered by an electric pump, the liquid coolant in this closed-loop system flows continuously through the motor, generator, inverter, and radiator. Heat removed from these electrical components is transferred to the surrounding atmosphere by the radiator. Like the engine-coolant system, the hybrid-coolant system also includes a tank that functions as an overflow reservoir.

Detailed information about the 2004 Prius and its operation and maintenance is provided in the three-volume repair manual published by the Toyota Motor Corporation [3–5].

2.1 DESIGN REQUIREMENTS

The high-voltage power circuit in the THS II, which includes the motor and generator, is designed to operate over a variable voltage range of 200–500 Vdc. This elevated-voltage design feature results in an increase in efficiency because electrical power can be supplied to the motor using less current. In addition, the elevated voltage allows the motor to operate at higher speeds where high emf would inhibit the speed of a lower voltage motor.

2.2 SYSTEM SUBASSEMBLIES

Major THS II subassemblies in the 2004 Prius include the:

- engine
- power-split device
- generator
- motor
- inverter
- battery

The specification for these subassemblies is shown in Table 2.1 (Sources include http://www.toyota.co.jp/en/tech/environment/ths2/ and http://www.toyota.com/vehicles/2005/prius/specs.html).

Table 2.1. Specification for THS II subassemblies

Subassembly	Property Description	Property Value
Engine	Type	1.5 liter gasoline (high-expansion ratio cycle)
	Maximum output	57 kW at 5000 rpm
	Maximum torque	115 Newton meter (Nm) at 4200 rpm
Motor	Type	Synchronous alternating current (ac) permanent magnet (PM) motor
	Maximum output	50 kW between 1200 and 1540 rpm
	Maximum torque	400 Nm between 0 and 1540 rpm
System*	Maximum output	82 kW at 85 km/h and higher
	Maximum torque at 22 km/h or lower	478 Nm
Battery	Type	Nickel-metal hydride
	Construction	28 each 7.2V modules connected in series
	Voltage	201.6V
	Power output	21 kW

*Maximum combined engine and hybrid-battery output and torque constantly available within a specified vehicle speed range.

[1] Although the reason for using two separate coolant systems cannot be confirmed, it is believed that this decision was made to allow the motor, generator, and inverter to operate well below 100°C, the boiling point of water.

2.2.1 Engine

The design of the Type 1NZ-FXE 1.5-liter engine in the 2004 Prius is based on the Atkinson Cycle in which compression stroke and expansion stroke duration can be set independently. The transverse-oriented, water-cooled, 4-stroke engine features 4 in-line cylinders, 16 valves, a double overhead cam with chain drive, and a 13:1 compression ratio. The high expansion ratio cycle engine design has helped to certify the vehicle as an advanced technology partial zero emission vehicle (ATPZEV).

2.2.2 Power-Split Device

Major transmission subassemblies in the THS II include the power-split device (planetary-gear set), the generator, the electric motor, and the reduction gears. The purpose for the power-split device is to allow power from the engine to turn the generator and the wheels simultaneously. In operation, shaft power from the engine is transmitted via the planetary carrier. The rotational shaft of the planetary carrier inside the gear mechanism is directly linked to the engine and transmits the motive power to the outer-ring gear and the inner-sun gear via pinion gears. The rotating shaft of the ring gear is directly linked to the motor and transmits traction-drive force while the rotating shaft of the sun gear is directly linked to the generator. Diagrams of the power-split device and the gear train that connect the motor to the front wheels are shown in Figs. 2.4 and 2.5, respectively. The actual gear arrangement is shown in Fig. 2.6.

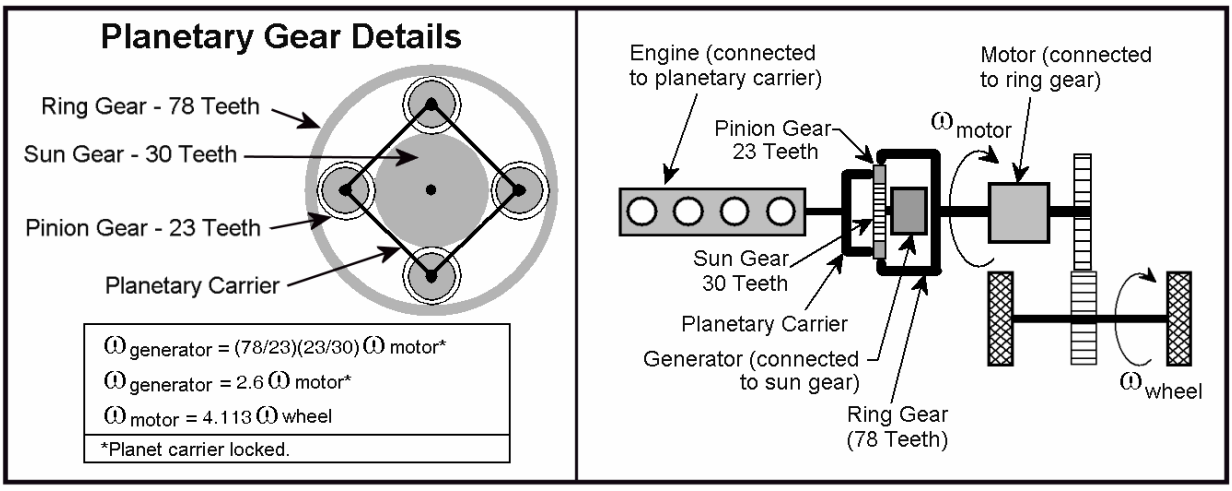

Fig. 2.4. Diagram of the 2004 Prius power-split device.

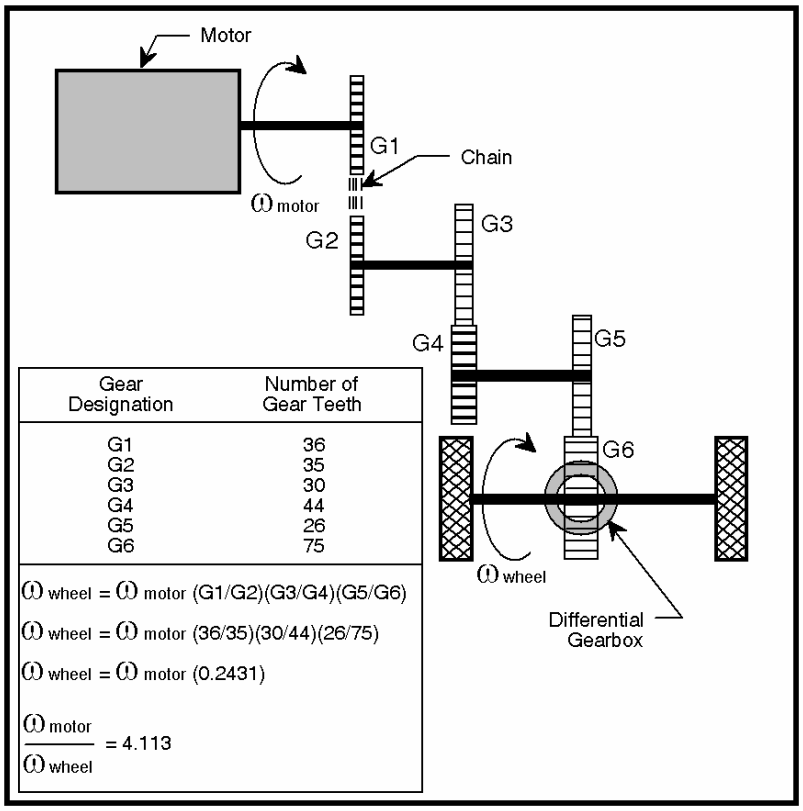

Fig. 2.5. Diagram of the 2004 Prius gear train between the motor and wheels.

Fig. 2.6. 2004 Prius gears with number of gear teeth shown.

2.2.3 Generator

The THS II includes a synchronous-type ac generator that rotates at high speeds up to 10,000 rpm. By rotating at high speeds, the generator, which is an eight-pole PM device, provides high-power density for charging the battery and supplementing motor power requirements. In addition, the generator also functions as the engine starter. At start up, the generator rotates the sun gear in the power-split device and thereby provides cranking power for the engine. The configuration of the generator rotor is shown in Fig. 2.7.

Fig. 2.7. 2004 Prius generator rotor.

2.2.4 Motor

The eight-pole, PMSM features high low-speed torque and high power output. It is designed as a high-efficiency, brushless direct current (dc) motor. The motor rotor is constructed with interior PMs and laminated stacked electromagnetic steel plates. The PMs are arranged in a V-shape as opposed to conventional radial alignment. In addition, with a high supply voltage up to 500V, the peak-power output of the motor is 50 kW. The configuration of the motor and stator are shown in Fig. 2.8. Additional details about the design and manufacture of the motor are contained in a report that was recently published by ORNL [6]. Supplementary information about locked rotor torque and current performance, which is addressed in Section 3.2.1, is contained in another ORNL report [2].

2.2.5 Inverter

The power control unit consists of the following subassemblies

- motor inverter,
- generator inverter,
- voltage-buck/boost converter,
- air-conditioning compressor inverter, and
- a 12V dc-to-dc converter.

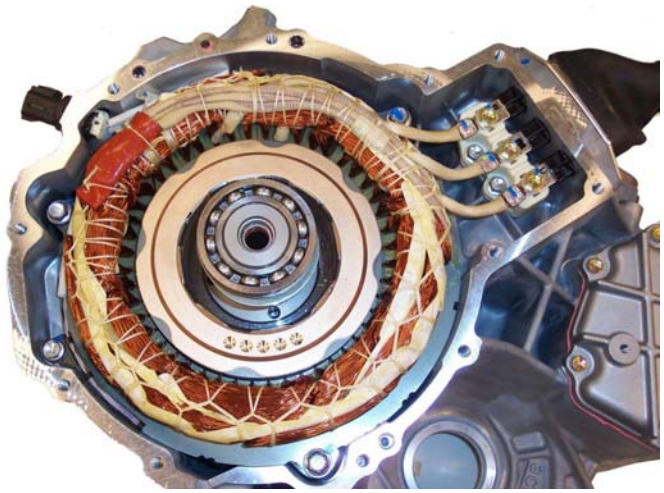

Fig. 2.8. 2004 Prius motor rotor and stator.

The unit, which is shown in Fig. 2.9, contains an inverter that produces 3-phase ac for driving the motor and includes a dc-to-dc converter that produces 12V for auxiliary equipment. It also includes a high-voltage, bi-directional, dc-to-dc converter that boosts the 200V battery up to a maximum of 500Vdc link, or bucks the higher voltage dc link (that may range from 200–500V) down to charge the 200V battery.

Fig. 2.9. 2004 Prius inverter and voltage converter unit.

2.2.6 Battery

A compact, high-performance nickel-metal hydride rechargeable battery is used in the 2004 Prius. The battery consists of 28 low-voltage modules (7.2V each) connected in series to produce a nominal 201.6V. It provides electricity to the motor and receives charging energy from the generator. The specified power output from the battery is 21 kW.

3. LABORATORY TESTING

Laboratory testing of the 2004 Prius hybrid electric drive system and its subassemblies is being conducted at ANL and ORNL. The objectives of these testing programs are to characterize the functional performance of the hybrid electric drive system and to understand the design methodology used in the construction of its various subassemblies, specifically the traction motor, inverter, generator, and coolant system.

3.1 ANL VEHICLE-LEVEL PERFORMANCE TESTS

This section describes in two subsections the early performance testing of the Prius and later test data that focuses on the operation of the voltage-boost converter.

3.1.1 Initial Performance Testing at ANL

Beginning in early 2004, a vehicle-level performance-testing program was initiated at ANL. Objectives of this ongoing collaboration are to determine the operating characteristics and to quantify efficiencies of the 2004 Prius hybrid electric drive system as installed in the vehicle and as operated based on algorithms contained in the ECU. The tests are being conducted at the APRF under both steady-state and dynamic conditions. To acquire the necessary electrical data, all accessible power-flow points were instrumented to measure voltage and current. Power measurements were obtained between the following locations:

- Generator and inverter (Phase A current, Phase B current, A-C line voltage, B-C line voltage),
- Traction motor and inverter (Phase A current, Phase B current, A-C line voltage, B-C line voltage),
- Boost converter and battery (battery current, battery dc voltage), and
- Boost converter to main inverters (dc voltage, current).

Test variables that were measured are identified in Table 3.1.

Table 3.1. Measurement variables for ANL testing program

Variable Description	Variable Designation	Measurement Type
Generator power	P_{genAC}	Electrical
Motor power out (to wheels)	P_{mtr}	Mechanical
Inverter power out (inverter to motor)	P_{mtrAC}	Electrical
Boost power high side	$P_{boostHI}$	Electrical
Battery power (battery dc link)	P_{BATT}	Electrical

Each test run was conducted with the air-conditioner compressor inverter and the auxiliary 12V dc-to-dc converter disabled. To ensure precise acceleration and speed settings during the tests, the accelerator position was remotely controlled.

The ANL chassis dynamometer is normally set up to monitor vehicle emissions under various driving cycles. Testing of a HEV requires a greater monitoring effort to cover the additional electrical devices incorporated in the vehicle. In addition, the joint ANL and ORNL testing effort requires very precise power measurements to fully characterize 2004 Prius performance. The test setup for the 2004 Prius

hybrid electric drive system involves current and voltage measurements at numerous points within the system. Figure 3.1 shows the configuration of the basic electrical system for the 2004 Prius hybrid electric drive system and the locations of the installed instrumentation. Details about the ANL inverter modifications are discussed in Section 4.3.

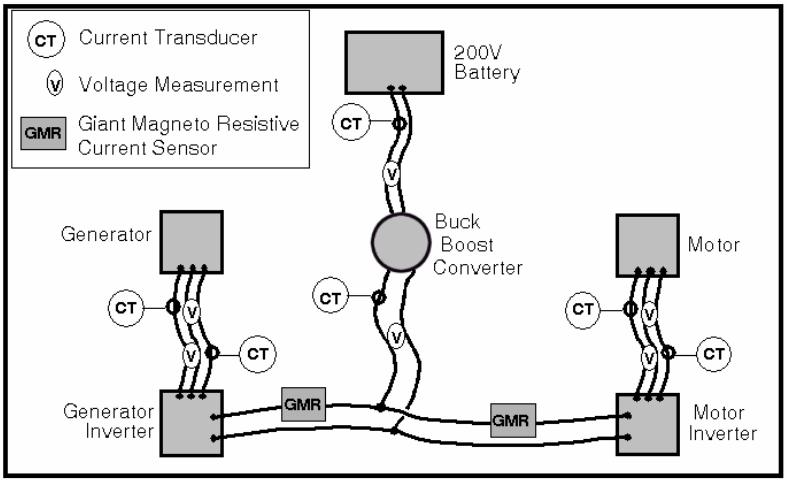

Fig. 3.1. Instrumentation locations for ANL testing.

An example time trace of data being acquired during the tests is presented in Fig. 3.2. It shows the power flow in different parts of the hybrid electric drive system with the vehicle speed overlaid on the graph. Review of this graph reveals that engine power is high when the vehicle is accelerating to higher speeds and drops to zero when the vehicle speed is constant, thus allowing the electric motor to propel the vehicle without assistance from the engine. At the highest speeds, however, the engine and the motor simultaneously supply power for the vehicle. Subsequent to the test, calibration checks of the power-sensing equipment indicated possible offsets and discrepancies in the data. Additional data is needed to fully characterize vehicle-level performance.

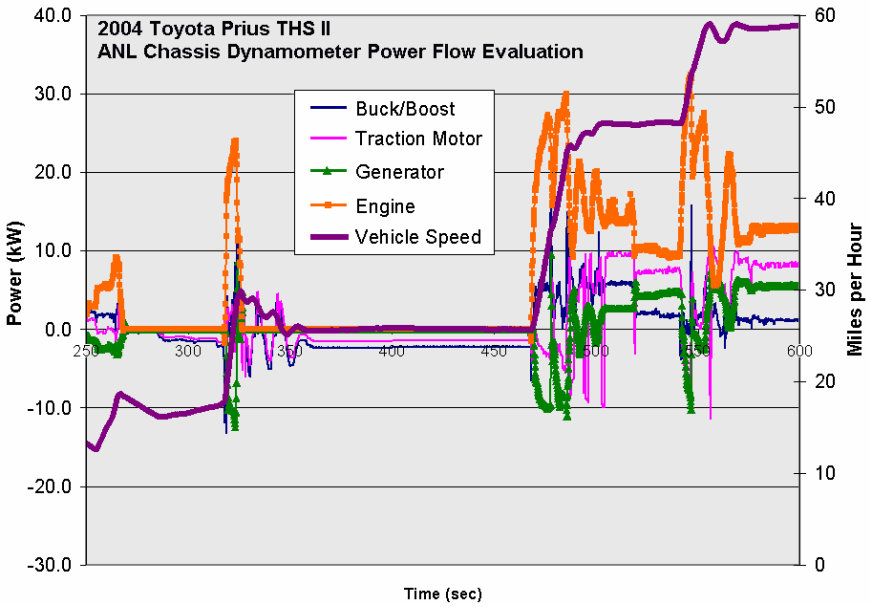

Fig. 3.2. Sample power measurements under varying speed conditions.

Another example data plot that illustrates the relationship between battery power, boost-converter power, and motor power is shown in Fig. 3.3. This data was acquired under controlled conditions in which all auxiliary equipment was switched off (i.e., air-conditioning compressor inverter and 12V dc-to-dc converter) so the battery, boost, and motor power levels would be directly related to each other. Boost power is very close to the battery power because boost converters have low losses. Motor electrical power should be approximately the same but slightly lower due to efficiency losses in the motor inverter. Gross efficiencies can be inferred from this data, but more detailed efficiency results from additional tests are needed.

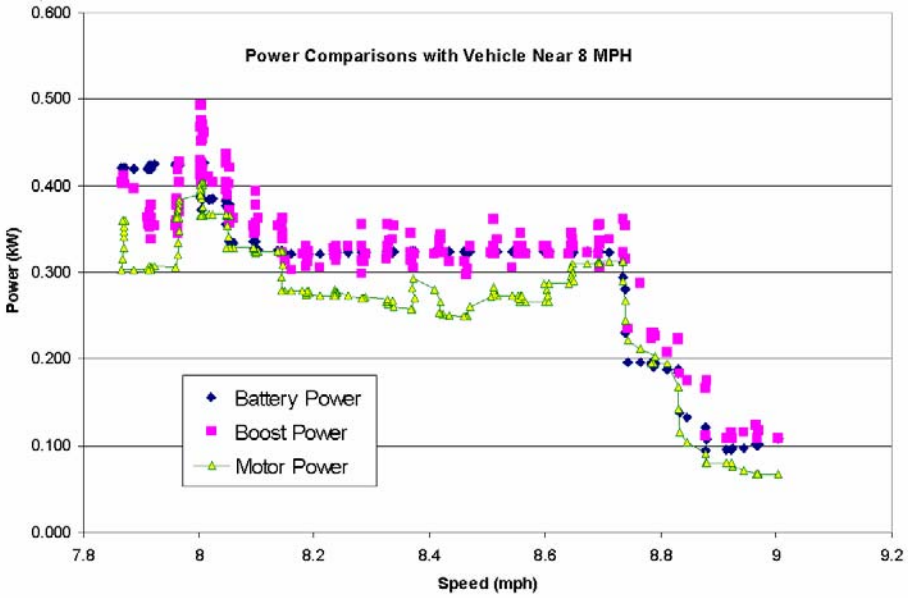

Fig. 3.3. Sample power measurements under controlled speed conditions.

Although this graph validates the measurement results, slight discrepancies in the data and other factors indicate the need to improve sensor calibrations and data acquisition system (DAS) settings prior to future tests.

3.1.2 Vehicle Data Characterizing Boost-Converter Operation

With planning underway for detailed performance testing at ORNL, it was necessary to review ANL data that made clear the operation of the voltage-boost circuit in the Prius. In addition, there was considerable technical interest in boost converters, including both their packaging (see Sections 5.2 and 5.3) and operation. (Note: ORNL converter test data and efficiency maps are provided in Section 3.3.4.) In the Prius HEV system, the PMSM obtains most of its power from the generator and the rest from the HEV-battery-converter-inverter system. Thus, the converter's power rating is less than half of the PMSM's rating.

Of high interest is how the generator voltage, which increases with vehicle speed, compares to the voltage that the ECU directs the converter to produce. In order to determine this, the generator back-emf data plot was modified[2] as shown in Fig. 3.4 to show, by extrapolation, the voltage-speed relationship at speeds up to 10,000 rpm. Also, the vehicle speed is included in the plot so that the data can be compared to vehicle operation data provided by ANL. Note that the peak voltage developed in the generator is in the variable

[2] The full set of generator data is provided in Section 3.2.2.2.

range of the dc converter when the vehicle is traveling from 25–65 miles per hour (mph). This relationship will prove useful in the discussion below.

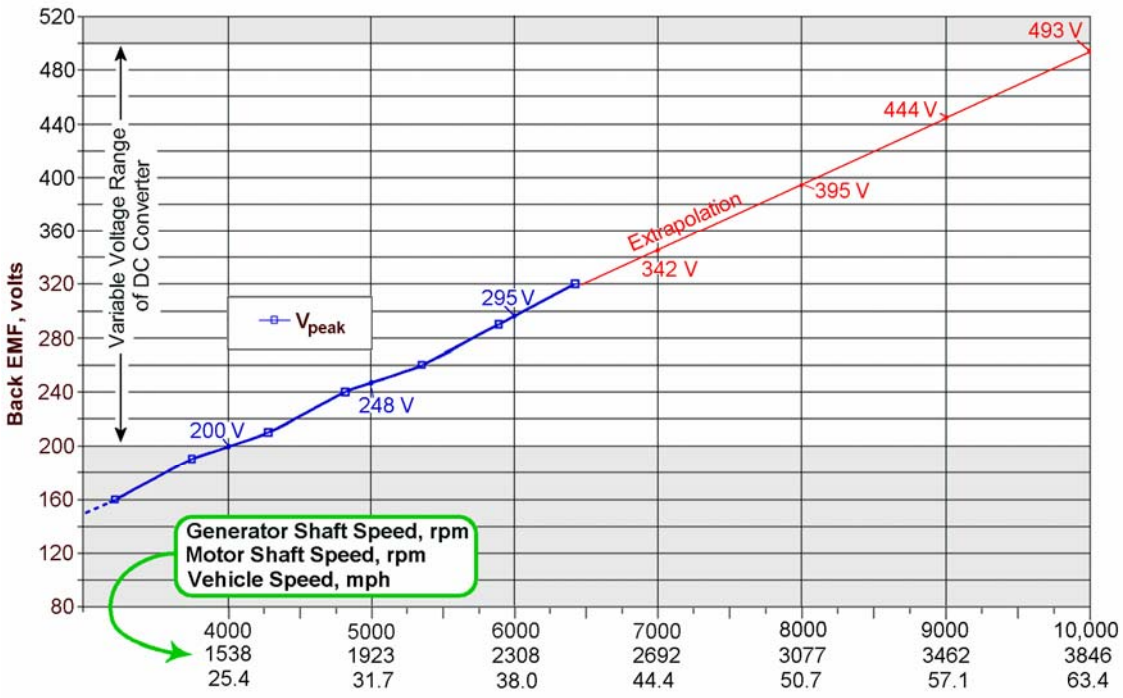

Fig. 3.4. Extrapolation of generator back-emf data for generator speeds up to 10,000 rpm.

Subsequent to the testing at ANL described in Section 3.1.1, ANL generated additional test data and, at ORNL's request, transmitted converter-related data to ORNL in April 2005. This data helped to characterize the operation of the voltage-boost converter relative to acceleration and vehicle speed. The voltage-buck operation is not reflected in the data, but clearly the battery-charging function requires a reduction from the generator and PMSM output voltages to a voltage a few volts higher than the 201.6 volts (V) battery voltage.

The plots that follow show the following five parameters: V and I output from the converter, accelerator pedal position output, brake-pedal position output, and vehicle speed. Note that positive current powers the PMSM and negative current charges the HEV battery. Units are excluded since the plots are intended to provide qualitative comparisons.

Figure 3.5 shows data from a drive cycle where the vehicle was accelerated to about 31.5 mph, based on chassis-dyne data, followed by braking. A portion of the y-axis scale is expanded to enlarge/clarify the plots at the bottom of the chart (also making the depiction qualitative). As indicated in the figure, there are three instances where a current spike from the output of the voltage-boost circuit preceded or accompanied a rise in the output voltage from the boost circuit. The voltage then remained elevated for different periods and then fell. Two occurred during acceleration and one at the end of the acceleration period. The data does not appear to provide a full picture of what is happening and this is not surprising since the ECU algorithm is unknown.

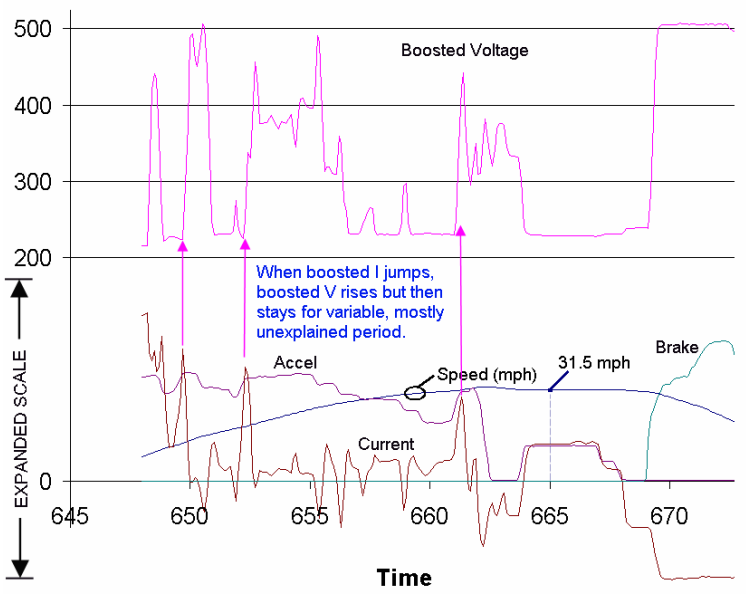

Fig. 3.5. Drive-cycle data from ANL showing voltage-boost converter response.

Note that braking causes a maximum boost to 500 V to support the regeneration battery-charging mode. Since ORNL testing will not include an evaluation of this process, periods of braking will be excluded from the drive-cycle plots which follow.

In Fig. 3.6, the second drive-cycle period shows an elevated voltage level corresponding to a rapid acceleration followed by an extended period of time at the minimum voltage (just above 200 V). This is followed by a few brief, voltage spikes of unknown causes that are postulated to be of no value to the operation of the inverter/motor system.

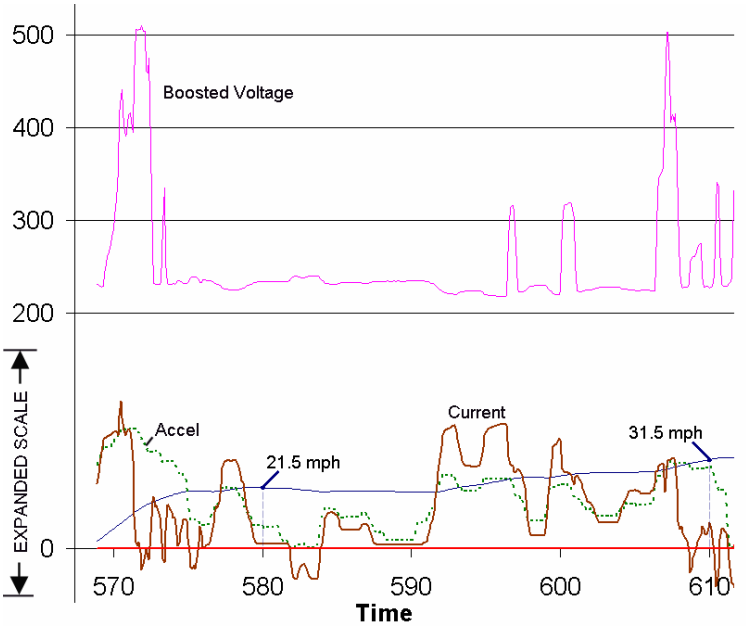

Fig. 3.6. Second drive-cycle data set from ANL showing voltage-boost converter response.

In Fig. 3.7, the third drive-cycle period shows a rapid acceleration followed by operation at vehicle speeds above 40 mph. These data show a sustained voltage boost to well above 300 V and the maximum of 500 V during acceleration. The plot depicts an intermediate voltage-boost state that occurs at these vehicle speeds.

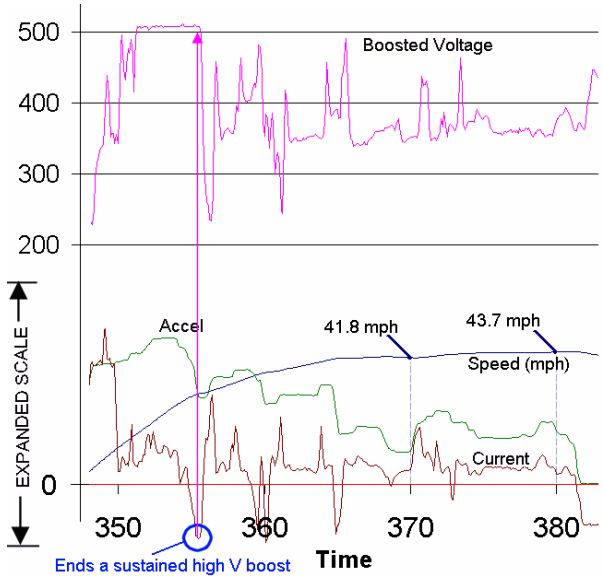

Fig. 3.7. Third drive-cycle data set from ANL showing voltage-boost converter response.

Much of what the preceding figures have shown is further clarified in the fourth drive-cycle plot in Fig. 3.8. In this case the vehicle is accelerated to about 68 mph. Because the level of acceleration is varied, the voltage boost swings between minimum and maximum several times. From 28.1–49.8 mph, maximum voltage results from both the acceleration process and the increasing speed. Between 49.8–59.7 mph, there is minimal tendency for voltage to drop below the maximum level. Above 59.7 mph, voltage remains at the maximum level. Notice that the plot also specifies the rotational speed of the PMSM[3] at specified points.

Figure 3.8 also shows the peak back-emf from the generator based on ORNL component testing as presented earlier in this section (Fig. 3.4). The points are plotted at the calculated equivalent vehicle speeds and then approximate interconnecting lines are added for clarity. The data shows how the boosted voltage rarely falls below the generator's peak voltage. Although the actual ECU algorithm for controlling the voltage boost is unknown, this plot and the preceding plots present a clear picture of how voltage is generally controlled during acceleration, high speeds, and braking. Because the rating of the converter prevents it from providing full power to the Prius motor, the converter was not used in performance characterization testing at ORNL.

Six additional plots of drive-cycle data from a different drive-cycle test are provided in Appendix A. These plots are useful in further characterizing the operation of the voltage-boost converter and the ECU-dictated converter-control scheme.

[3] The rotational speed of the PMSM (rpm) is 60.66 times the vehicle speed in mph. This is based on the constant gear ratio of the Prius, wheel/tire diameter, and conversion of units.

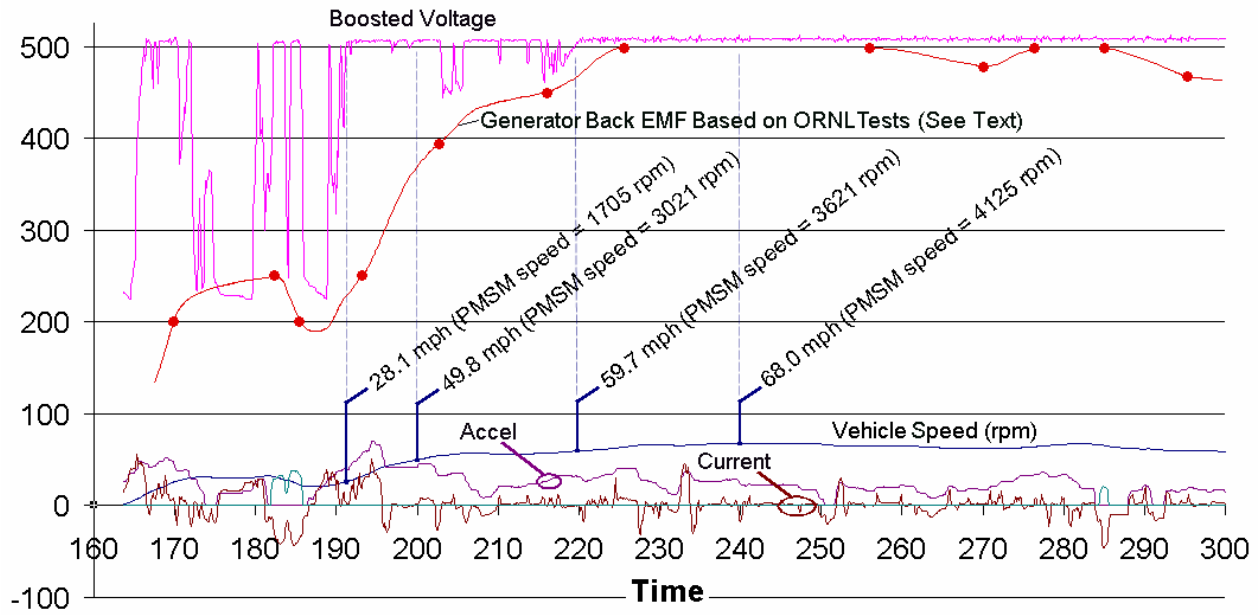

Fig. 3.8. Drive-cycle data set from ANL/ORNL showing voltage boost at high speeds (ANL data).

3.2 ORNL SUBSYSTEM-LEVEL PERFORMANCE AND VALIDATION TESTS

The hybrid electric drive system for the 2004 Prius was also tested at ORNL under a variety of operating conditions to characterize its electrical and mechanical performance. Objectives of the testing program were to measure motor and generator back-emf voltages, evaluate motor starting torque capacity, and determine gearbox-related power losses over a specified range of shaft speeds and lubricating oil temperatures. To eliminate effects of engine friction from the evaluation, the engine was removed from the system prior to the tests.

Accomplishing the testing program objectives required connecting the hybrid electric drive system to a dynamometer that was capable of providing the power needed to turn the system components at specified rotational speeds. To ensure that both axles rotated at the same speed, the differential was modified so the internal gears of the differential could not rotate. By blocking rotation of these gears, it was possible to measure torque from one of the two drive wheel axles. In this modified configuration, the gear-reduction ratio, which is a function of the number of gear teeth, was determined to be 4.113 motor rotations to one axle rotation.

To understand effects of oil temperature on power loss, a system for heating the gearbox lubricating oil to a specified nominal temperature was developed and used during the tests. In this blocked differential configuration, the following measurements were obtained:

- The gear ratio from the motor shaft to the dynamometer was measured, calculated, and documented.
- The gear, windage, cogging, and other friction losses were measured without energizing the generator or the motor. Measurements were obtained with the engine spline free spinning and with it locked.

For initial motor testing, the engine input spline was allowed to float with either the motor or the dynamometer providing the driving power. During the generator tests, the engine spline was fixed from

rotating which effectively locks the planetary-carrier arm. In this configuration, the planetary-gear train transmitted torque to the generator shaft. Details of the power-split device and the gear train that connects the motor to the wheels are presented in Figs. 2.4 and 2.5 (see Section 2).

To provide a better understanding of the thermal management system, data collected as part of the overall testing effort included (1) gearbox lubricating oil temperature, and (2) hybrid-drive-coolant system flow. A diagram showing the lubricating and cooling oil inside the three compartments of hybrid drive housing is presented in Fig. 2.3 (see Section 2). This figure also presents the hybrid-drive-coolant system flow rate and pressure that were determined as part of the testing effort. Besides lubricating the bearings and gears, this oil also removes excess heat from the gears, motor, and generator and transfers it to the hybrid drive system coolant.

3.2.1 Locked Rotor Tests

A series of locked rotor tests [2] were performed in 2004 and 2005 to determine the general operating capabilities of the traction motor. The 2005 test used a new mechanical-gear mechanism capable of precisely positioning and locking the rotor based on readings from the absolute position sensor in the Prius.

The motor-driven gear mechanism was used to position the motor shaft and rotate it incrementally in degree segments while otherwise remaining locked. Torque values were obtained by supplying sinusoidal current to the motor windings at varying degrees of shaft angle. The resulting data were used to produce torque-vs.-shaft-angle plots, which are shown in Fig. 3.9 for various current levels. Current and corresponding torque values are listed in Table 3.2. Following the test, it was verified that no demagnetization damage[4] occurred due to rotor heating.

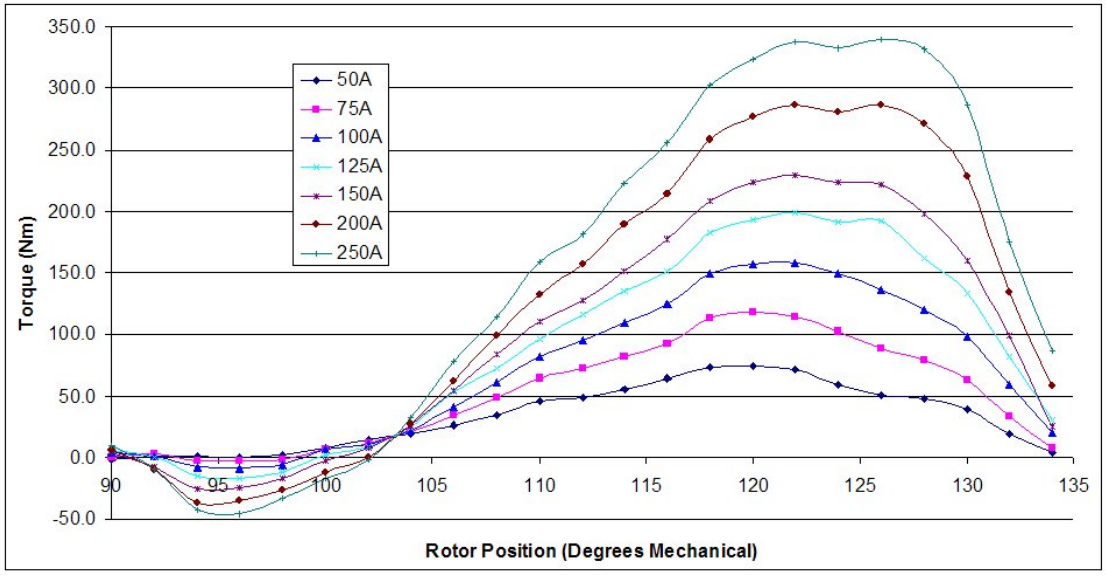

Fig. 3.9. Motor-shaft angle vs. torque (rotor locked).

[4] Although this potential was based on thermal tests conducted on the motor in November 2004, the likelihood of demagnetization is very low based on before and after back-emf tests.

Table 3.2. Motor torque vs. motor-shaft angle

Motor-Shaft Angle, Degrees	Motor-Shaft Torque, Nm						
	50A	75A,	100A,	125A,	150A	200A	250A
90	-1.9	-0.6	3.5	5.3	3.6	6.0	10.0
92	0.7	2.4	0.7	0.0	-7.6	-9.6	-10.1
94	1.0	-2.8	-8.1	-15.0	-25.7	-37.6	-43.3
96	0.2	-3.0	-9.0	-17.0	-24.7	-35.4	-46.2
98	1.9	-2.3	-5.8	-12.0	-17.3	-26.7	-33.8
100	7.3	6.1	6.1	2.0	-3.5	-11.7	-16.4
102	14.5	11.8	10.4	9.0	7.4	0.0	-1.9
104	19.6	20.8	22.0	24.0	25.8	27.0	31.7
106	25.8	34.0	41.0	53.0	54.8	62.0	78.1
108	34.1	48.3	61.0	72.0	83.6	99.2	114.2
110	45.5	64.0	82.0	96.0	109.9	132.0	158.5
112	48.2	72.4	95.0	116.0	127.8	157.0	181.6
114	55.8	81.9	109.0	135.0	151.0	189.2	222.0
116	63.9	92.6	125.0	151.0	177.4	214.3	255.0
118	73.1	112.5	149.0	182.0	208.1	258.6	302.0
120	74.0	117.7	157.0	193.0	223.0	277.0	324.0
122	70.9	114.1	158.0	199.0	229.0	286.1	337.0
124	59.1	102.1	149.0	191.0	223.0	280.4	332.0
126	50.2	89.0	136.0	192.0	221.0	286.6	339.0
128	47.3	79.0	120.0	162.0	198.2	271.2	331.0
130	38.8	63.5	98.0	133.0	159.6	228.2	287.0
132	19.0	33.0	59.0	82.0	99.7	134.2	175.0
134	3.4	7.1	20.4	30.0	25.3	58.3	87.0

The seven peak-torque values for the different current levels are plotted in Fig. 3.10. These peak values are based on June and August 2005 data, with a preference to August 2005 data in the cases where slight differences exist. This series of tests was effective in characterizing the starting torque capability of the 2004 Prius traction motor.

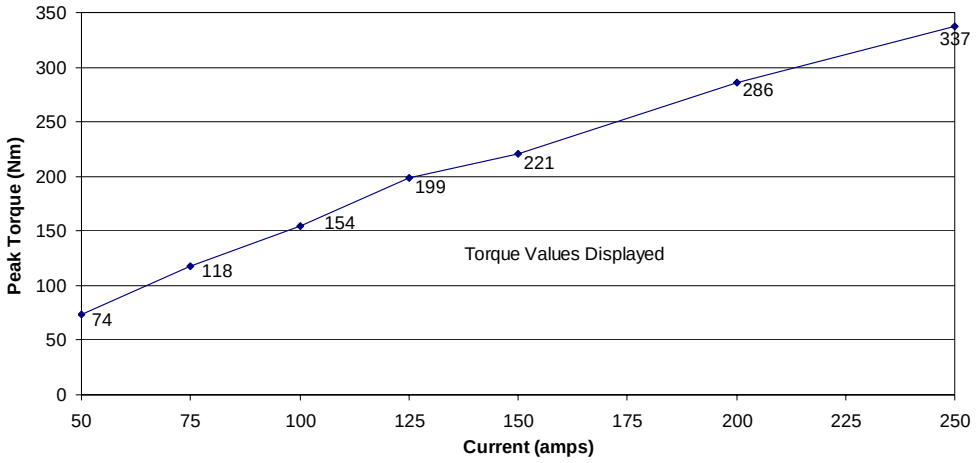

Fig. 3.10. Locked rotor peak torque as a function of current.

3.2.2 Back-emf Tests

The back-emf voltage generated by the motor and the generator was measured using two slightly different hybrid electric drive system configurations. Test conditions and subsystem arrangements for the motor and generator tests are defined in Table 3.3. During the tests, an oscilloscope was used to measure both rms[5] (Vrms) and peak (Vpeak) back-emf voltage values.

Table 3.3. Test conditions for back-emf voltage measurements

Test Condition	Motor Tests	Generator Tests
Shaft speed range, rpm	500–6000	1000–6500
Oil temperature range, °C	25–80	25–80
Motor rotor	Installed	Installed
Oil pump	Installed	Installed
Sun gear	Installed	Installed
Planetary gears	Installed	Installed
Rotating subassemblies:		
• Motor	Functional	Functional
• Generator	Idle	Functional
• Planetary gears	Idle	Functional

3.2.2.1 Motor tests

Measured back-emf voltage values from the motor are shown in Table 3.4 and plotted in Fig. 3.11. The lubricating oil temperature during this motor test was a nominal 25°C. It should be noted that the Vpeak to Vrms ratio is greater than the square root of 2 because of the harmonics content in the back-emf. The results of the back-emf test were verified one year later, just prior to the full design range testing/mapping (Section 3.3), and the agreement between the two data sets was excellent.

Table 3.4. Back-emf voltage measurements for the 2004 Prius motor

Axle Speed, rpm	Motor-Shaft Speed, rpm	Axle Torque, Nm	Electrical Frequency, Hz	Scaled Back-emf (Vrms)	Scaled Back-emf (Vpeak)
122	502	8.0	33.8	42.0	75
243	1000	8.4	66.5	85.7	150
365	1502	9.3	99.8	132.3	225
486	1999	10.2	134.4	181.6	300
608	2501	10.8	168.1	221.8	350
729	2999	11.3	200.2	269.3	425
851	3501	12.0	233.9	315.7	500
972	3999	12.6	265.4	354.6	575
1094	4501	13.1	295.7	405.5	625
1215	4999	13.6	333.0	440.4	700
1337	5500	14.6	366.3	503.4	775
1458	5998	15.6	401.3	539.8	850

Note: Testing was conducted with the differential gears blocked from rotating and oil near room temperature.

[5] Root mean square (rms).

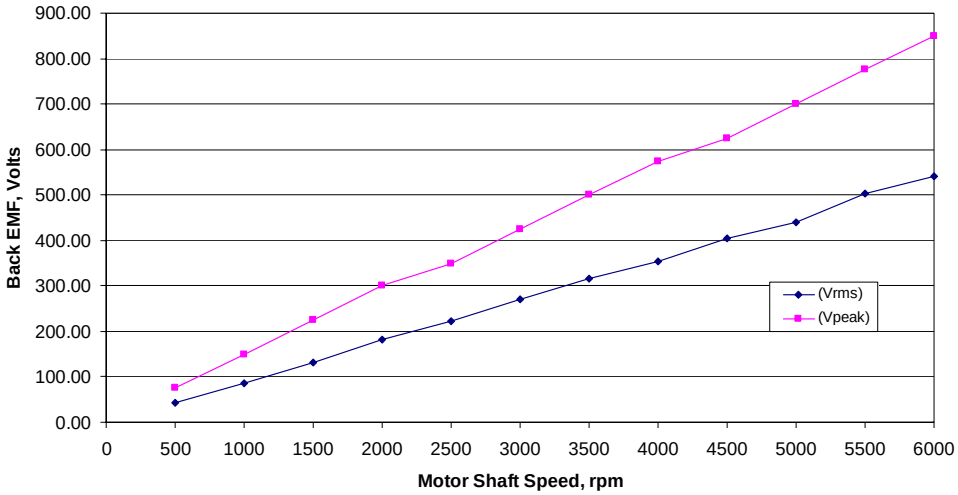

Fig. 3.11. Motor back-emf voltage vs. motor-shaft speed.

3.2.2.2 Generator tests

Measured back-emf voltage values from the generator are shown in Table 3.5 and plotted in Fig. 3.12. The lubricating oil temperature during this generator test was a nominal 80°C.

Table 3.5. Back-emf voltage measurements for the 2004 Prius generator

Axle Speed, rpm	Generator Shaft Speed, rpm	Axle Torque, Nm	Frequency, Hz	Scaled Back-emf (Vrms)	Scaled Back-emf (Vpeak)
100	1070	8.2	70.0	31.6	52.5
150	1605	9.4	109.4	49.4	80.0
200	2140	9.6	141.3	67.0	110.0
250	2675	9.0	180.6	83.5	135.0
300	3210	9.1	213.3	96.5	160.0
350	3745	9.5	247.9	113.5	190.0
400	4280	10.2	287.0	134.5	210.0
450	4815	10.8	320.6	144.5	240.0
500	5350	11.3	357.9	167.0	260.0
550	5885	11.6	392.2	182.0	290.0
600	6420	12.2	430.5	195.0	320.0

Note: Testing was conducted with the differential gears blocked from rotating and a nominal oil temperature of 80°C.

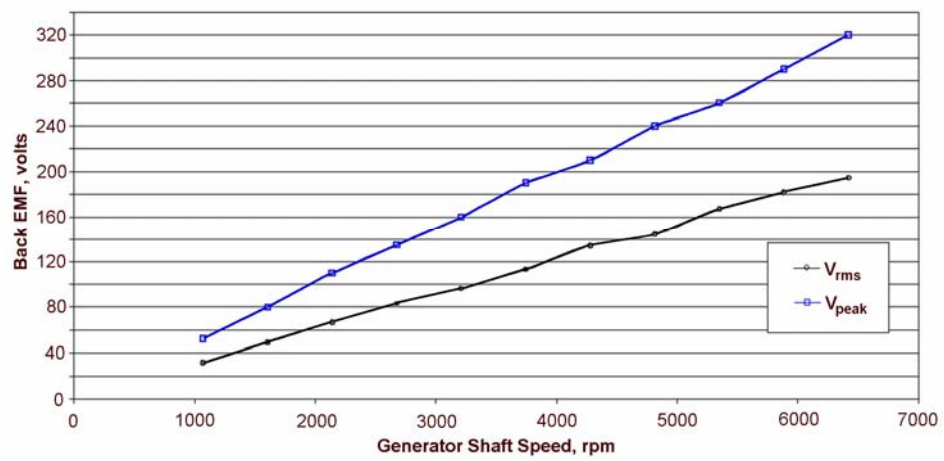

Fig. 3.12. Generator back-emf voltage vs. generator shaft speed.

In order to mechanically link the generator into the system, the engine shaft was not allowed to rotate during the tests (i.e., the planetary carrier was fixed from rotating). Using this arrangement allowed the generator to either drive or be driven by the hybrid drive gear train. The location of the planetary carrier relative to the other hybrid electric drive system components is shown in Fig. 2.4 (see Section 2).

3.2.3 Hybrid Drive System Loss Tests

Three types of power losses that affect the overall efficiency of the hybrid electric drive system were studied. These losses, which are reported in watts (W), include: (1) gear losses; (2) motor-rotor losses; and (3) planetary gears, sun gear, and generator-rotor losses. Determining the magnitude of each of these types of losses was achieved by separately testing three hybrid drive system configurations at different motor-shaft speeds and lubricating oil temperatures. Subassemblies installed as part of each configuration are identified in Table 3.6.

Table 3.6. Subassembly configurations for loss determinations

Subassembly	Configuration A	Configuration B	Configuration C
Engine	Not installed	Not installed	Not installed
Motor rotor	Installed	Removed*	Removed
Generator rotor	Installed	Installed	Removed
Sun gear	Installed	Installed	Removed
Planetary gears	Installed	Installed	Removed
Main drive gears, drive chain, and differential	Installed	Installed	Installed

*A substitute rotor that provides no loading was installed in place of the motor rotor in order to provide the necessary mechanical support for the adjacent gearbox and planetary components.

Overall power loss for the entire hybrid drive system was determined by testing the components and subassemblies included in Configuration A. Losses associated with the motor rotor were determined by testing the components and subassemblies included in Configuration B. These tests were conducted with the motor rotor removed and a simulated rotor[6] installed in its place. For Configuration C, additional

[6] The simulated rotor, consisting of a dummy shaft and bearings, was intended to keep the other components in their normal positions.

components including the generator rotor, sun gear, and planetary gears were removed leaving only the main drive gears, drive chain, and differential. Under these test conditions, it was possible to determine the gear losses. This testing approach also made it possible to determine losses associated with the planetary gears, generator rotor, and sun gear by subtracting the motor-rotor losses and the gear losses from the losses for the entire hybrid electric drive system. Loss values determined with the lubricating oil near room temperature are shown in Table 3.7 and plotted in Fig. 3.13. This data was compiled based on tests of all three configurations.

Table 3.7. Summary of hybrid drive system losses[1]

Axle Speed, rpm	Motor-Shaft Speed, rpm	Gear Losses, W	Motor-Rotor Losses, W	Planetary Gears, Generator Rotor, and Sun-Gear Losses, W	Hybrid Drive System Losses, W
120	494	74.9	19.8	7.1	102
243	1000	158.5	31.6	23.7	214
366	1506	261.8	60.2	33.2	355
484	1991	369.8	109.0	40.5	519
608	2501	487.9	135.9	63.6	687
731	3007	617.2	161.7	84.2	863
851	3501	745.2	205.3	118.8	1069
972	3999	915.6	242.1	125.5	1283
1095	4505	1058.2	297.4	145.2	1501
1215	4999	1220.8	323.9	186.5	1731
1335	5492	1425.2	404.9	214.3	2044
1460	6006	1645.3	472.8	264.9	2383

[1]Testing was conducted with the differential gears blocked from rotating and oil near room temperature.

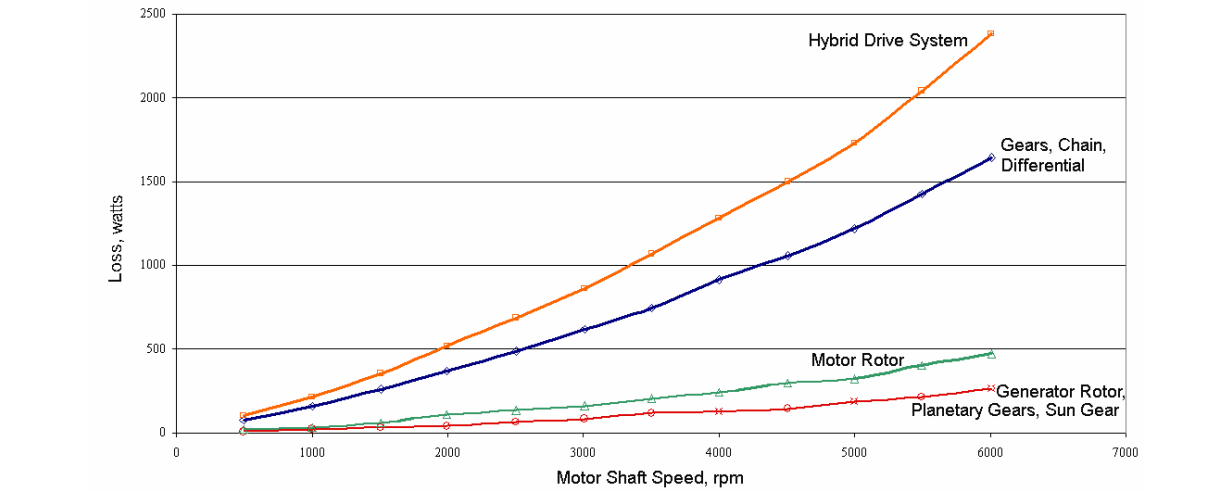

Fig. 3.13. Hybrid electric drive system and component/subassembly losses at 25°C.

Losses that were determined for Configuration B at various elevated lubricating oil temperatures are listed in Tables 3.8–3.13. As Fig. 3.14 indicates, losses tend to decrease as the lubricating oil temperatures increase, presumably due to viscosity changes.

Table 3.8. Configuration B losses at a nominal oil temperature of 28°C

Axle Speed, rpm	Motor-Shaft Speed, rpm	Axle Torque, Nm	Losses, W	Oil Temperature, °C
122	502	5.8	72.8	27.0
243	1000	6.7	170.4	27.0
365	1502	7.6	291.1	27.0
486	1999	7.9	400.2	28.0
608	2501	8.4	534.6	28.5
729	2999	8.9	681.0	29.0
851	3501	9.4	837.3	29.0
972	3999	9.8	997.0	29.5
1094	4501	10.3	1180.5	30.0
1215	4999	10.7	1360.7	30.5
1337	5500	11.2	1565.0	31.5
1458	6006	12.1	1849.0	32.0

Table 3.9. Configuration B losses at a nominal oil temperature of 40°C

Axle Speed, rpm	Motor-Shaft Speed, rpm	Axle Torque, Nm	Losses, W	Oil Temperature, °C
122	502	5.3	66.6	40.5
243	1000	6.0	152.6	40.5
365	1502	6.7	256.7	40.5
486	1999	7.2	364.7	41.0
608	2501	7.7	490.0	41.0
729	2999	8.2	627.4	41.5
851	3501	8.5	757.1	42.0
972	3999	9.1	925.8	42.5
1094	4501	9.5	1088.8	43.0
1215	4999	10.2	1297.1	44.0
1337	5500	10.6	1481.1	44.5
1458	6006	11.3	1726.8	45.0

Table 3.10. Configuration B losses at a nominal oil temperature of 50°C

Axle Speed, rpm	Motor-Shaft Speed, rpm	Axle Torque, Nm	Losses, W	Oil Temperature, °C
122	502	5.2	65.3	50.0
243	1000	6.0	152.6	50.5
365	1502	6.5	249.0	51.0
486	1999	7.0	354.6	51.5
608	2501	7.4	470.9	51.0
729	2999	7.9	604.4	51.5
851	3501	8.3	739.3	52.0
972	3999	8.6	874.9	52.0
1094	4501	9.1	1043.0	52.5
1215	4999	9.7	1233.5	53.0
1337	5500	10.2	1425.2	53.5
1458	6006	10.7	1635.1	54.5

Table 3.11. Configuration B losses at a nominal oil temperature of 60°C

Axle Speed, rpm	Motor-Shaft Speed, rpm	Axle Torque, Nm	Losses, W	Oil Temperature, °C
122	502	5.0	62.8	59.5
243	1000	5.5	139.9	59.5
365	1502	6.2	237.5	60.0
486	1999	6.8	344.5	60.0
608	2501	7.2	458.2	60.0
729	2999	7.9	604.4	60.0
851	3501	8.3	739.3	60.0
972	3999	8.6	874.9	60.0
1094	4501	8.9	1020.0	60.5
1215	4999	9.4	1195.4	61.0
1337	5500	10.0	1397.3	61.5
1458	6006	10.6	1619.8	62.0

Table 3.12. Configuration B losses at a nominal oil temperature of 70°C

Axle Speed, rpm	Motor-Shaft Speed, rpm	Axle Torque, Nm	Losses, W	Oil Temperature, °C
122	502	4.7	59.0	70.0
243	1000	5.5	139.9	70.0
365	1502	6.2	237.5	70.0
486	1999	6.8	344.5	70.0
608	2501	7.1	451.8	70.0
729	2999	7.7	589.1	69.5
851	3501	8.2	730.4	69.5
972	3999	8.3	844.4	69.5
1094	4501	8.8	1008.6	70.0
1215	4999	9.1	1157.2	70.5
1337	5500	9.6	1341.4	71.0
1458	6006	10.1	1543.4	71.5

Table 3.13. Configuration B losses at a nominal oil temperature of 80°C

Axle Speed, rpm	Motor-Shaft Speed, rpm	Axle Torque, Nm	Losses, W	Oil Temperature, °C
122	502	4.0	50.2	82.5
243	1000	4.4	111.9	82.0
365	1502	5.5	210.7	80.5
486	1999	6.1	309.0	80.5
608	2501	6.6	420.0	80.5
729	2999	7.2	550.9	81.0
851	3501	7.8	694.8	81.0
972	3999	8.2	834.2	81.0
1094	4501	8.5	974.2	81.0
1215	4999	8.8	1119.1	81.5
1337	5500	9.2	1285.5	82.0
1458	6006	9.7	1482.3	82.0

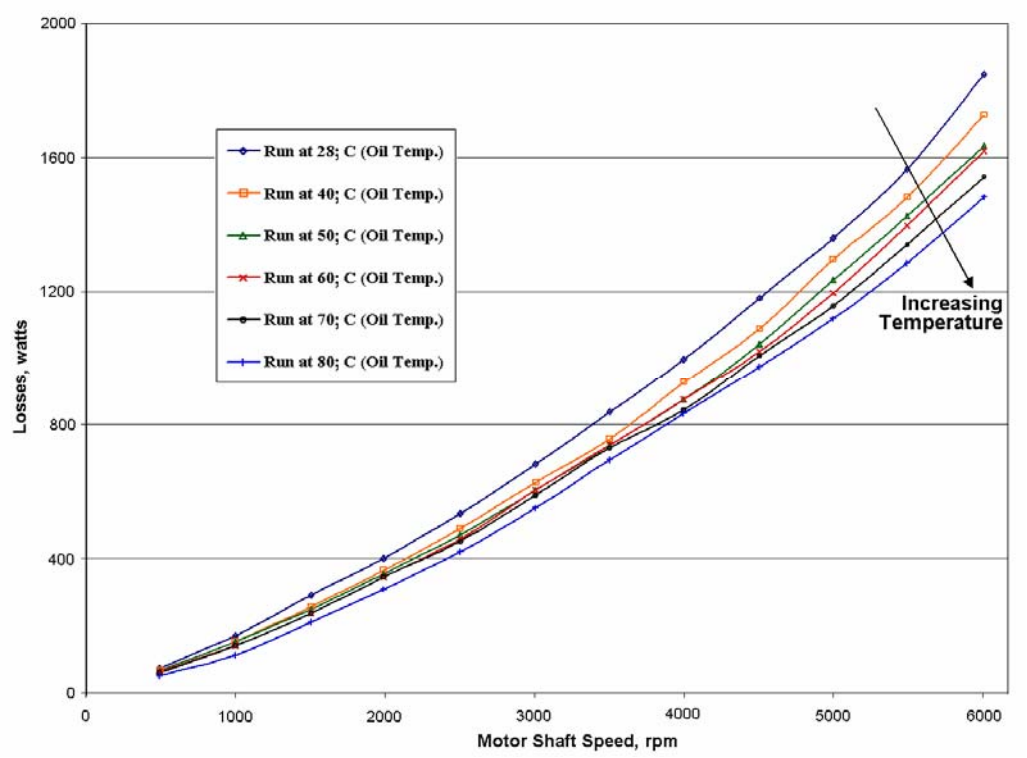

Fig. 3.14. Configuration B losses as a function of oil temperature.

3.3 HEV SYSTEM TESTING OVER THE FULL DESIGN RANGE

From the time that the benchmarking project began, one of the primary goals was to operate the Prius HEV system in a test cell and collect operating and performance data over the full speed range and over the full shaft-loading range. This presented considerable challenges as discussed in Section 1.4.

The following summarizes the major technical efforts during 2004 and 2005 leading up to HEV system testing:

- Instrumenting the inverter and motor hardware,
- Planning and preparing a controller algorithm to maximize torque and provide field weakening,
- Resolving persistent electromagnetic interference (EMI) problems in the feedback control loop,
- Setting gains in proportional integral (PI) controllers partly by trial and error,
- Using a motor model for testing/verifying the controller algorithm,
- Preparing a DAS, and
- Calibrating all essential equipment and verified sensors.

The intention of the full-design-range Prius testing is to characterize the performance of the Prius PMSM, inverter, and buck/boost-converter[7] subsystems. This will not necessarily reflect the operation of these items in the Prius vehicle where the ECU algorithm dictates operation, but rather it will reflect the full capabilities of these Prius subsystems when operated to maximize torque and/or efficiency over the full speed range. Thus, this report provides HEV subsystem design information, packaging information, and data that fully define the performance potential of the as-described hardware.

[7] Tested separately at lower power levels after testing the other two subsystems.

3.3.1 Test Configuration

A simplified depiction of the test configuration for Prius performance characterization tests is illustrated in Fig. 3.15. The left-hand portion of the figure shows computer systems for (1) controlling the operation of the Prius HEV system, (2) real-time monitoring of thermal and electrical parameters, and (3) data acquisition/storage. The figure shows that the Yokogawa PZ 4000 power analyzer and the Keithley 2700 DAS collect all electrical, thermal, and mechanical parameters. A closed-loop coolant system is used to regulate the temperature and flow rate of the coolant sent to the inverter and PMSM.

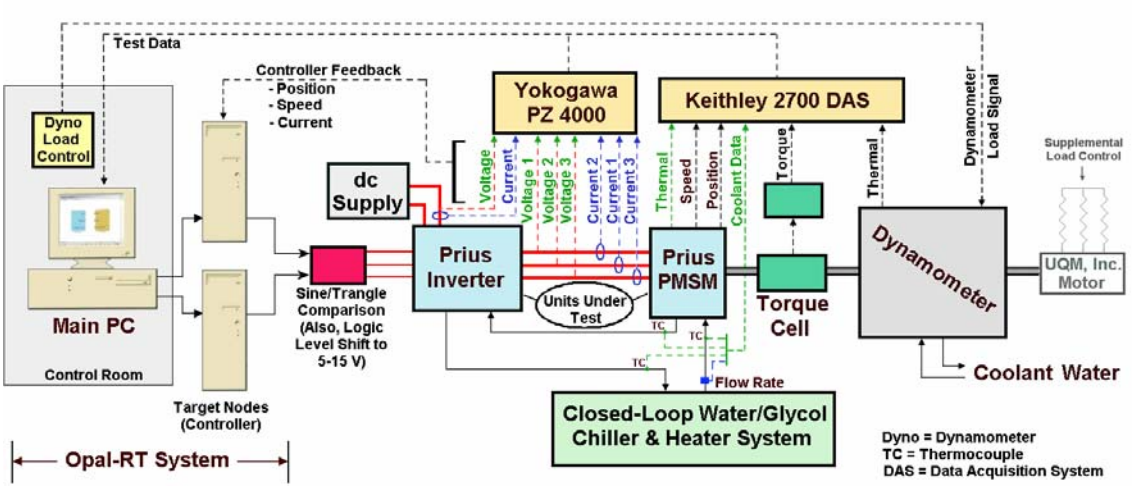

Fig. 3.15. The test configuration for Prius performance characterization tests.

The motor was modified for this test so that the rotor is directly coupled to the shaft; thus, the dynamometer rotational speed matches that of the PMSM rotor. This eliminates issues relating to gear losses. Figure 3.16 shows the subassemblies and test-related hardware in the laboratory just prior to the final sequence of tests. At the end of testing, the Solectria motor was replaced by a synchronous motor from UQM, Inc. to provide supplemental loading at load speeds.

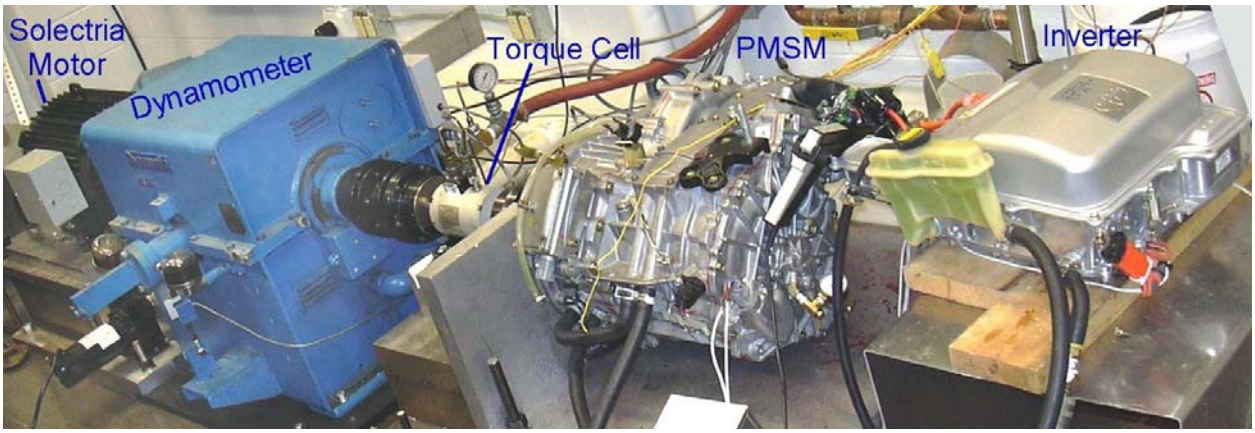

Fig. 3.16. The test hardware for Prius performance characterization tests.

3.3.2 General Test Plan and Data Verification

This section provides (1) details relative to the test plan for the motor/inverter performance tests, (2) data sampling details, and (3) an investigation into higher-than-expected inverter efficiency data.

General Test Plan

The test data were obtained from an array of sensors and from a power analyzer. A Himmelstein torque cell was installed between the dynamometer and the PMSM. The Himmelstein torque cell provided the shaft loading. External equipment was also available for providing cooling and coolant temperature measurements. Motor power measurements were obtained using a Yokogawa PZ4000.

Sensors in the inverter, PMSM, and dynamometer test fixture provided the following electrical and thermal data:

dc voltage to inverter	voltage taps
dc current to inverter	one current transformer (CT)
PMSM input current	two CTs, rms processor circuit
PMSM input voltage	two voltage taps, rms processor circuit
Shaft speed, unprocessed	existing Prius sensor (resolver)
Position, unprocessed	existing Prius absolute position sensor (resolver)
Position and speed	Tawagama encoder (Section 4.3.3)
Torque	Himmelstein dynamometer torque cell
Inverter-heat sink	two thermocouples (TCs), motor bridge A and B
PMSM coolant in/out	two TCs
PMSM stator windings	three TCs
PMSM cooling oil	one TC, bottom of casing (internal)
Motor casing	one TC, top of casing (internal)
Dynamometer coolant in/out	two TCs
Coolant-flow rate	one flow meter

The plan for collecting test data was roughly bounded by published data [7] from Toyota indicating what the speed and load ranges were for the 2004 Prius motor. These data were adapted and plotted in Fig. 3.17.

The testing was generally limited by the top rated speed of the Prius motor (i.e. 6000 rpm) and peak-power ratings, which are reported by the manufacturer to be 30kW continuous[8] and 50 kW (68 hp) from 1200–5000 rpm for 20 s. The test data that was obtained does not necessarily agree with these specifications. The peak-torque ratings of the motor are 400 Nm (295 lb.-ft) from 1–1200 rpm consistent with power rating time limitations.

[8] In earlier thermal testing at ORNL [1], the continuous motor ratings were determined to be 15 kW using 105°C coolant and 21 kW using 35°C coolant. Therefore, much of the performance testing was time-restricted.

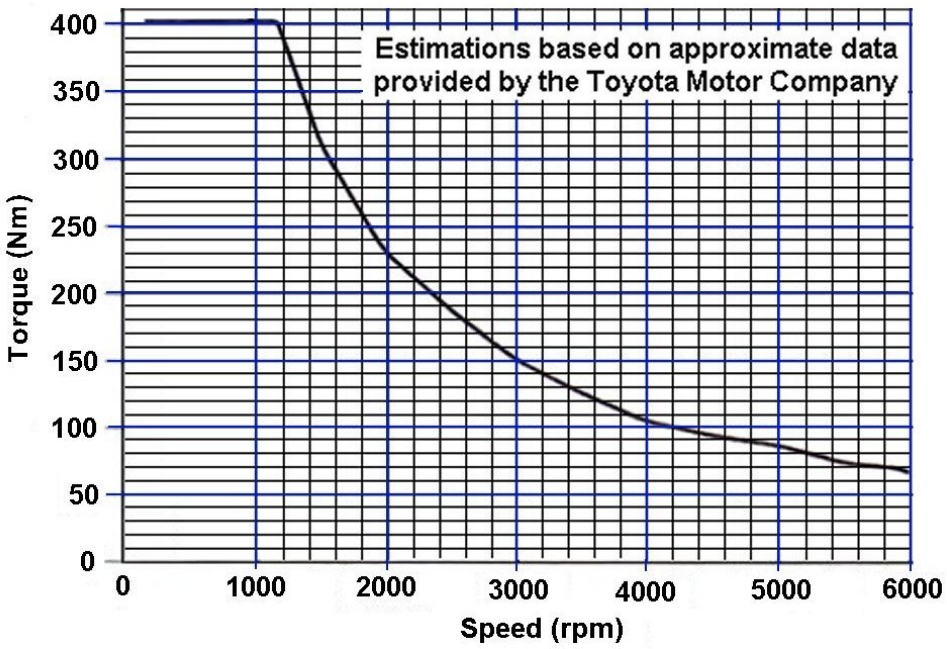

Fig. 3.17. Maximum torque-speed performance specifications for the 2004 Prius.

Other important specifications include those listed in Table 3.14.

Table 3.14. Cooling and coolant temperature and flow limits

Parameter	Limit	Basis
Maximum temperature of cooling oil (°C)	~160–170	To support effective winding cooling
Maximum temperature of stator winding (°C)	200	Elevated limit – see text below
Normal temperature of coolant (°C)	65	[Ref. 7]
Typical, measured coolant temperature (°C)	55	Average of ANL vehicle test data[9]
Published minimum flow rate of coolant (L/min)	10	[Ref. 7]
Actual flow rate of coolant (L/min)	10.6	Measured using Prius pump/piping

In the Prius vehicle, the stator-thermal protection is set at 174°C, which indicates that Toyota is protecting the winding as if it is a Class H motor winding. Class H allows operation at up to 180°C for an average life of 20,000 hrs. Literature shows that Class H can be operated at just above 200°C and still have a 5000 hr life (Apogee Interactive, Inc.: http://elpaso.apogee.net/md/mfnrins.asp). Thus, operating up to 200°C for **<10 hrs**, as for this test, would be inconsequential as far as the stator life is concerned. Also, transmission cooling oil with a high flash point (246°C) was substituted for the Toyota spec oil and placed in the motor casing.

HEVs use intermittent-duty motors. The Prius motor must deliver torques in the 300–400 Nm range for only seconds at a time during hard accelerations. The motor is not thermally designed for anything more. However, this performance-mapping test requires operating in the very high torque range for up to a minute or more to set field weakening and collect redundant sets of data. This is why is was necessary to

[9] The ANL Prius vehicle test data show that 50°C was not exceeded in a mild urban drive cycle, while 60°C was not exceeded in the most demanding drive cycle that the vehicle could track (Pittsburgh cycle). Thus, 55°C is selected for the coolant temperature.

(1) allow stator temperatures to go very high, (2) set the coolant-flow rate higher than in the Prius vehicle, and (3) use very cold coolant temperatures for a portion of the testing.

For performance testing, coolant flow was supplied to the Prius inverter/PMSM system with an inlet temperature of 55°C with a flow rate of ~7 L/min. Obtaining certain low-speed, high-torque data well into the intermittent-duty portion of the operating window required lowering the coolant temperature substantially to 0°C and increasing the flow rate to 7–10 L/min. A fan was aimed at the motor casing for the entire test for limited convection cooling as typically occurs during vehicle operation. The current for the inverter was controlled based on controller algorithms developed specifically for Prius operation and/or operator control settings.

The testing entailed varying speed and then load through several levels in an iterative fashion. At low speeds, data was collected in 100–200 rpm increments; at high speeds, where efficiency changes more gradually, data was collected in 400–500 rpm increments. At each speed, the torque was increased through a series of levels as data is collected. Data was recorded at every 10 Nm for loading up to ~120% torque if temperature limits were not exceeded. At each speed/torque condition, direct-axis current (i_d) was varied through several values to find the minimum necessary level, which is known to correspond to the highest motor efficiency.

Each test condition (i.e., torque at a given speed) was maintained for at least 30 seconds unless temperature limits are about to be exceeded, in which case a note was made to that effect. At each test condition, 10 or more data points were recorded for use in averaging in order to eliminate the effects of data scatter. Inverter current and voltage waveforms were recorded with the motor operating at 1200 rpm and 2500 rpm with a maximum rated torque load.

Data Sampling

Regardless of speed and therefore electrical frequency, a sample length was used that contains at least five fundamental cycles for each test speed. This ensures that information is not omitted and that power measurements are consistent. To provide additional consistency, the power analyzer was set to trigger on one of the ac phase currents. Since the sample rate varies with the sample length and thus with test speed, a specific sample length was not used throughout the tests, but can be approximated to be 2.5 mega samples per second.

The data acquisition program sampled data from multiple measurement instruments every 4–5 seconds. For each speed and torque, at least five samples were taken and each sample was stored in a row of a spreadsheet. Therefore, after moving to a different operating point, steady-state conditions were first verified and then the row numbers corresponding to the correct data were logged. Furthermore, the data for each operation point was averaged and the efficiency maps provided below were generated using the averaged data.

High Inverter Efficiency Investigation

During testing, inverter data at certain speed and load combinations showed efficiencies that were as high as 99.0%, which is just beyond the expected range. Because only precision, calibrated instrumentation and sensors were used, it was believed that inaccuracies (if indeed any existed) could only be caused by the noise/EMI observed in the inverter-output current signals. Several solutions and/or special tests were identified.

Researchers investigated all but Item 3 of the following potential solutions to the high efficiency issue:

1. Take additional data using internal-current shunts to compare with suspect data,
2. Locate the power analyzer and CT power supply closer to the motor and inverter using shorter cables,
3. Make use of the CTs that Toyota has built into the inverter (higher signal-to-noise ratio but accuracy must be checked carefully),
4. Look for the root cause of the high EMI, and
5. Investigate the observed fact that when we remove the voltage signal coming from the 500 Vdc supply to one of the Yokogawa power analyzer inputs, the noise from the three-phase CTs drops down somewhat. (This signal coupling effect was subsequently reduced by reconfiguring equipment/signal lines and adding additional grounds/shields.)

The most significant outcome of the above investigation resulted when several special tests were run in February 2004 to verify/validate the performance-mapping data recorded in the prior month.

The special tests included the following:

1. Testing Using Shunts – Subsystem testing was performed at low current using *internal* Yokogawa shunts, which is the most precise power measurement configuration possible. The three-phase inverter-to-motor lines were routed through the power analyzer for this testing. The results matched earlier test data using CTs on the three-phase lines.
2. Use of Filtering – Data was obtained with and without digital filters on the three-phase voltage and current with no significant difference in power and efficiency measurements.
3. Use of Pseudo Neutrals – Data was obtained using external pseudo neutrals on the three-phase lines and then using the impedance of the power analyzer for the pseudo neutral. There was no significant difference in power and efficiency measurements.
4. Line/Channel Isolation – Inverter input/output (I/O) lines were connected/disconnected to the power analyzer in all combinations to verify isolation of channels. In this way, inverter I/O electrical data were fed to the power analyzer sequentially. Again, no significant difference in power and efficiency could be seen.

The above testing greatly increased the confidence that ORNL researchers had in the performance-mapping tests and led to the conclusion that there were indeed certain speed/load combinations in which the inverter performed with very high efficiency. The inverter efficiencies are expected to be high for these operating conditions since the pulse-width modulation (PWM) control signal is over-modulated to create the maximum voltage available from the power supply. This means that the inverter is switching less often per fundamental cycle and therefore switching losses are very low.

3.3.3 Motor/Inverter Test Data and Efficiency Maps

This section provides Prius subsystem performance-mapping data including efficiency contour mapping plots. The most challenging data to obtain were those at high load levels since the Prius motor is an intermittent design and high thermal excursions in the stator were frequent. Overheating was not a problem in the inverter integrated power electronics module (IPEM). For full loading at speeds below 1300 rpm, it was necessary to use an auxiliary-synchronous motor to supplement the loading from the eddy-current dynamometer. Those changes that were necessary in the cooling of the Prius motor (see Section 3.3.1) were deemed unlikely to have any significant effect on the electrical data obtained from the inverter and Prius motor.

The motor efficiency contour map, ranging from 300–6000 rpm, is presented in Fig. 3.18. It shows efficiencies peaking at 93–94% in the 1750–3000 rpm range at moderate torque levels (50–150 Nm). The lowest efficiencies are evident at several fringe regions of the contour, especially at low-speed, high-

torque conditions. Since one of the primary applications of the motor is to accelerate the vehicle from a stop, the low-speed and/or high-torque regions are quite significant.

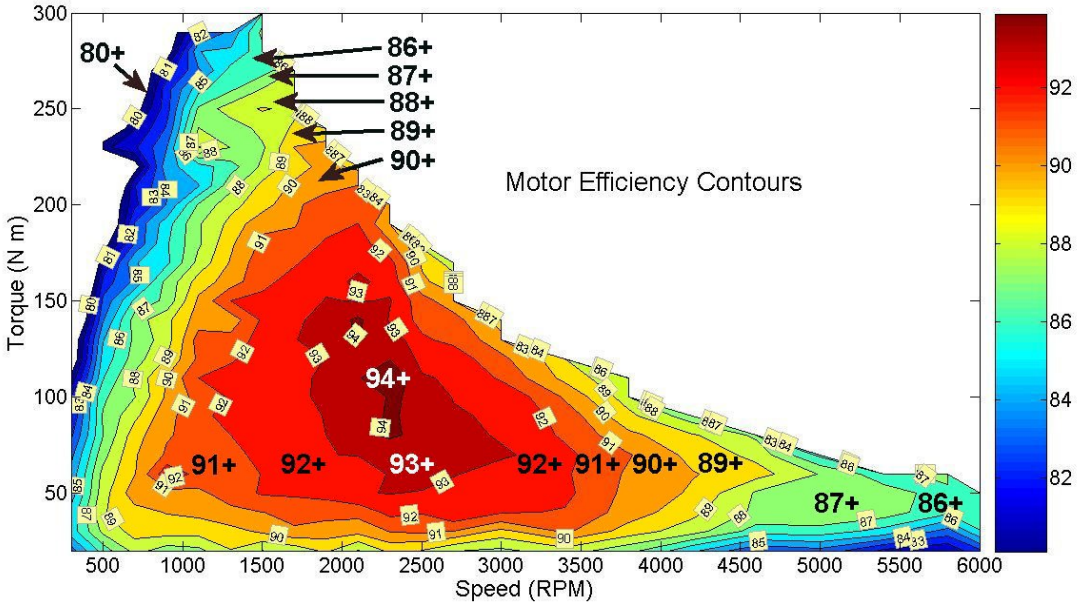

Fig. 3.18. 2004 Prius motor efficiency contour map.

The inverter efficiency contour map, ranging from 300–6000 rpm, is presented in Fig. 3.19. It shows a large area of high 98–99% efficiencies above ~1800 rpm. Although colored regions generally denote a spanned efficiency range of 1%, the regions denoted as "99" had 99.0% efficiency in 23 torque-speed settings, 99.1% efficiency in 13 torque-speed settings, 99.2% efficiency in 6 torque-speed settings, and >99.2% efficiency in 1 torque-speed setting. The higher-than-expected efficiencies led to data verification tests (Section 3.3.2). At lower motor speeds, inverter efficiency drops down gradually to 92% and even lower in small regions of the contour. Clearly, motor torque levels generally have little effect on inverter efficiency.

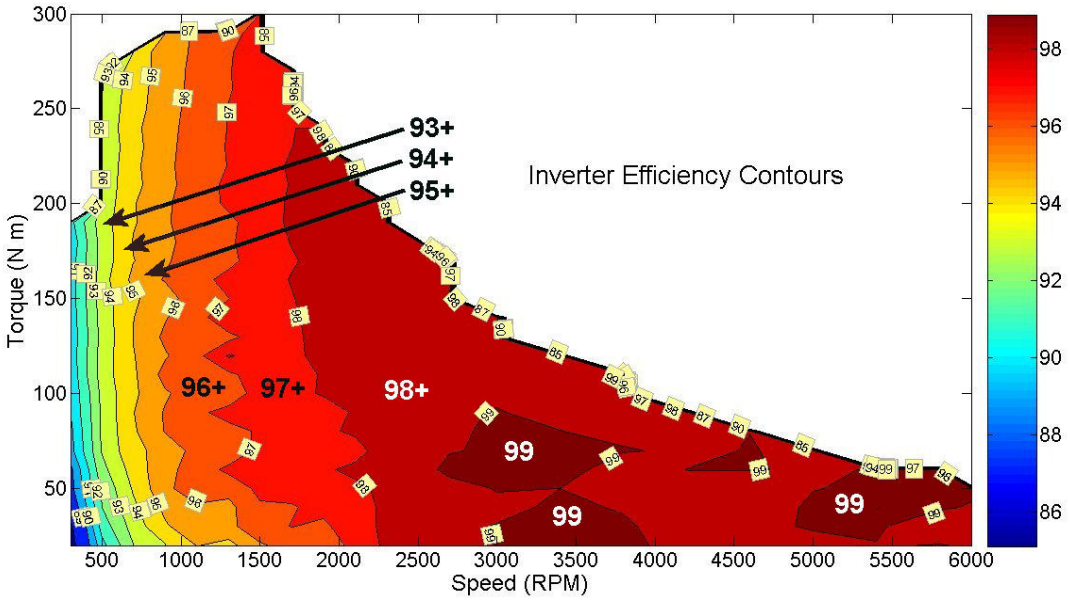

Fig. 3.19. 2004 Prius inverter efficiency contour map.

The combined motor/inverter efficiency contour map ranging from 400–6000 rpm is shown in Fig. 3.20. Motor/inverter efficiency is in the 92–93% range from ~2200–3000 rpm (depending on load) over a range of moderate torque levels (60–140 Nm). The most significant region of relatively low efficiencies is at speeds below 1500 rpm, especially at higher load levels.

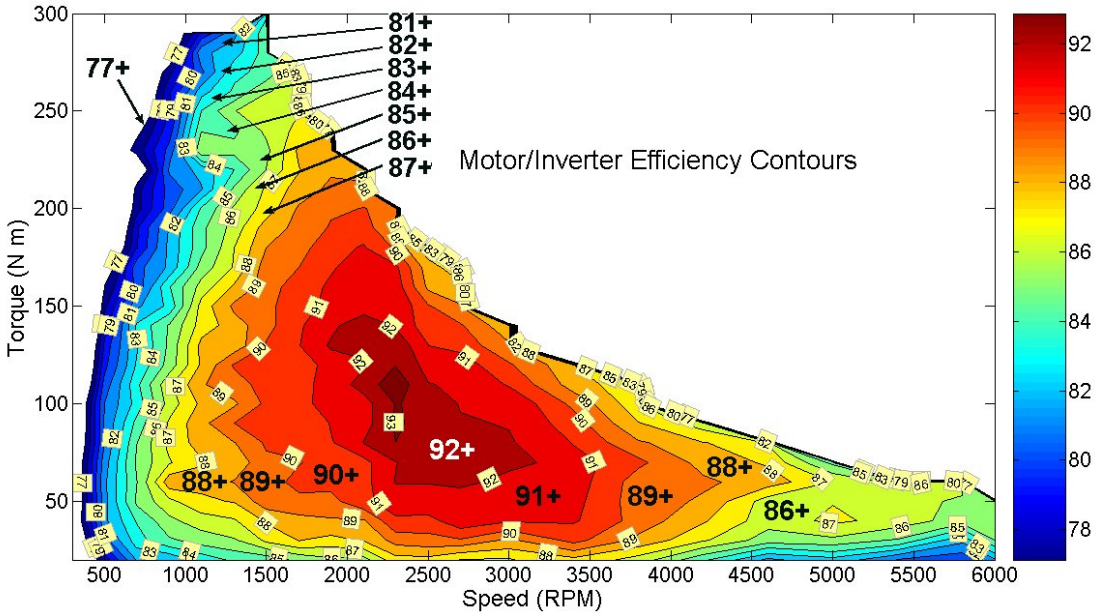

Fig. 3.20. 2004 Prius combined motor/inverter efficiency contour map.

A summary set of mechanical, operational, electrical, and thermal data obtained from the Prius subsystem performance-mapping test is provided in the table found in Appendix B. In support of FCVT objectives, the full set of test data has been made available to technical partners as needed. Data on the performance of the buck/boost converter is provided in the next section.

3.3.4 Buck/Boost-Converter Test Data and Efficiency Maps

This section contains boost-converter information based on converter, inverter, and motor system testing in the ORNL test cell which immediately followed the testing described in Section 3.3.3. This testing was constrained by the power rating of the converter, which is less than half the peak-power rating of the motor. The testing of the boost converter was performed at minimum-, mid-, and maximum-output voltages. The voltage-buck performance of the converter was not tested.

The input voltage to the boost converter was set at 233 Vdc throughout the test. This voltage was based on ANL's drive-cycle data that showed the converter's dc input fairly steady at ~230V. Although the Prius battery voltage is 201.6 Vdc, the generator is apparently responsible for an elevated voltage during vehicle operation. The Vdc output of the converter was set at 240, 365, and 500, and these output settings comprised the three parts of the test.

The converter tests were carried out under the following conditions:

- Motor speed: 1500 rpm
- Motor shaft torque: 0–130 Nm in increments of 10 Nm
- Motor shaft mechanical Power: 0–20.4 kW
- Boost converter output power range: 0–25 kW
- Motor, converter, and inverter coolant temp: 55°C
- Coolant flow rate: 7 Liters/minute

Figure 3.21 shows the boost-converter efficiency versus output power for all three output voltages and Fig. 3.22 shows efficiency versus output current. Polynomial curve fitting is used where oscillations are evident in the data. The most apparent conclusion is that the efficiency drops as the output voltage of the boost converter increases. Additionally, for all output voltages the efficiency is lowest for high power/current conditions and, to a somewhat lesser extent, when power/current is very low. The efficiency is at the minimum, 96.7%, when the maximum boost and power is required.

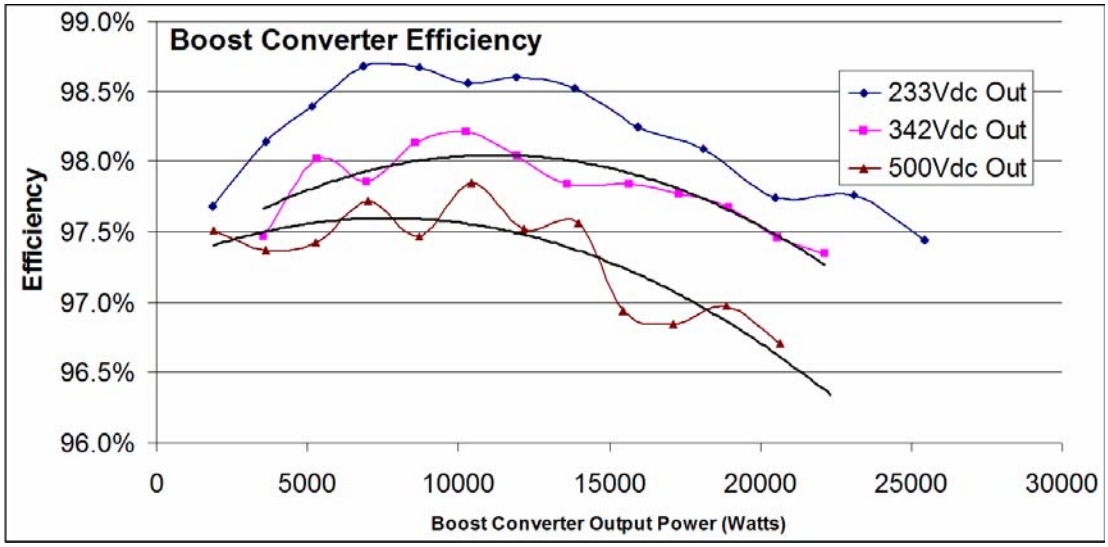

Fig. 3.21. Boost-converter efficiency vs. output power.

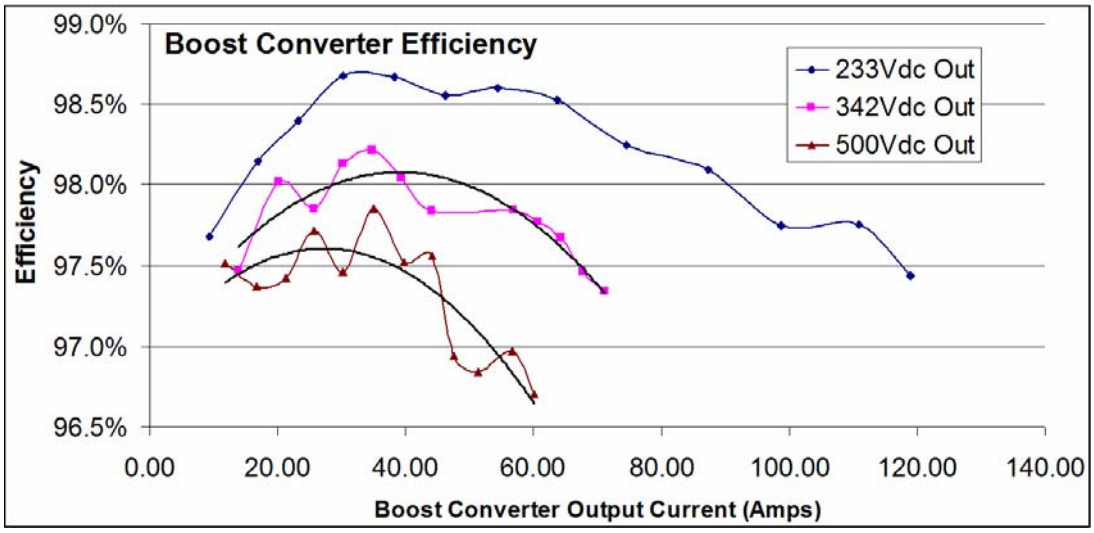

Fig. 3.22. Boost-converter efficiency vs. output current.

The motor load, efficiency, and electrical data obtained from the converter test are tabulated in Table 3.15. The data is presented in three sections (denoted by heavy lines) to show results using the three different voltage output settings of the converter.

Table 3.15. Boost-converter test data including efficiency, motor load, and electrical parameters

	Efficiency (%)			Power (W)			Input rms		Output rms	
Torque	Converter	Inverter-Motor	Total	In	Out	Mech.	Vdc	Idc	Vdc	Idc
10.00	**97.7**	85.2	83.2	1888	1844	1571	232	8.6	236	9.3
20.00	**98.1**	86.8	85.1	3690	3621	3142	232	16.2	235	16.9
30.00	**98.4**	91.7	90.2	5222	5138	4712	232	22.8	235	23.2
40.00	**98.7**	91.6	90.4	6951	6860	6283	232	30.2	235	30.2
50.00	**98.7**	90.3	89.1	8813	8695	7854	232	38.6	234	38.2
60.00	**98.6**	91.5	90.2	10446	10295	9425	232	45.3	234	46.2
70.00	**98.6**	92.1	90.8	12104	11934	10996	232	52.5	234	54.5
80.00	**98.5**	90.8	89.5	14046	13838	12566	232	60.9	233	63.7
90.00	**98.2**	88.6	87.1	16240	15955	14137	232	70.5	233	74.6
100.00	**98.1**	86.7	85.0	18470	18118	15708	231	80.4	232	87.2
110.00	**97.7**	84.3	82.4	20965	20492	17279	231	91.1	232	98.7
120.00	**97.8**	81.5	79.7	23650	23119	18850	231	102.6	231	110.9
130.00	**97.4**	80.2	78.2	26118	25449	20420	231	113.3	231	118.9
10.00	**98.1**	80.8	79.3	1982	1944	1571	231	8.7	358	7.5
20.00	**97.5**	88.6	86.4	3636	3544	3142	231	16.4	345	13.9
30.00	**98.0**	88.7	87.0	5418	5311	4712	231	24.0	345	20.2
40.00	**97.9**	90.2	88.3	7119	6966	6283	231	31.5	344	25.7
50.00	**98.1**	91.4	89.7	8753	8589	7854	231	38.6	344	30.2
60.00	**98.2**	91.8	90.2	10454	10267	9425	231	46.1	343	34.8
70.00	**98.0**	92.0	90.2	12186	11946	10996	231	53.3	343	39.4
80.00	**97.8**	92.4	90.4	13903	13602	12566	231	60.8	342	44.1
90.00	**97.8**	90.2	88.2	16022	15676	14137	231	70.2	341	57.0
100.00	**97.8**	90.7	88.7	17710	17314	15708	231	77.6	341	60.6
110.00	**97.7**	91.2	89.0	19407	18956	17279	230	85.2	340	64.2
120.00	**97.5**	91.6	89.2	21120	20583	18850	230	92.5	339	67.8
130.00	**97.3**	92.2	89.8	22751	22146	20420	230	99.5	339	71.1

Table 3.15. Boost-converter test data including efficiency, motor load, and electrical parameters (cont'd)

	Efficiency (%)			Power (W)			Input rms		Output rms	
Torque	Converter	Inverter-Motor	Total	In	Out	Mech.	Vdc	Idc	Vdc	Idc
10.00	**95.5**	82.3	78.5	2000	1910	1571	231	9.6	495	6.3
20.00	**97.5**	86.6	84.5	3719	3627	3142	231	16.7	468	11.8
30.00	**97.4**	89.1	86.8	5429	5286	4712	231	24.6	463	16.7
40.00	**97.4**	89.6	87.3	7199	7012	6283	231	32.5	462	21.4
50.00	**97.7**	90.4	88.4	8889	8685	7854	231	40.0	461	25.7
60.00	**97.5**	90.2	87.9	10721	10449	9425	231	48.1	460	30.3
70.00	**97.8**	90.3	88.4	12440	12172	10996	231	55.4	460	35.0
80.00	**97.5**	90.0	87.8	14314	13958	12566	230	63.3	458	39.8
90.00	**97.6**	91.5	89.2	15845	15458	14137	230	69.6	458	44.1
100.00	**96.9**	91.7	88.9	17670	17129	15708	230	77.6	457	47.6
110.00	**96.8**	91.6	88.7	19482	18866	17279	230	85.5	456	51.3
120.00	**97.0**	91.3	88.5	21302	20656	18850	230	93.5	455	56.6
130.00	**96.7**	91.5	88.5	23083	22322	20420	230	101.3	454	60.2

4. INVERTER, CONTROLLER, AND Z-SOURCE ACTIVITIES

This section begins by briefly assessing the early and upgraded Prius inverter designs based on disassemblies to reveal its architecture and method of cooling. An earlier description of the inverter and its components is provided in Section 2.2.5. This section also describes the modifications performed on the 2004 inverter by ANL to support performance testing at ORNL. Next, the controller development which is essential for operating the HEV system outside the vehicle is summarized. Lastly, the Prius inverter is compared to the new, experimental Z-source inverter design.

4.1 INVERTER ARCHITECTURE OVERVIEW

After careful study of a 2003 and 2004 Prius inverter, differences were noted between the two models. The 2004 inverter/converter package has roughly the same volume as the 2003 unit; however, the 2004 package contains the new buck/boost converter.

The 2004 Prius inverter is cooled using a cold plate located in the center of the package. This cold plate serves as a separator between the generator-motor-boost sections that are located above the cold plate and the air-conditioning compressor inverter and dc-to-dc converter located below the cold plate. The cold plate transfers excess heat from the inverter to the hybrid drive system coolant as it circulates through internal passages in the cold plate. A flow diagram for the hybrid drive system coolant is presented in Fig. 2.3. The power electronic active switching devices for the main inverter sections (motor and generator) are packaged in one IPEM that contains 18 insulated-gate bipolar transistors (IGBTs). The buck/boost-converter power electronics are contained in a separate module from the IPEM.

The main dc-link capacitors in the 2004 Prius are slightly smaller in volume than those in the 2003 Prius and are packaged in a plastic module making them different from the commercially available can-type electrolytic capacitors used in the 2003 model. Most of the integrated circuits in the 2004 Prius are identified with a Toyota label, as compared to those in the 2003 unit that used commercially available electronic components primarily from International Rectifier (IR). However, the circuits appear to be basically unchanged.

4.2 INVERTER MODIFICATIONS

A 2004 Prius inverter was modified at ANL with installation of instrumentation to allow monitoring of the system to provide electrical power and thermal data from the inverter and converter. The inverter was returned to ORNL and used for the PMSM/inverter tests after being modified with conventional sensors that are similar in design and configuration to those installed in the ANL inverter for chassis-dyne testing.[10]

The instrumentation modifications performed on the ORNL inverter by ANL include the installation of:

[10] Additional inverter instrumentation was required to achieve ANL chassis-dyne testing goals and this effort was included as part of the benchmarking project. The additional instrumentation involves developmental sensors and installation techniques including (1) installation of Giant Magneto Resistive (GMR) current sensors directly on the dc bus bars (embedded in the IPEM) to sense current in the feed to the traction motor inverter section, and (2) installation of GMRs on the dc bus bars that feed the generator inverter section.

1. Shunt-style current sensors on dc-link bus bars on both the 200V and 500V sides of the boost converter,
2. Voltage divider sensing points on the 200V and 500V bus bars,
3. A shunt-style current sensor on the 12V auxiliary charging system, and
4. TCs at power electronic devices as described below.

After the modifications were performed, it was realized that the buck/boost converter has only ~40% the peak power rating of the PMSM. This is because the generator provides most of the power to the PMSM, and the HEV battery and converter provide less than half the power. For these reasons, the converter was not used during full-power laboratory testing of the inverter/PMSM system.

TCs were installed between certain power electronics components such as the IGBT modules and the cold plate. Figure 4.1 depicts the placement of TCs on the cold plate in the area on which the IPEM is mounted where two TCs were located under motor inverter IGBTs and two under generator IGBTs.

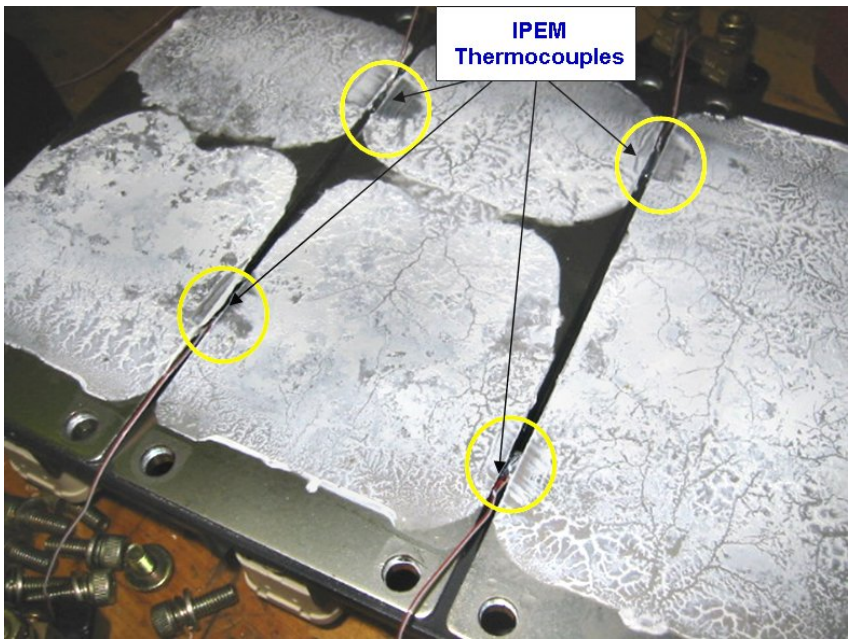

Fig. 4.1. TC placement at IPEM area of cold plate (2004 Prius inverter).

4.3 CONTROLLER DEVELOPMENT

In order to perform subsystem-level tests, the inverter/PMSM system had to be severed from the vehicle control system or ECU. The ECU not only controls essentially all vehicle electrical systems, but it also contains a sophisticated algorithm for the operation of the inverter/PMSM system over the full design range. Therefore, the ECU may certainly be considered as part of the HEV traction-drive system.

This project is designed to test the operation of the inverter/PMSM system to determine their capabilities and performance apart from the ECU-specified operation. If this was not the case, the project could not continue because it is not possible to determine precisely what the ECU algorithm is intended to do. For instance, does the ECU attempt to maximize torque or performance? How do the ECU algorithm goals change with vehicle speed or other operational parameters? How does the ECU's control of PWM change with speed and by what algorithm does the ECU control the voltage boost in the dc converter?

ORNL developers decided to create an entirely new controller that would operate the inverter/PMSM system at maximum torque per current from 1–6000 rpm. This would provide the answer to what the Prius traction system is capable of producing. Since the Prius motor is an interior PM design, developers knew that the model would have to be capable of operating a salient PM motor; the saliency is due to the fact that the reactances for the direct and quadrature axes are not equal, $X_d \neq X_q$. Furthermore, the voltage-boost circuit alone would not enable the system to attain speeds close to 6000 rpm; therefore, a field-weakening scheme would have to be used. Lastly, speed and position feedback signals from the motor would be essential for the new control system.

4.3.1 Establishing the Need for Field Weakening

The Prius inverter/PMSM drive system relies partly on a control system that increases the dc-link voltage such that the field-weakening current, i_d, is zero. Up to a certain speed, this is the most efficient way to operate the motor but there is a speed at which the back-emf voltage is greater than the voltage supplied by the inverter (related to the dc-link voltage).

The 500 Vdc link produces a maximum voltage of 390 V_{LL}(rms) during a six-step inverter-square wave operation based on:

$$V_{LL(RMS)} = \frac{\sqrt{3}}{\sqrt{2}} \frac{4}{\pi} \frac{V_d}{2} = 0.78 V_d$$

Using $V_{LL(RMS)} = 390$, the back-emf test data indicate that the corresponding motor speed is:

$$390 \frac{1}{1.338} = 291.5\ Hz \Rightarrow 4372\ rpm$$

The 1.338 Hz/V_{LL}(rms) relationship is based on ANL and ORNL back-emf test data. Thus, the theoretical maximum speed without field weakening and under no-load conditions is 4372 rpm. This calculation neglects inverter-voltage drop, so the actual upper speed limit for operation without field weakening is lower, likely in the range 3250–3750 rpm (see Fig. 4.2). This speed limit decreases even further as the motor is loaded.

Reluctance torque increases as L_d - L_q is maximized as evident in the second term of the following torque equation:

$$T = P_n \phi_m i_q + P_n (L_d - L_q) i_d i_q$$

If L_q is greater than L_d (which is the case for the Prius based on static measurements: 5 mH and 1.92 mH, respectively), then the contribution from the reluctance torque is positive only if i_d is negative (i.e., the application of field weakening). The quadrature-axis current (i_q) is positive in motoring operation and the number of pole pairs, P_n, is always positive. Therefore, to maximize the torque-per-ampere ratio, i_d must be negative. Thus, Toyota has clearly designed the motor to operate with field weakening.

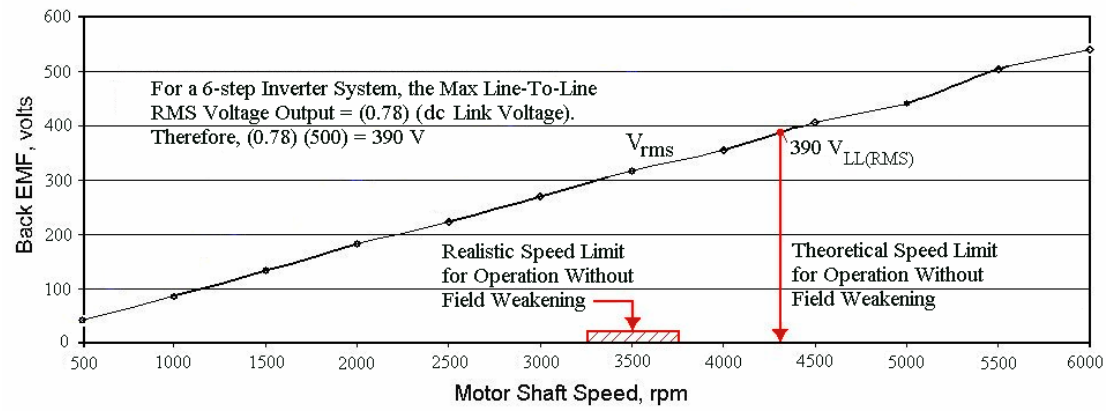

Fig. 4.2. Limitations in operation of PMSM where field weakening is not used.

The total torque, including reluctance torque, was originally measured during locked rotor tests. However, in system testing over the full torque and speed range, the approach take was to "explore" for the right value of i_d (field weakening) to find the optimal efficiency point. Specifically, during the full performance speed-torque mapping tests, torque and speed are maintained constant and the rms current is monitored as the field-weakening current i_d is varied. The value of i_d which maximizes the torque-per-ampere ratio is then defined as an optimal point. Varying i_d not only has a profound effect on the torque, but at high speeds i_d must be supplied or the motor will not operate. In practical terms, it was observed that efficiency was highest when the minimum i_d was applied that permitted stable motor operation.

4.3.2 Controller Software

The algorithm for the controller was divided into three speed regimes, (1) a low-speed regime where operation is limited by current, (2) a mid-speed regime where operation is limited by voltage and current, and (3) a high-speed regime where operation is limited by voltage. In each case, the code was designed to maximize torque per current in a salient, PMSM over a wide speed range with voltage boost set to the 500 volt maximum.

First, a model of a salient PMSM was setup and simulated in Simulink/Opal-RT. This was developed to help in verifying the controller algorithm. The machine model in the in the direct/quadrature coordinate system is given by:

$$L_d \frac{di_d}{dt} = -R_S i_d + n_p \omega L_q i_q + u_d \,, \tag{1}$$

$$L_q \frac{di_q}{dt} = -R_S i_q - n_p \omega L_d i_d - K_m n_p \omega + u_q \,, \text{ and} \tag{2}$$

$$J \frac{d\omega}{dt} = n_p K_m i_q + n_p \left(L_d - L_q\right) i_d i_q - \tau_L \,. \tag{3}$$

Where R_S = stator resistance, n_p = number of pole pairs, ω = rotational speed (rad/s), L = inductance, J = the inertia constant, i = current, u = voltage, K_m = the torque constant in the dq frame, and τ_L = load torque.

The field weakening problem is to maximize the torque, that is

$$n_p K_m i_q + n_p \left(L_d - L_q\right) i_d i_q \,.$$

Subject to the following constraints:

$$V = \sqrt{u_d^2 + u_q^2} \le V_{max}\,, \text{ and} \tag{4}$$

$$I = \sqrt{i_d^2 + i_q^2} \le I_{max}\,. \tag{5}$$

A controller algorithm was developed that for any fixed speed, ω, derives the values of $i_d(\omega)$, $i_q(\omega)$, $u_d(\omega)$, and $u_q(\omega)$ that maximize torque for motoring and minimize the torque for braking.

This is broken down into three cases

1. $\sqrt{i_d^2 + i_q^2} = I_{max}, \sqrt{u_d^2 + u_q^2} \le V_{max}$,
2. $\sqrt{i_d^2 + i_q^2} \le I_{max}, \sqrt{u_d^2 + u_q^2} = V_{max}$, and
3. $\sqrt{i_d^2 + i_q^2} = I_{max}, \sqrt{u_d^2 + u_q^2} = V_{max}$.

This was further developed in a Matlab™ program that solves a static optimization problem. The control algorithm was used on the simulated PMSM with excellent agreement. The next step was to validate the simulation model with data from the Prius machine.

Having a very high power density, the Prius motor operates well into the saturation regime. This has added complexity to the motor modeling and controller development efforts. Furthermore, the agreement between the model and motor operation data has not been as good as expected. Recent research papers [8,9] indicate that the flux linkage in the *q* axis depends on *both* the *d* and *q* currents. This also appears true for the *d* axis flux linkage. Therefore, the model required revision so that it corresponded better with the data; furthermore, additional finite-element analysis (FEA) runs were deemed necessary to account more accurately for saturation. These efforts are expected to lead to an improved understanding of how a high energy-density, interior PM motor such as the Prius should be modeled and controlled.

4.3.3 Controller Hardware

The RT-LAB real-time computing platform from OPAL-RT Technologies was used to model and replace the Prius control system. The RT-LAB system interfaces with the MATLAB SIMULINK software for quick controller development without tedious programming. The system consists of a host PC running a user-selected operating system and two target PCs running the QNX Neutrino operating system. One of the PCs is a dual-processor computer with additional counter, encoder, and analog/digital I/O boards.

The model of the Prius controller and a user interface is built in MATLAB SIMULINK using both built-in SIMULINK blocks and RT-LAB blocks as illustrated in Fig. 4.3. This figure is an upper-level representation; most blocks can be opened for additional detail. Using the Real-Time Workshop Toolbox of SIMULINK, the model is converted to C-source code and the executable is uploaded to the target PCs. The controller software runs on two target PCs that communicate with each other through a firewire connection while the host PC is used to command the controller through an Ethernet connection. The

software allows the control development to be flexible and versatile, with the capability of quickly making required development changes. This approach bypasses some of the more difficult hardware development efforts required to allow the inverter to be controlled outside the vehicle. It also enhances the ability to make changes during testing, if required.

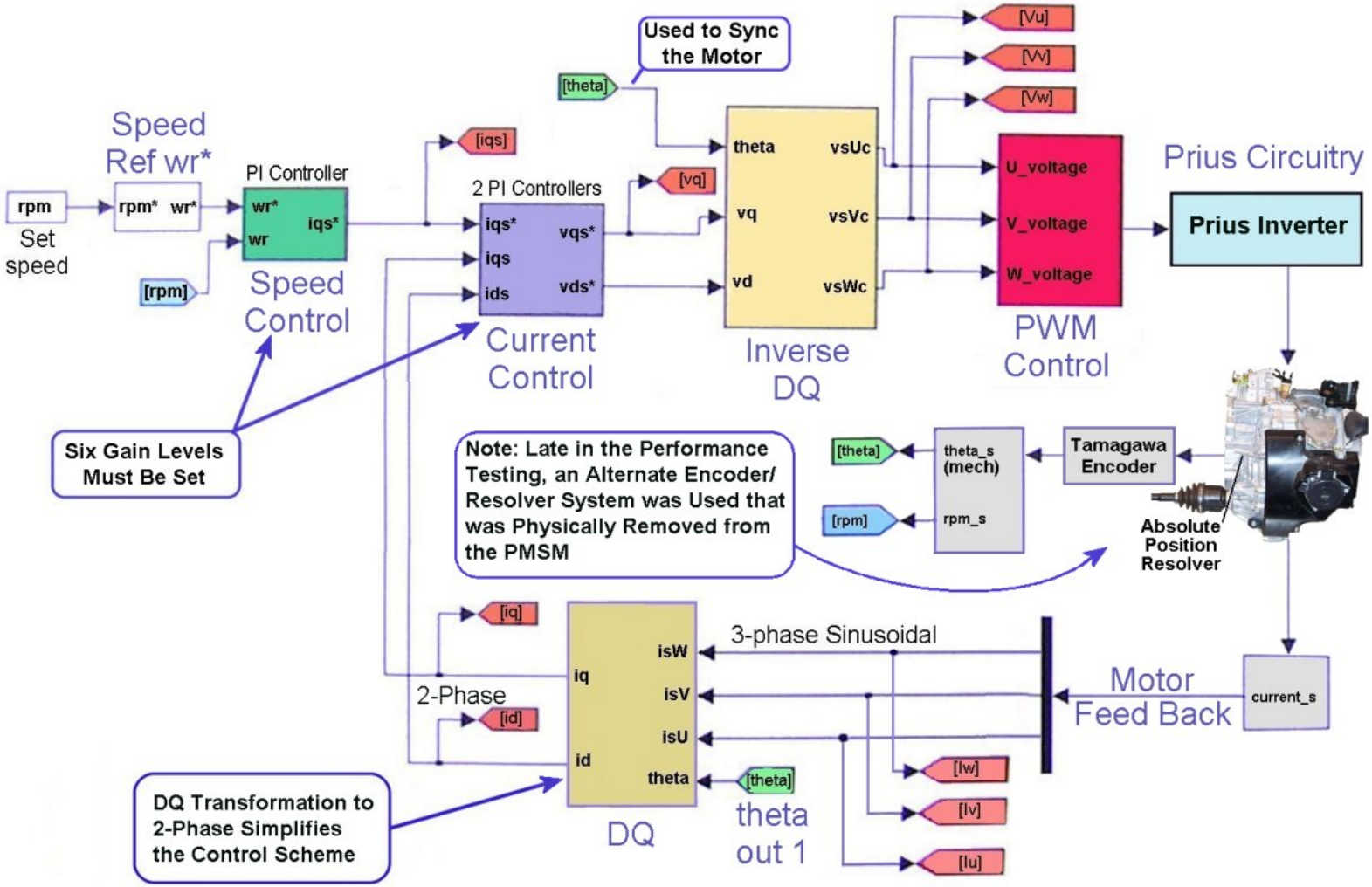

Fig. 4.3. Upper-level flow diagram of Prius controller system.

4.4 COMPARISON OF PRIUS INVERTER AND Z-SOURCE INVERTER

The Prius contains a conventional inverter for powering the PMSM with a voltage-boost circuit that is helpful in both reducing the stresses in the switching devices and expanding the motor's constant power speed ratio (CPSR). On the negative side, the dc-to-dc boosted PWM inverter topology suffers the cost and complexity associated with the two-stage power conversion.

In 2004, Fang Peng of Michigan State University performed a study [10] for ORNL that compared conventional inverter systems to a new inverter topology, Z-source, for applications including HEV systems and fuel-cell vehicles. The dc-to-dc boosted PWM inverter and Z-source basic circuit topologies are represented in Fig. 4.4. The comparison study was based on the use of a 50 kW (max) fuel-cell stack providing power to a 34 kW (50 kW max) Solectria AC55 motor for traction drive.

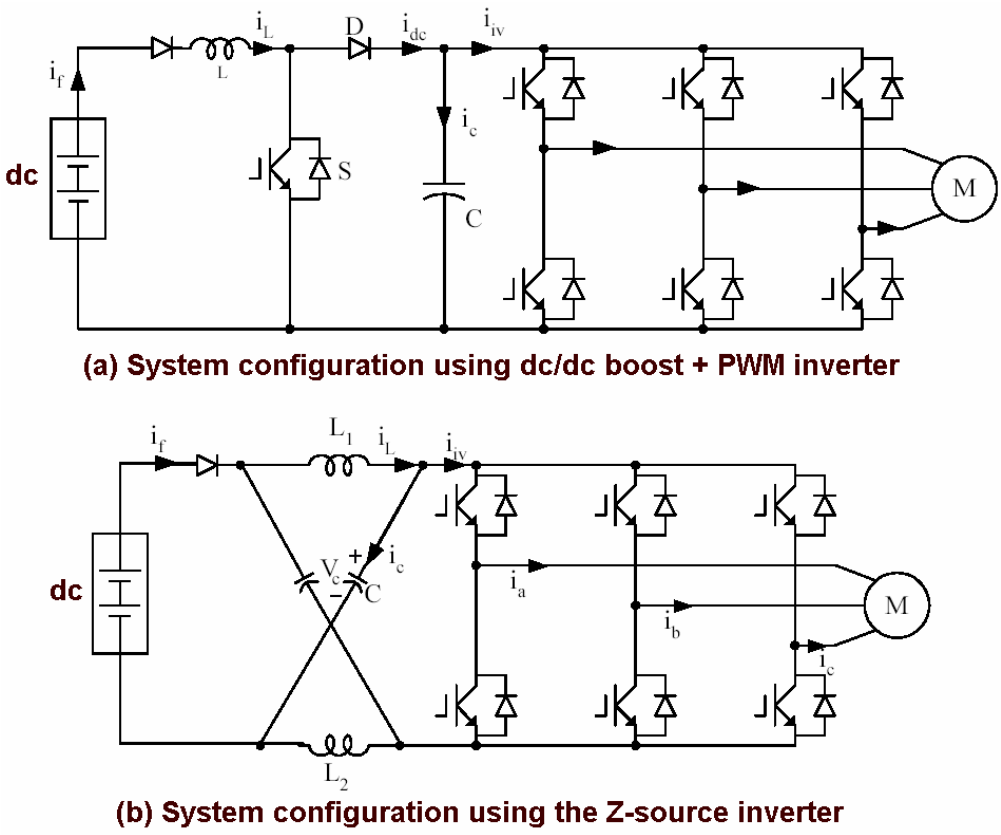

Fig. 4.4. Configurations for (a) conventional boosted inverter and (b) new Z-source inverter.

The study considered switching device power (SDP) as a means of quantifying the voltage and current stress (or requirement) of the inverters. Total SDP is the aggregate of SDP of all the switching devices used in the circuit.

Equations were developed to compare inverter SDPs for the following conditions:

- Maximum power: 50 KW
- Motor power factor at max power: 0.9
- Boost-converter output: 420 V

The equations produced results indicating that the Z-source inverter benefited from a lower total average SDP than the conventional boosted converter (199 kVA vs. 225 kVA); however, this was reversed in the case of total *peak* SDP (605 kVA vs. 528 kVA).

Perhaps the key findings of the study were efficiency data produced for the different inverter topologies. Table 4.1 indicates that, for five different power levels, the inverter efficiencies were higher for the Z-source inverter by 0.7% on the average. Considering the motor-inverter system, the Z-source system efficiency was higher in all cases except at the 50 kW power level. The average improvement at the motor-inverter system level was significantly higher at 0.87%. These data are plotted in Fig. 4.5.

Table 4.1. Efficiency comparisons of inverter topologies and inverter/motor systems

Power (kW)	Inverter Efficiency			System Efficiency		
	Conventional with Boost	Z-Source	% Improve-ment	Conventional with Boost	Z-Source	% Improve-ment
10	0.964	0.973	0.93	0.936	0.949	1.39
20	0.966	0.973	0.72	0.917	0.93	1.42
30	0.966	0.973	0.72	0.902	0.913	1.22
40	0.965	0.971	0.62	0.89	0.896	0.67
50	0.964	0.969	0.52	0.88	0.877	-0.34

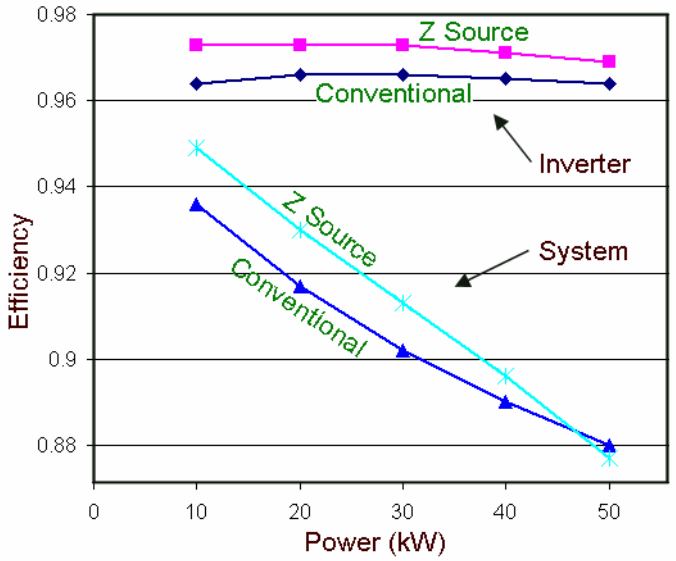

Fig. 4.5. Efficiency comparisons of inverter topologies and inverter/motor systems.

The potential advantages of using the Z-source inverter include the following:

1. Nearly a 1% improvement in system efficiency,
2. Improved reliability since shoot-through cannot cause failure,
3. Elimination of in-rush current facilitates startup,
4. Reduced vulnerability to EMI and related misgating-induced failures, and
5. Reduced cost through the elimination of dc-to-dc boost-conversion circuit.

5. HEV SYSTEM MANUFACTURING AND PACKAGING

This section will present certain details relating to the manufacturing, assembly, and packaging of the HEV system in the 2004 Prius. This information will help to more fully characterize the design and to determine key parameters, such as specific power and power density, in support of the FCVT program.

5.1 PMSM

Figure 5.1 shows three views of the PMSM housing with selected dimensions[11] called out. As indicated, about 3/4th of the casing houses the PMSM rotor and stator and the remainder encloses part of the gearbox. The portion of the casing that houses the PMSM is roughly cylindrical and that is the geometry used for the purposes of estimating the PMSM casing volume. Based on the average of three measurements of casing diameter, the cylinder diameter can be assumed to be ~29.9 cm. The depth of the PMSM housing extending from the end plate to the surface identified in the upper left photo in Fig. 5.1 is 20.5 cm. This results in a volume of 14,400 cm^3 excluding the three-phase terminal-block housing and the cooling passages that protrude from the surface of the casing. Including all three volumes results in a total of 15,400 cm^3 (15.4 L). This volume and the 50 kW peak-power specifications result in a peak-power density of 3.25 kW/L.

The mass of the PMSM was determined in order to estimate the specific power. The masses of the components of the Prius PMSM are:

Stator:	25.9 kg
Rotor:	10.2 kg
Case:	6.36 kg (machined – see below)
Case cover:	2.49 kg
Total mass of motor:	**45.0 kg**

The casing for the PMSM has (1) a portion that encloses one end of the gear box, and (2) compartments that enclose the gear-shift-lever-to-shift-plunger linkages. These areas are unrelated to the PMSM and were therefore machined off of the structure to obtain a new 6.36 kg mass (the original casing mass was 13.9 kg). The resulting specific power for the PMSM is 1.11 kW/kg.

[11] The casing in the figure was obtained from a 2003 Prius; however, the dimensions were obtained from the very similar 2004 casing used in performance testing.

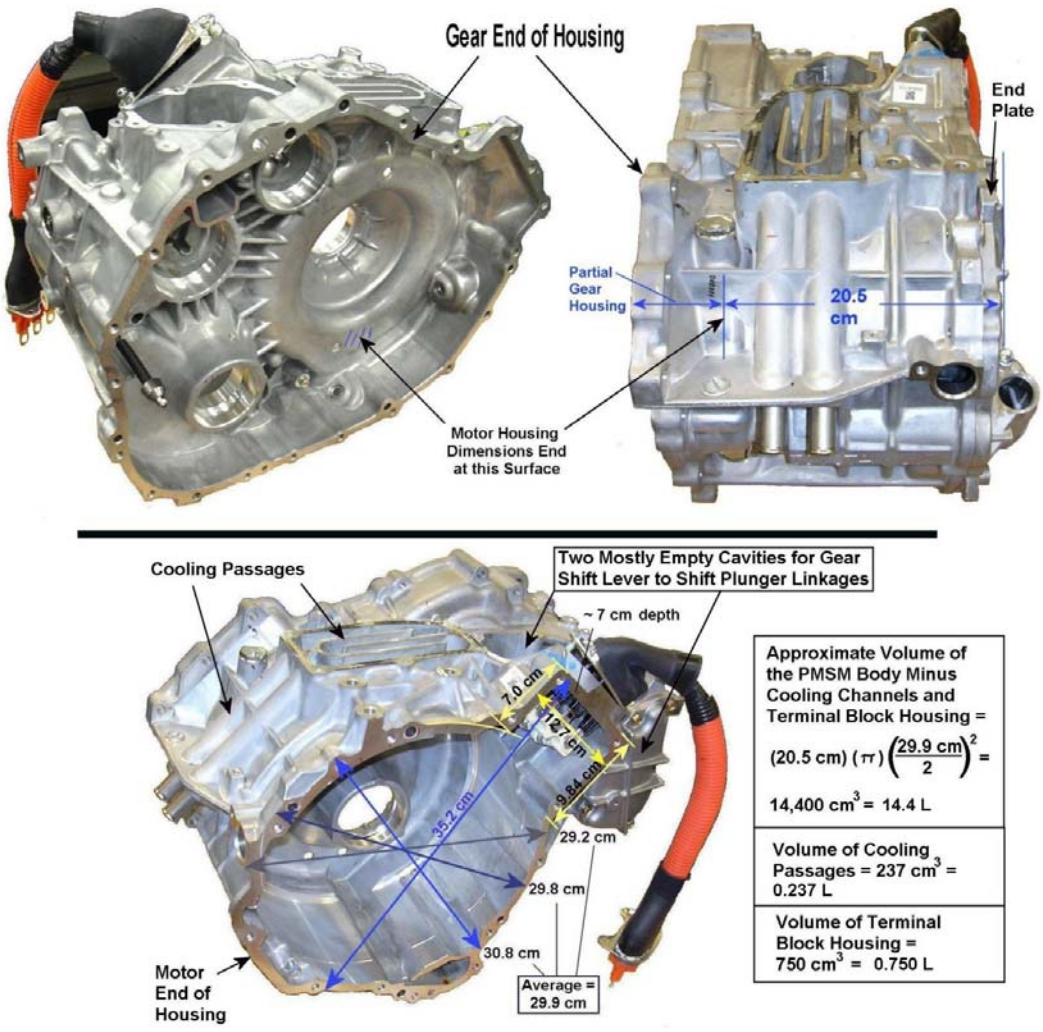

Fig. 5.1. Casing of the 2004 Prius PMSM with dimensions and volume calculations.

5.2 INVERTER/CONVERTER

As indicated in Section 2.2.5, the inverter package contains several important circuits that include the

- Motor inverter
- Generator inverter
- Buck/boost converter
- Air-conditioning compressor inverter
- A dc-to-dc inverter

Figure 5.2 shows how these circuits are packaged in the inverter casing. The PMSM inverter and generator inverter driver circuitry is contained on a circuit board mounted below the inverter capacitor module and above the power module that contains the IGBTs and diodes for both inverter circuits. The power module contains 6 IGBTs and 6 diodes for the generator inverter and 12 IGBTs and 12 diodes for the PMSM inverter to support its higher power rating (6 pairs of IGBTs are wired in parallel). The power module is mounted on a water-cooled cold plate for cooling. Adjacent to the inverter circuitry is the buck/boost converter (500-V clamp on the boost) and its associated IGBTs. The voltage is boosted from

200V to 200–500V for motor operation and bucked from the same 200–500V range for charging the 200V battery.

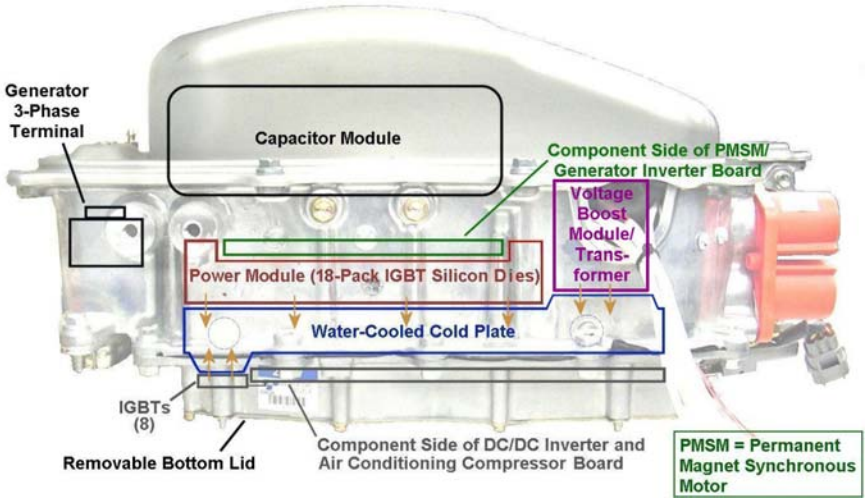

Fig. 5.2. Overall subsystem packaging in the 2004 Prius inverter/converter.

At the bottom of Fig. 5.2 is another compartment that is accessible by opening the bottom lid. This compartment holds a large circuit board containing (1) the inverter for powering the air-conditioning compressor, and (2) the dc-to-dc converter that takes the 200–500V bus and provides 13.8V for charging the battery and powering accessories. IGBTs for both circuits are mounted on the bottom of the cold plate. Many of the components and subassemblies mentioned above will be seen in the figures provided below.

Figure 5.3 shows the inverter casing with the lid removed. Most evident are the capacitor module, voltage-boost module and the main electrical connections. High current bus bars make all of the connections to the capacitor module, motor and generator terminals, and the boost converter.

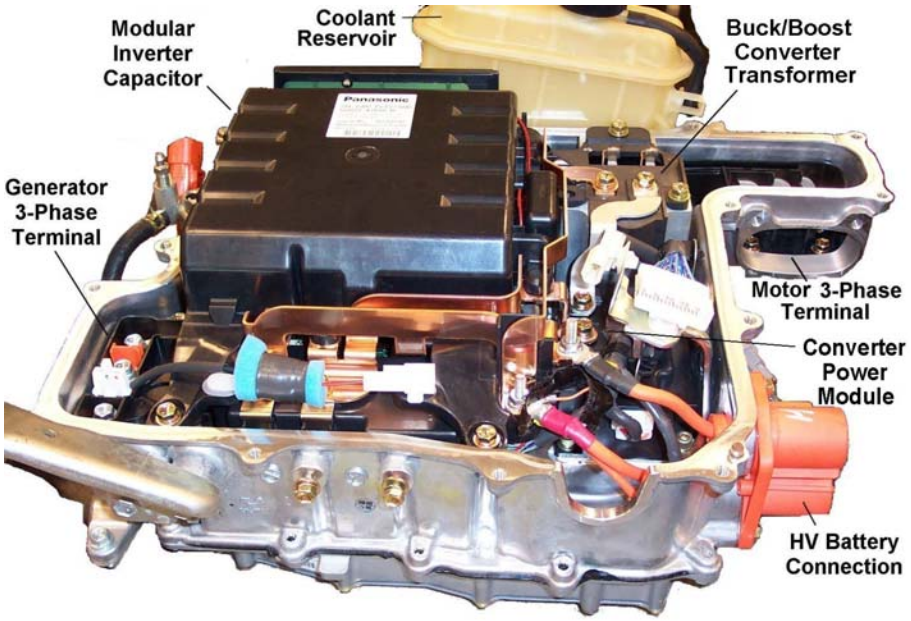

Fig. 5.3. Overview of packaging in an opened 2004 Prius inverter/converter.

Figure 5.4 shows a similar view of the inverter casing but with the capacitor module removed. The general location of the buck/boost converter is indicated; however, the power electronic devices are located down near the cold plate and are not visible. The inverter-driver board is partially visible and the positions of the three motor bus bar terminals and three generator bus bar terminals indicate that the driver board is functionally divided into an upper half containing the motor inverter and a lower half containing the generator inverter.

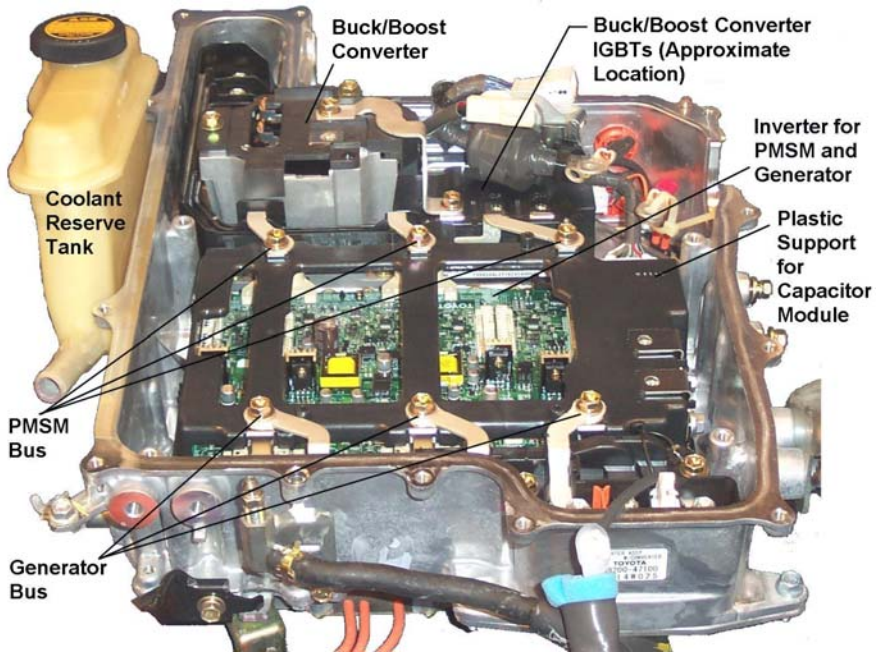

Fig. 5.4. Overview of packaging in a 2004 Prius inverter/converter with capacitor module removed.

The six bus bar "connections" are actually junctions *above* the driver board. They cause the currents to pass through current sensors located on the driver board and the conductors continue down until electrical connections are made on the power module.

The inverter-driver board in earlier year models had several IR chips and in later year boards these were often relabeled as "Toyota." The basic logic or architecture of the circuits remained the same. IR gate driver and bridge drivers are described on the IR internet site (http://www.irf.com/product-info/cic), and the circuit design is somewhat unique. For instance, the IR gate driver approach eliminates the need for an isolated upper branch when driving the IGBT. This results in significant parts savings. The only requirement is that the circuit must turn on the lower branch first. This approach is reflected in the Toyota inverter-driver boards.

The empty inverter/converter casing is shown in Fig. 5.5. The photo shows the high usage the casing design makes of the cold plate surface area for the cooling of the IPEM, the voltage-boost transformer, and the buck/boost converter. The inverter cold plate measures 250mm X ~255 mm X ~19 mm for a total volume of 1.21 L, excluding additional aluminum surrounding the cold plate where component mounting holes are located. The power module, converter, and transformers mount on this cold plate. The IPEM alone requires a cold plate measuring 250mm X ~155 mm X ~19 mm for a total volume of 0.74 L.

The IPEM is shown in Fig. 5.6 with the cover removed. This IPEM photo was taken by ANL during their disassembly and instrumenting of the 2004 Prius inverter for ORNL. The six pairs of parallel-wired IGBT dies for the motor inverter are shown on the top and the six IGBT dies for the generator inverter are shown on the bottom. The 200V battery terminal posts are shown on the right. Figure 5.7 provides a

close-up of a single IGBT die and related diode die. This image was obtained looking through the silicone gel.

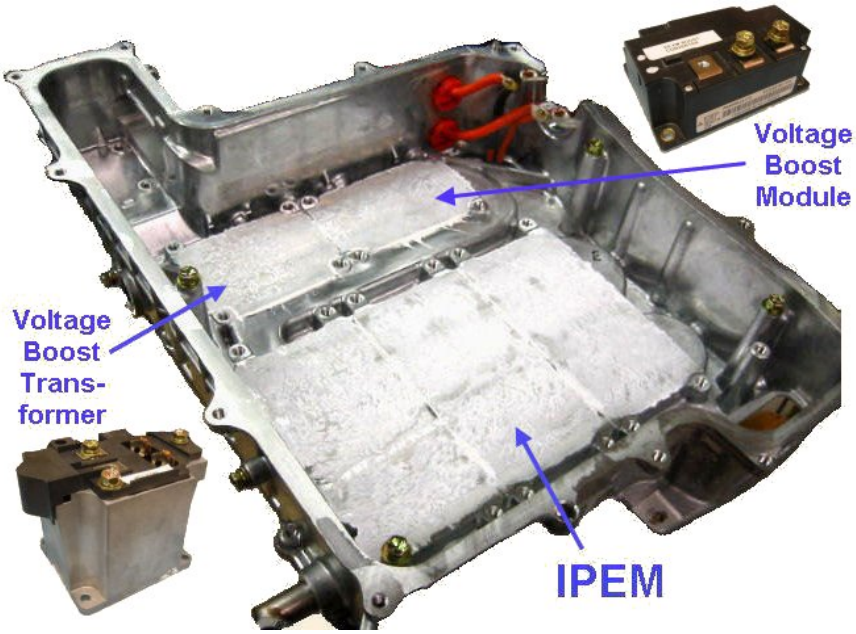

Fig. 5.5. Empty inverter/converter housing showing cold plate surfaces.

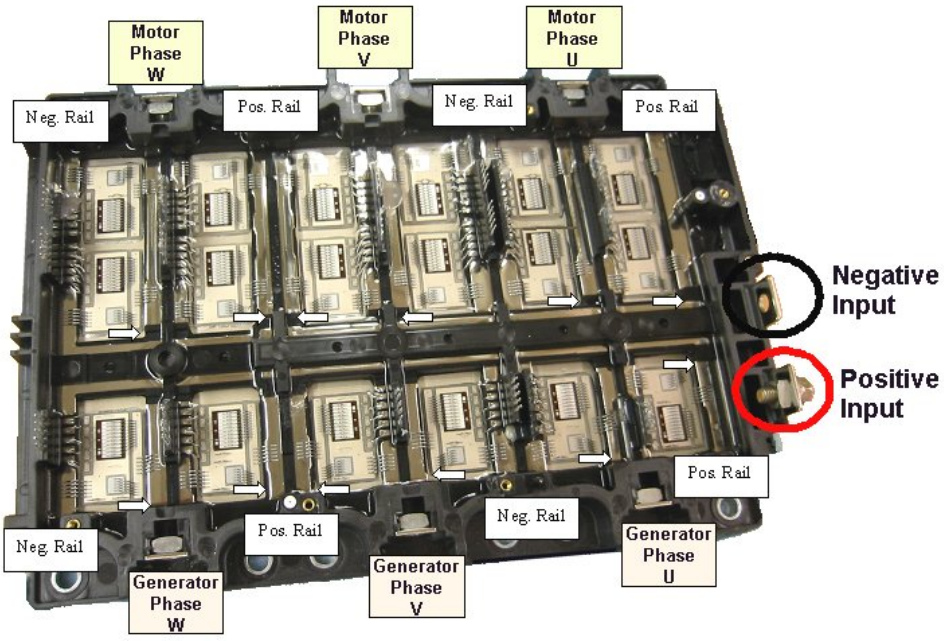

Fig. 5.6. Power module 18-pack dye array in a 2004 Prius inverter (photo provided by ANL).

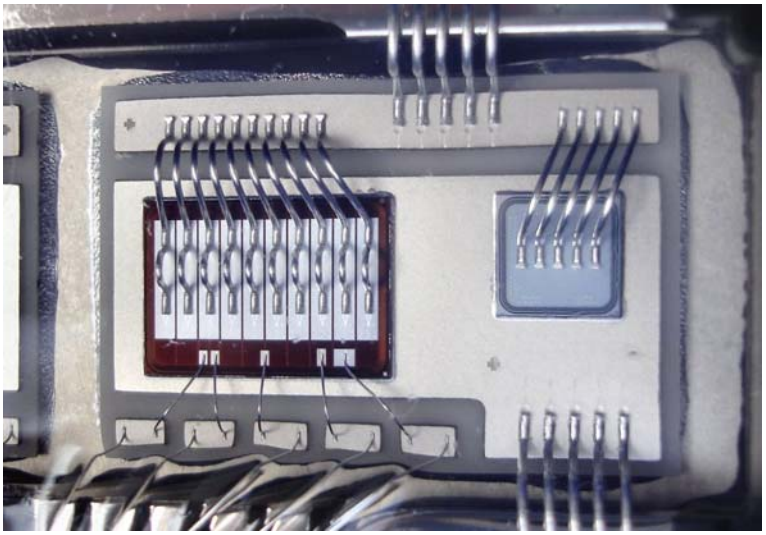

Fig. 5.7. Close-up of an IGBT/diode pair in the 2004 Prius inverter.

Figure 5.8 shows a board located in a separate compartment located under the water-cooled cold plate. As mentioned above, this board contains the inverter for powering the air-conditioning compressor and the dc-to-dc converter. The converter takes the 200–500V bus and provides 13.8V for charging the battery and powering accessories such as lights, the audio system, and ECU. The inverter is located across the top of the board in the figure and the dc-to-dc converter circuitry fills up the remainder of the compartment (i.e., about 75% of the volume shown).

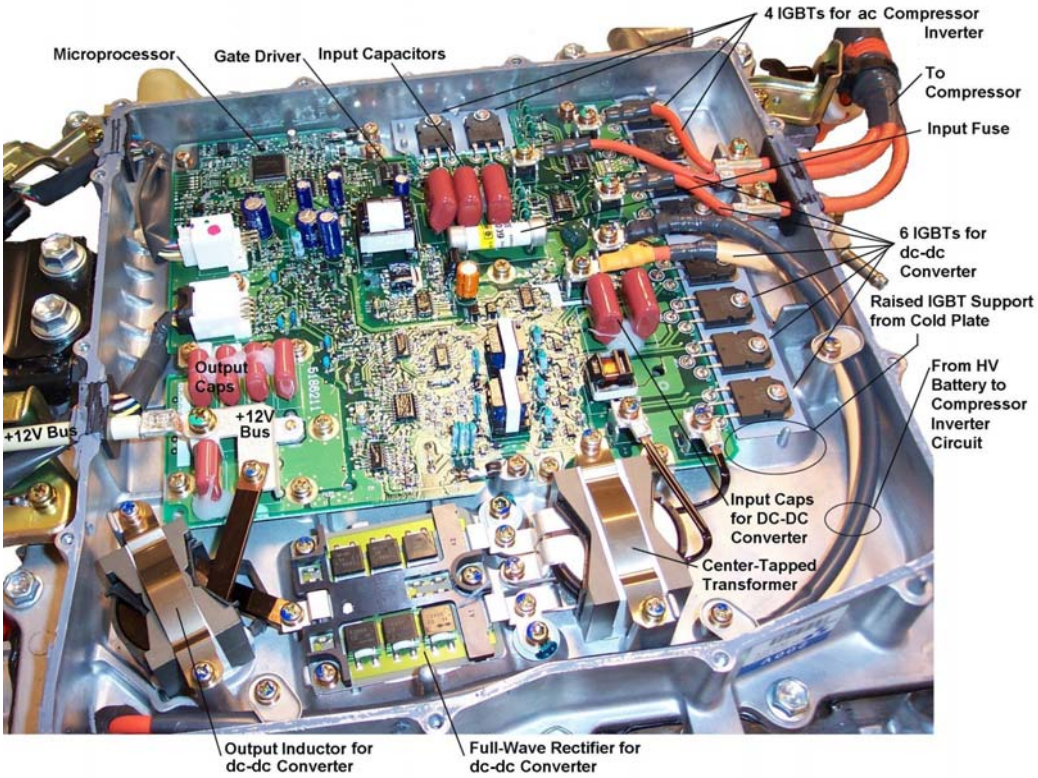

Fig. 5.8. Packaging of the 2004 Prius compressor inverter and dc-to-dc converter circuit.

The volume and mass of the inverter/converter casing was assessed to determine the peak-power density and specific power for the power electronics. Figure 5.9 indicates the overall mass and volume of the unit. The volume of the lid was calculated in four parts with a few simplifying assumptions in order to produce a reasonably close estimate of volume. Likewise volume estimates were derived for the mid section and the bottom section. The motor operation is supported by 1/2 of the inverter-driver board, 2/3 of the IPEM, and all of the voltage-boost circuit. The fact that half the driver board can be disregarded has only a small bearing on the volume. Thus, power density can be approximated by the motor power rating of 50 kW and the volumes of the lid and mid sections, which together total 14.5 L. Thus, the peak-power density is 3.45 kW/l. The volumes occupied by the housing for the three-phase connection to the motor and the connector for the HEV battery were not included since these can be located anywhere on the casing that is convenient to the designer making the actual volume penalty negligible. The volume used in the calculation could likely be reduced by ~25% if a designer so desired. This is because of the circuits not supporting the operation of the motor and because there is some amount of wasted space in the lid surrounding the capacitor module for the purposes of improved styling/appearance (the inverter/converter casing lid is quite visible/predominant when the Prius hood is raised).

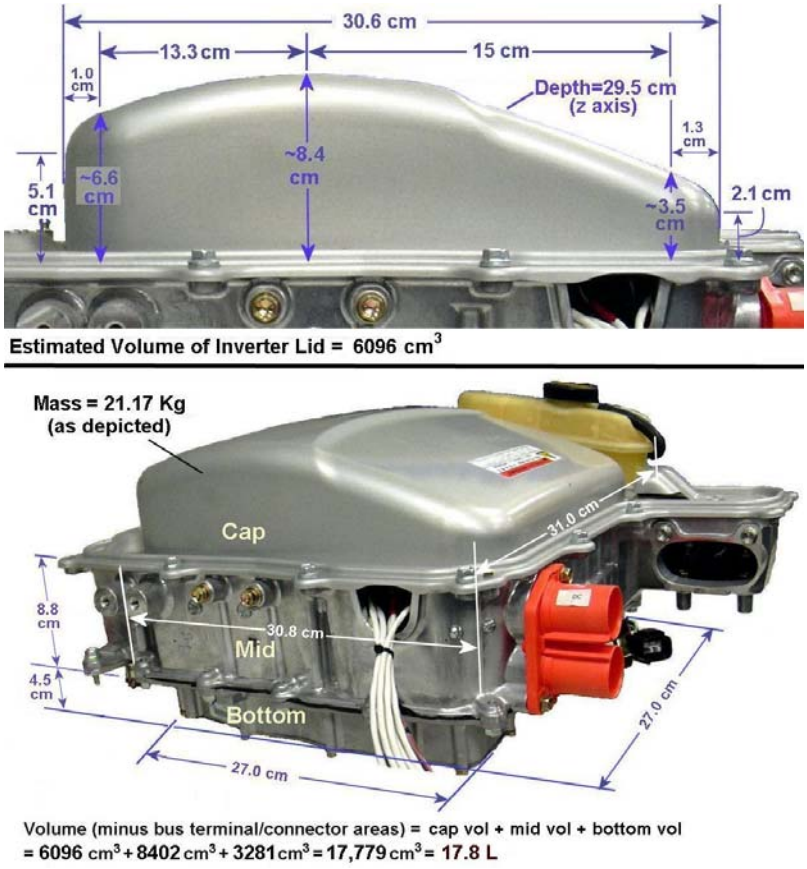

Fig. 5.9. Overall volume and mass of the 2004 Prius inverter/converter.

The mass of the inverter/converter unit was also closely considered to develop an estimate of specific power. The mass of the bottom compartment housing and internal components for the dc-to-dc converter and ac compressor inverter were excluded from the full mass (21.17 kg) since these circuits are not part of the PMSM/inverter system. This resulted in 19.37 kg. The resulting specific power is 2.6 kW/kg which, as in the case of the power density, could easily be improved for the same reasons discussed above.

No discussion of the PMSM and inverter/converter would be complete without a description of the cooling system that serves both. The cooling system is comprised of a 12-V electric pump (344 g), four 5/8-inch hoses, and a small, lightweight radiator. A single radiator structure, weighing 2.05 kg, serves both the engine and the hybrid subsystems including the PMSM and the inverter/converter. The portion of the radiator serving only the hybrid subsystems has (1) a mass estimated to be ~0.55 kg, and (2) dimensions of 16 mm X 706 mm X 101 mm for a total volume of 1.14 L. Figure 5.10 shows the radiator after being separated from the air-conditioning condenser that was located behind it.

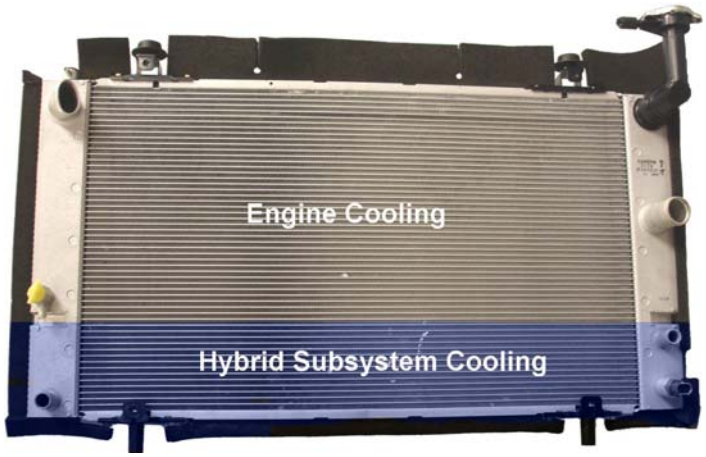

Fig. 5.10. Radiator for Prius engine (upper) and hybrid subsystems (lower).

5.3 CONVERTER COMPONENTS

Due to recent, high interest in converter design, additional details are provided on the 2004 Prius voltage-boost-converter circuit. The general circuit diagram in Fig. 5.11 shows that the converter contains two IGBTs and two diodes instead of one of each. This allows for two-way power flow – battery to integrated power module (IPM) and IPM to battery. During periods of maximum power demand from the IPM/PMSM system, the converter provides ~20 kW and the vehicle generator supplies ~30 kW. This power split allows a reduction in size of the high-cost HEV battery and the converter. Therefore, the power rating of the converter is ~20 kW, not 50 kW.

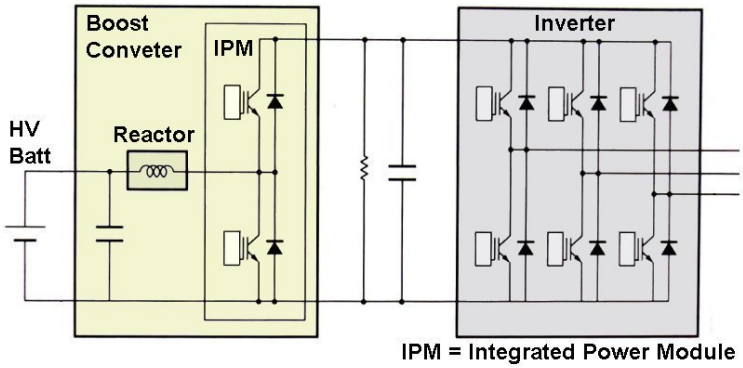

Fig. 5.11. General circuit schematic of the Prius inverter.

Figure 5.12 shows the disassembly of the IPM. Figure 5.12(a) shows the gate-driver board with a 18-pin connector on the left, Fig. 5.12(b) shows the EMI shield located immediately below the gate-driver board, and Fig. 5.12(c) shows the IGBTs and diodes. The gate-driver board contains circuitry that includes

protection logic for short circuit, over current, over temperature, and under-voltage conditions. Since non-standard chip numbers were observed, further information was not readily attainable.

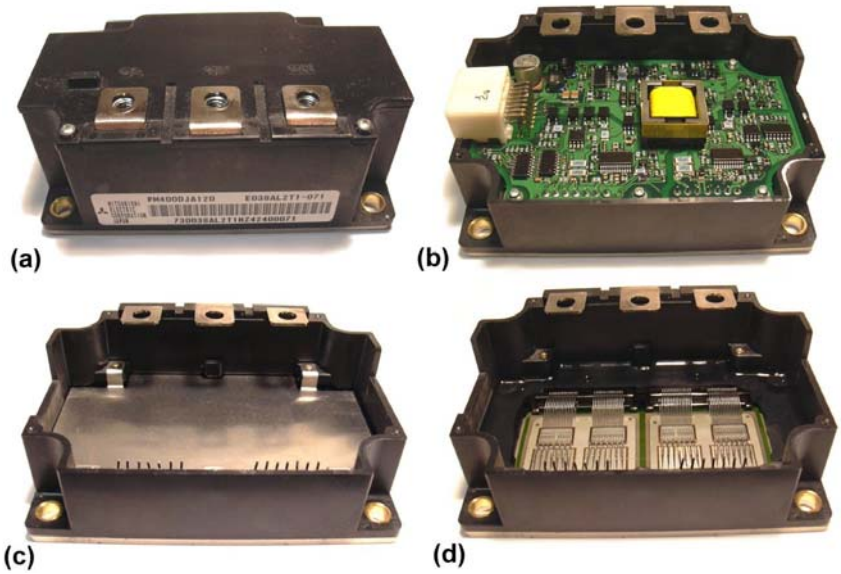

Fig. 5.12. Disassembly of the converter power module.

A close-up of the IGBTs and diodes, immersed in a high-temperature silicone sealer/gel and conformal coating, are shown in Fig. 5.13. Note that the IGBTs and diodes are paired (connected in parallel) to meet current requirements. This produces a total silicon surface area of 7.84 cm^2 for the two IGBT pairs and 3.78 cm^2 for the two diode pairs or 11.6 cm^2 total for the IPM. The volume of the IPM is 421 cm^3 if treated as a simple rectangle or ~375 cm^3 if derived in a more precise manner (subtracting cut-away areas from the top and the four corners). The mass of the IPM is 0.662 kg.

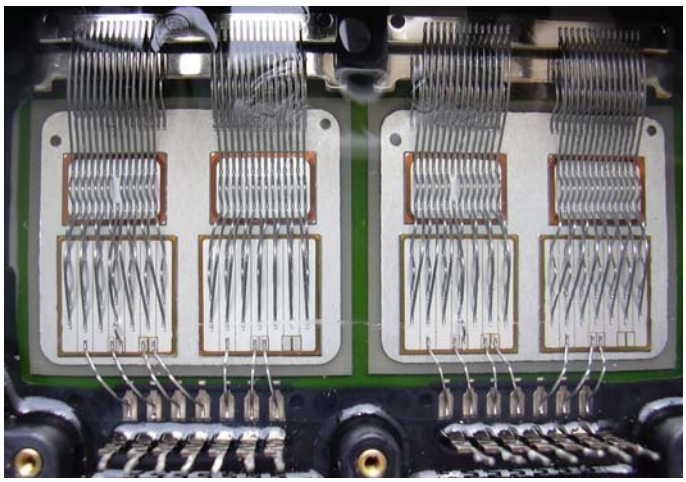

Fig. 5.13. Close-up of converter IGBTs and diodes.

The voltage-boost converter auto transformer (or reactor) is shown in Fig. 5.14. The mass of the transformer is 2.57 kg. The geometry of the transformer casing has several curves, angles, indentations, etc.; however, a close approximation of its total volume is ~742 cm^3. Excluding any type of cold plate, the volume and mass totals for the ~20 kW boost converter (IPM and transformer) are ~1.12 L and

3.23 kg, respectively. These estimates are modified below to include portions of the casing and cold plate.

Fig. 5.14. Voltage-boost converter auto-transformer.

The following derivations of converter volume consider even the cold plate and/or the converter volume enclosed by the casing:

Volume Calculation Approach A: The cold plate surfaces for the converter are shown in Fig. 5.15 (left photo). The volume of the cold plate under the two converter components (including adjacent mounting holes) is 19 mm X 100 mm X 250 mm = 0.48 L. However, this approach ignores the space enclosed by the converter portion of the casing.

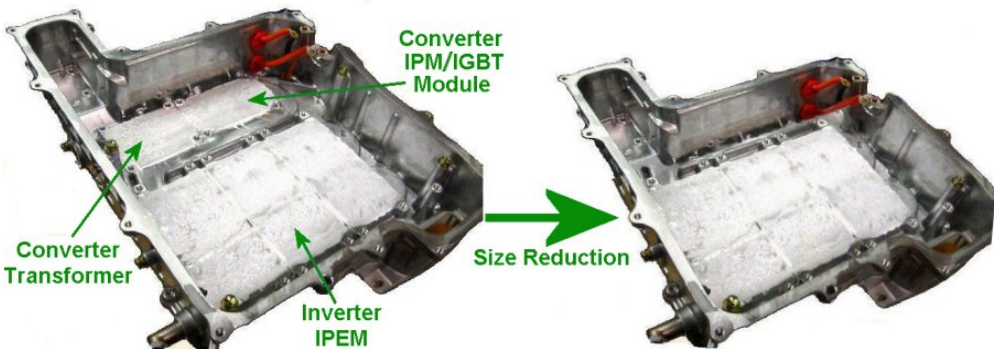

Fig. 5.15. Conceptual change to inverter/converter casing for excluding the buck/boost converter.

Volume Calculation Approach B: Comparing the two casing designs in Fig. 5.15, consider the entire volume that includes the cold plate, converter components mounted on it, and surrounding space enclosed in the casing. This overall volume is 335 mm X 100 mm X 140 mm = 4.7 L.

Again comparing casing designs in Fig. 5.15, it is estimated that converter uses 15% of the casing mass. Since the casing shell is 6.45 kg, the casing mass dedicated to the converter is ~1 kg.

Conclusions: Accounting for the transformer, IPM, and casing the total converter system volume is 4.7 L and the mass is 4.2 kg. From this information, specific power and power density can be determined keeping in mind that the rating of the buck/boost converter is ~20 kW.

Table 5.1 summarizes the estimates of volumes, masses, power density, and specific power presented earlier in this section.

Table 5.1. Physical characterization of the PMSM, inverter, converter, and cooling system

Item	Volume, L	Peak power density, kW/L	Mass, kg	Specific power, kW/kg
PMSM	15.4	3.25	44.9	1.11
Inverter/converter assembly	14.5	3.45	19.4	2.6
COOLING SYSTEM				
Full radiator assembly	4.19	-	2.05	-
Radiator: portion for hybrid cooling	1.14	-	0.55	-
Hybrid cooling water pump	~0.6	-	0.344	-
BUCK/BOOST CONVERTER				
Converter assembly (complete)	4.7	4.3	4.2	4.8
Transformer	0.74	-	2.57	-
Power module	0.38	-	0.66	-

6. SUMMARY AND CONCLUSIONS

The performance benchmarking of the 2004 Prius PMSM and inverter systems was accomplished through system inspections/evaluations, a review of manufacturing and packaging, controller development in preparation for testing, and laboratory evaluations that included back-emf tests, locked rotor tests, loss tests, and full-range performance testing of the HEV system. In essence, the overall approach of this project was to thoroughly define the systems and then perform a detailed evaluation of their performance in a controlled laboratory environment. This approach proved to be technically sound and successful.

Specifically, the subsystem-level performance testing involved:

- Collecting back-emf voltage waveforms for both the PMSM (and generator),
- Performing locked rotor tests at varying torque angles (over the range, 90–134°),
- Determining gear, bearing, and other friction losses for various operating speeds and lubricating oil temperatures, and
- Mapping motor/inverter performance over the full speed and shaft-loading ranges using 50°C and 90°C motor/inverter coolant temperatures.

6.1 FINDINGS AND OBSERVATIONS

Subassembly-level testing at ORNL revealed that gearbox related friction losses were found to be significant. These losses are approximately 2.4 kW at a motor speed of 6000 rpm. The predominant loss of about 1.6 kW is associated with the main reduction gears and drive chain while the motor, power-split device, and generator yielded losses of about 0.8 kW. Gear-train losses are primarily associated with oil splashing within the hybrid drive housing and oil slinging from the generator and motor rotors to provide needed lubrication and removal of excess heat. These losses, which are summarized in Table 6.1, were determined with the lubricating oil at or near room temperature (about 25°C). The tests also revealed that overall losses decreased about 20% when the temperature of the lubricating oil increased from 27–80°C. This finding indicates that total losses for the hybrid electric drive system equal approximately 1.9 kW at a lubricating oil temperature of 80°C.

Table 6.1. Summary of gear-train losses at 25°C

Subassembly	Contribution to Loss, %
Reduction Gears and Drive Chain	68
Motor Rotor	21
Generator and Planetary Gears	11

Gear-reduction ratios were determined and documented for both the motor rotor and the generator rotor (with engine spline locked). This determination was primarily performed to allow accurate calculation of speed, torque, and loads but the findings also provided a basis for comparison with other drives and to identify engineering choices and compromises that were made as part of the overall design process. The following relationships are based on results of the gear-reduction determinations:

$$\text{2004 Prius Motor Speed} = (4.113)\ (\text{axle speed})$$

2003 Prius Motor Speed = (3.905) (axle speed)

2004 Prius Generator Speed = (10.7) (axle speed with engine spline locked)

Motor and generator testing yielded back-emf voltage and frequency data. During the tests, a dynamometer drive was used to control motor speed and generator speed. Results of the back-emf testing are summarized in Table 6.2.

Table 6.2. Summary of back-emf test results

Test Conditions	Results
Motor back-emf (6000 rpm)	540 Vrms
Motor voltage constant	1.33 Vrms/Hz
Generator back-emf (6420 rpm)	195 Vrms
Generator voltage constant	0.46 Vrms/Hz

A series of locked rotor tests was performed to determine general operating capabilities of the traction motor. In particular, the torque and current were studied during the locked rotor tests to characterize the startup torque capability of the motor. Current and corresponding torque values are presented in Table 6.3 and discussed in detail in Ref. [1].

Table 6.3. Summary of motor current and torque test results

Current, A	Maximum Torque, Nm
75	140
150	260
250	400

The benchmarking project partially supported and funded the thermal testing of the Prius motor. These tests were successful in determining the continuous ratings of the Prius motor design at coolant temperatures ranging from 35–105°C. This information has not been released by the Toyota Motor Company. The ratings at base speed (1200 rpm) were projected from test data at 900 rpm. The continuous ratings were determined to be 15 kW using 105°C coolant, and 21 kW using 35°C coolant. As indicated in the full report on these thermal tests [1], these ratings are well below the 30 kW target of the DOE FCVT program.

The final testing of the Prius is the mapping of motor/inverter performance over the full speed and shaft-loading ranges using primarily 55°C motor/inverter coolant temperatures. In early test runs while using only calibrated instrumentation, test data showed higher-than-expected inverter efficiency. This led to a series of tests designed to (1) verify the test procedures/approaches in use, and (2) provide a higher level of confidence in the test data.

The subsystem performance-mapping data tests were successfully completed in March 2006. The test data enabled ORNL researchers to generate the efficiency contour mapping plots for the motor, inverter, and combined motor/inverter system shown in Fig. 6.1. These are discussed in Section 3.3.3.

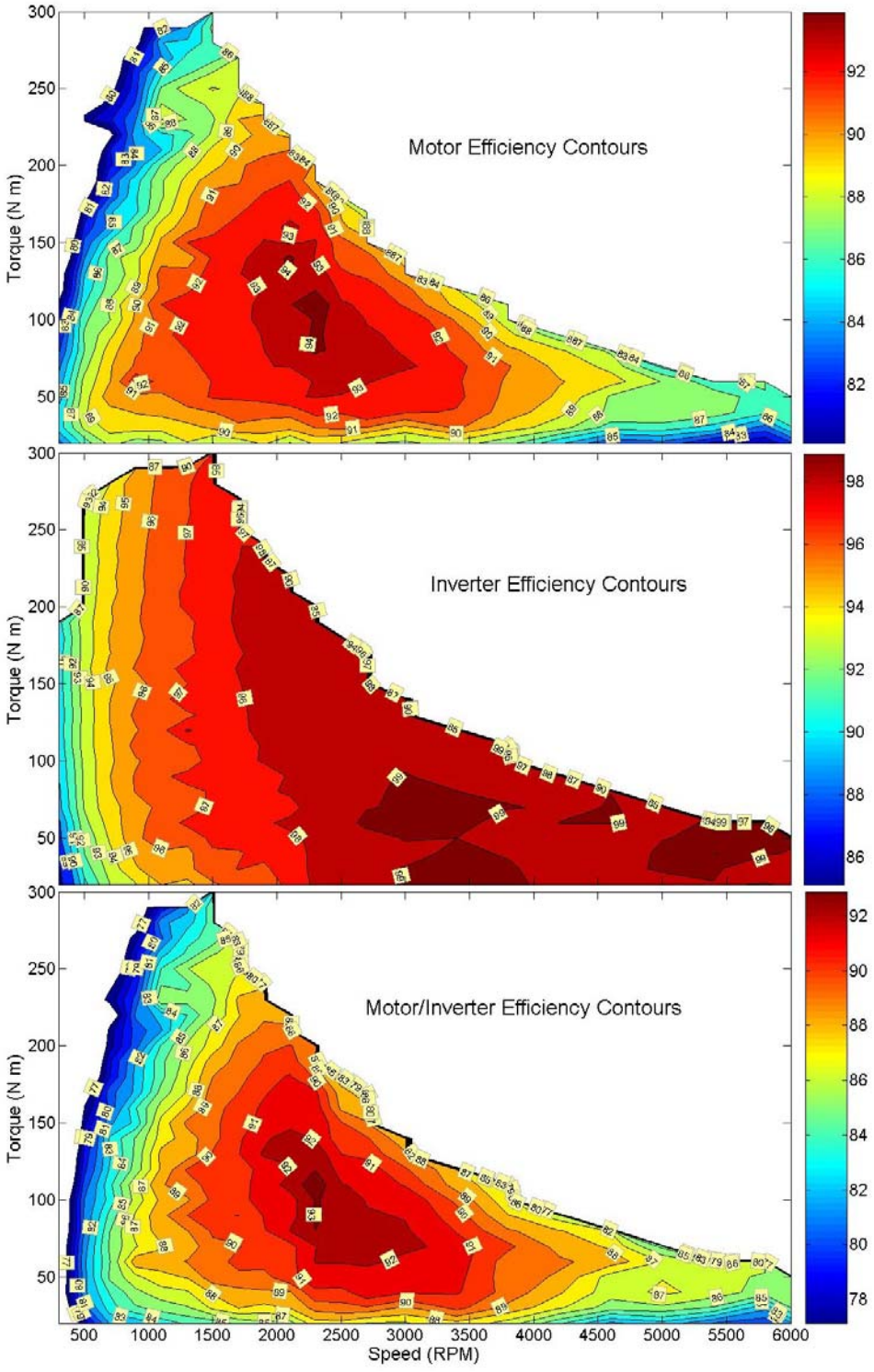

Fig. 6.1. Prius combined efficiency contour maps.

The results of the Prius testing have provided a wealth of information on these innovative, high-power-density subsystems that would not have been available otherwise. The design and packaging information and data from various subsystem tests have been in very high demand over the last couple years necessitating the dissemination of these data to FCVT researchers even before the publishing of this report. The planning and management of the FCVT project itself has benefited from various sets of data including estimates of power density, specific power, and detailed characterizations of the motor, inverter, converter, and planetary-gear train subsystems.

6.2 NEEDED RESEARCH AND DEVELOPMENT

During FY2006, ORNL will perform benchmark testing of the hybrid Accord traction-drive system. The test data and design, packaging, and fabrication assessment will be combined to enable analysts to determine how the Accord system compares to the Prius system and program technology targets (peak-power-to-weight and -volume ratios). Other hybrid systems will be considered for limited analysis based on resources and the needs of the FCVT program.

Hybrid sport utility vehicles (SUVs) are emerging on the market and may represent significant deviations from existing hybrid technology. There may be some innovations in the drive system that merit benchmarking studies. Clearly, HEV systems sized appropriately for SUVs are of greatest interest to domestic manufacturers who have aggressively begun to introduce HEV systems into SUVs. Nationally, it is important to improve vehicle fuel efficiency to significantly reduce oil imports. This can be done most effectively on a vehicle-model basis by focusing on those with the poorest fuel efficiencies. With the global demand for oil increasing, fuel prices will increase significantly for years to come — no original equipment manufacturer (OEM) wants to find itself in poor fuel efficiency standings relative to other OEMs. There is also the potential for the return of Corporate Average Fuel Economy (CAFE) standards or similar requirements/incentives; however, increasing fuel prices are perhaps the most powerful incentive.

REFERENCES

1. J. S. Hsu, S. C. Nelson, P. A. Jallouk et al., *Report on Toyota Prius Motor Thermal Management*, ORNL/TM-2005/33, UT-Battelle, LLC, Oak Ridge National Laboratory, Oak Ridge, Tennessee, February 2005.
2. J. S. Hsu, C. W. Ayers, C. L. Coomer, R. H. Wiles, S. L. Campbell, K. T. Lowe, and R. T. Michelhaugh, *Report on Toyota/Prius Motor Torque Capability, Torque Property, No-Load Back-EMF, and Mechanical Losses*, ORNL/TM-2004/185, UT-Battelle, LLC, Oak Ridge National Laboratory, Oak Ridge, Tennessee, October 2004.
3. *Prius Repair Manual*, **1**, Pub. No. RM1075U1, Toyota Motor Corporation, 2003.
4. *Prius Repair Manual*, **2**, Pub. No. RM1075U2, Toyota Motor Corporation, 2003.
5. *Prius Repair Manual*, **3**, Pub. No. RM1075U3, Toyota Motor Corporation, 2003.
6. J. S. Hsu, C. W. Ayers, and C. L. Coomer, *Report on Toyota/Prius Motor Design and Manufacturing Assessment*, ORNL/TM-2004/137, UT-Battelle, LLC, Oak Ridge National Laboratory, Oak Ridge, Tennessee, August 2004.
7. *Prius New Car Features 2004*, Toyota Motor Corporation, 2004.
8. N. Bianchi, S. Bolognani, and B. J. Chalmers, "Salient-Rotor PM Synchronous Motors for an Extended Flux-Weakening Operation Range," *IEEE Transactions on Industry Applications*, **36**(4), July/August 2000.
9. S. D. Rubira and M. D. McCulloch, "Control Method Comparison of Doubly Fed Wind Generators Connected to the Grid by Asymmetric Transmission Lines," *IEEE Transactions on Industry Applications*, **36**(4), July/August 2000.
10. F. Z. Peng, *Z-Source Inverter for Hybrid Electric and Fuel Cell Vehicles*, Michigan State University, March 2004.

APPENDIX A
DRIVE-CYCLE PLOTS SHOWING CONVERTER OPERATION

This appendix supplements Section 3.1.2 by further characterizing the operation of the voltage-buck/boost converter using Prius drive-cycle data.

All of the figures in this appendix plot the same five parameters: voltage and current output from the converter, accelerator pedal position output, brake-pedal position output, and vehicle speed. These five are identified in each plot. Note that positive current powers the PMSM and negative current charges the HEV battery. As in Section 3.1.2, units are omitted from the plots since only qualitative and/or trend-related relationships are discussed.

Figure A-1 shows a rapid acceleration and how this acceleration locked the boosted voltage at the 500 V maximum. The highest and most sustained current occurs during the acceleration. The figure also shows how, whenever the accelerator pedal is momentarily released, battery charging begins immediately. The braking in the last third of the plot produces a high, sustained charging current that closely mirrors the output obtained from the brake-pedal transducer.

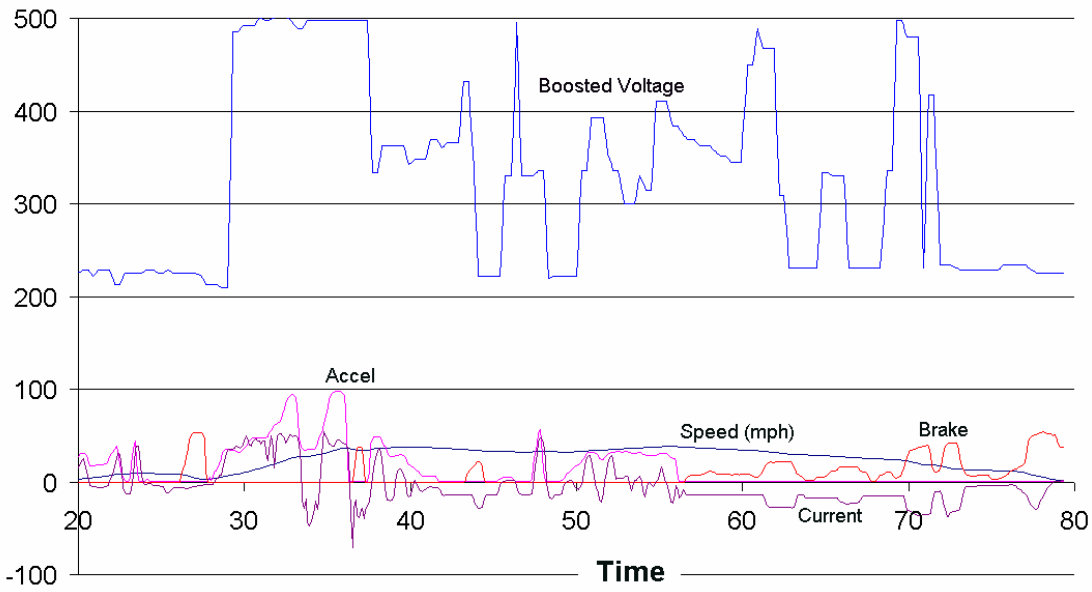

Fig. A-1. Drive-cycle plot chosen to illustrate a rapid acceleration (ANL data).

Figure A-2 shows a smooth, rapid acceleration that almost continuously maintains the boosted voltage at the maximum level. The sustained period of braking has a similar effect on the boosted voltage until the vehicle speed becomes low. The plotted data spans only ~30 s.

Figure A-3 was selected for its choppy converter output voltage. The boosted voltage stays at full output nearly continuously until the accelerator pedal output begins to level off. Immediately following this and until braking, the voltage and current fluctuate in a way that cannot be fully explained based on the data shown. The voltage has a 350-V floor most likely due to the vehicle speed (from 250–265 s, the speed ranged from 38.6–43.3 mph). A "zero-current zone" can be seen around 270 s where neither traction drive nor charging occurs. In the same timeframe, boosted voltage settled at 400 V, presumably as determined only by vehicle speed. Reduced accelerator pedal output results in charging current in several instances. The period of braking in the last fourth of the plot creates a charging current proportional to the amount of braking.

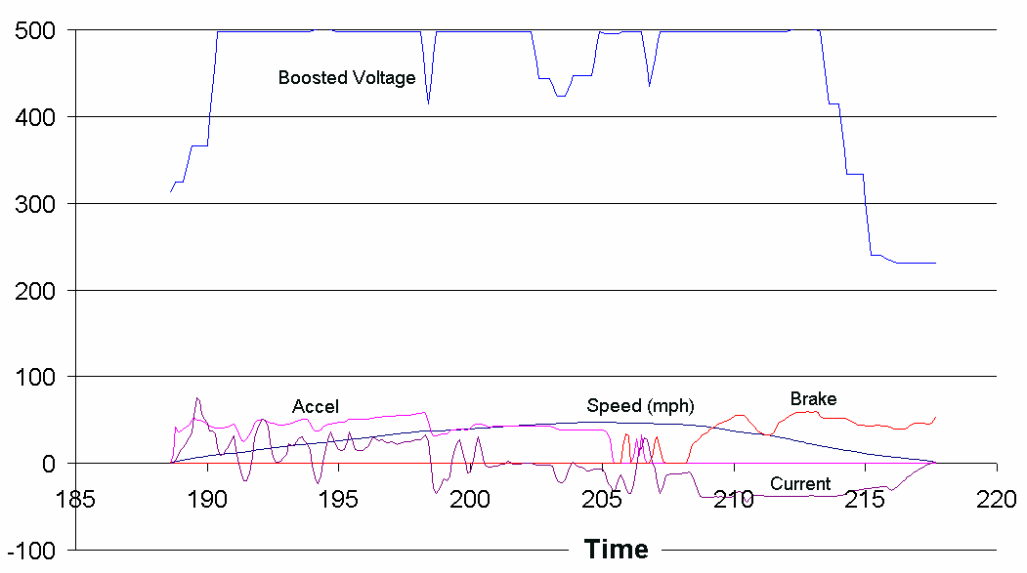

Fig. A-2. Second drive-cycle plot chosen to illustrate a rapid acceleration (ANL data).

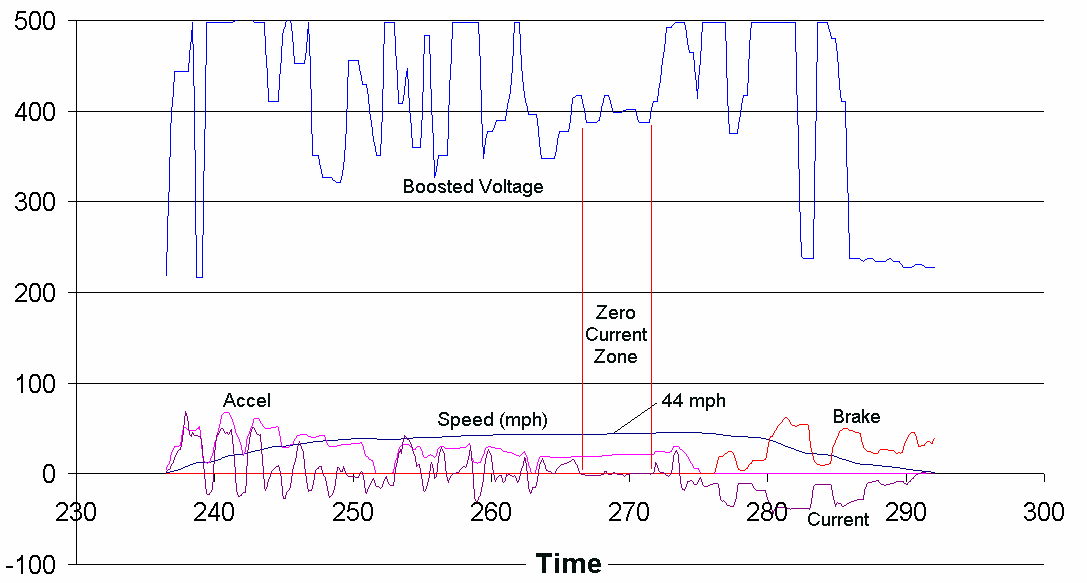

Fig. A-3. Drive-cycle plot chosen to illustrate a fluctuating boosted voltage (ANL data).

Figure A-4 was selected for its very gradual and slightly fluctuating acceleration. The slow acceleration had a dramatic effect on the boosted voltage, which was far lower than seen in preceding examples. There are many releases of the accelerator pedal with the corresponding reverse-current flow. As the speed continues to gradually increase, the boosted voltage floor rises from 215–315 V, and then to 350 V. The voltage fluctuations cannot be correlated with the corresponding current or other data shown in the figure. Because the fluctuations are very brief relative to other parameters, their significance is questionable. Therefore, Fig. A-5 was generated to compare vehicle speed to a smoothed-out[12] portion of the boosted voltage plot. Except for the flat topping of the voltage plot, there is clearly some level of

[12] A time-based, moving-window average was used around each point in the plot.

correlation. This flat topping would have been eliminated had the vehicle speed increased another ~10 mph.

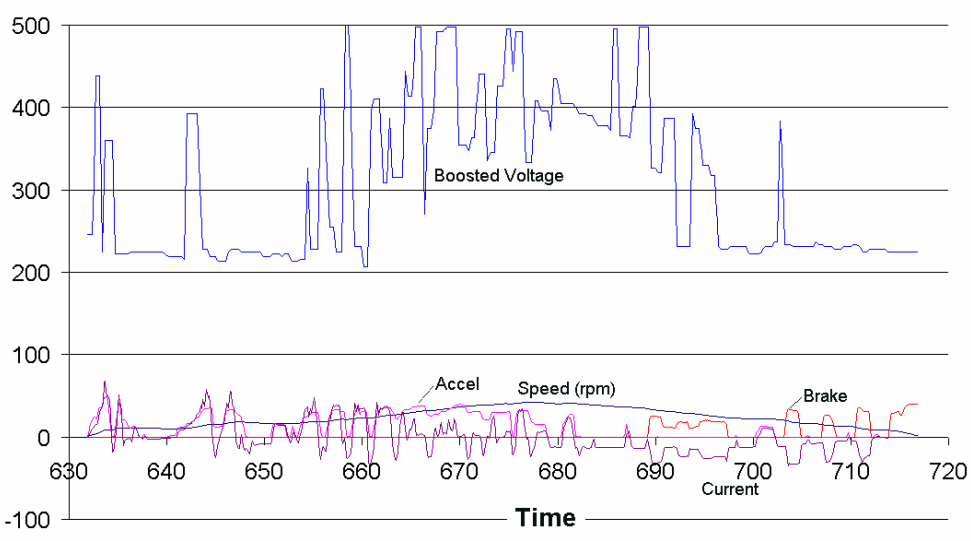

Fig. A-4. Drive-cycle plot chosen to illustrate a gradual acceleration (ANL data).

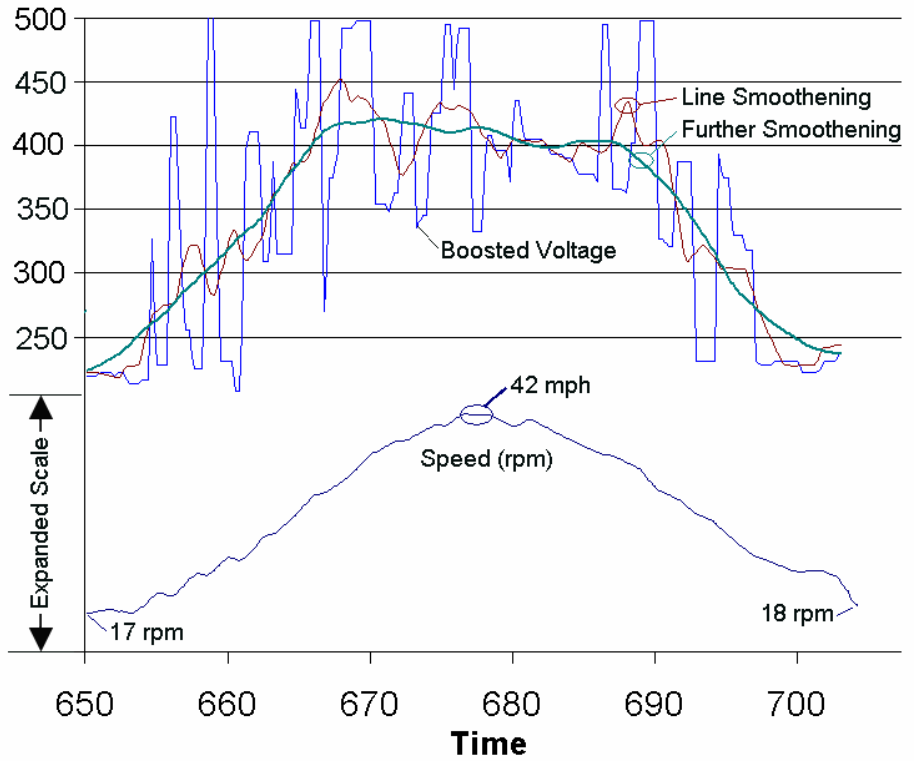

Fig. A-5. Consideration of curve smoothening on the boosted voltage plot (ANL data).

Spanning over three minutes (333 s.), Fig. A-6 is the longest-duration plot of drive-cycle data presented in this report. This figure was selected for its longer duration and continuously changing operating conditions (i.e., accelerator and brake positions). This produced a complex plot; however, trends of interest can still be seen. At first, the widely fluctuating boosted voltage with many very brief changes did not prove to be instructive or informative. Therefore, a time-based smoothening filter was applied. As indicated by the vertical, dotted lines, many of the peaks in the smoothed voltage plot correspond to

peaks in the speed; however, with some degree of offset. The offset suggests that the voltage peaks were instrumental in bringing the vehicle to the speed peaks. Not surprisingly, numerous current peaks also appeared to be responsible for bringing the vehicle to the speed peaks.

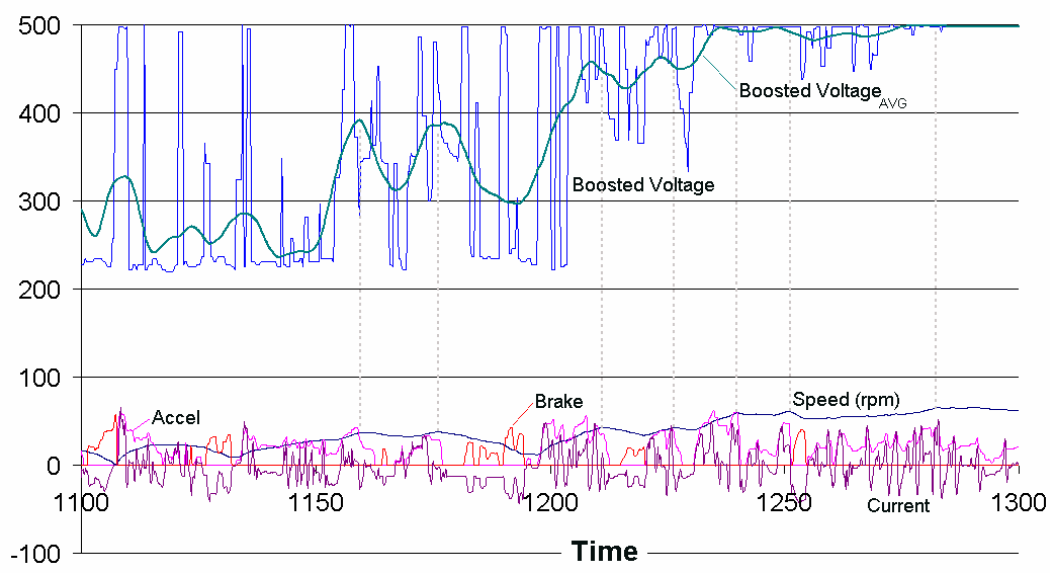

Fig. A-6. Drive-cycle plot chosen to illustrate a high level of change for each parameter (ANL data).

Figure A-7 was selected for its steady-state, high-speed conditions. Basically, only accelerator pedal position and current are changing. The positive current is made up of small spikes especially at times when the accelerator pedal is depressed. The absence of sustained positive current reflects how the vehicle operation is highly reliant on the engine and not the motor. Numerous, brief battery-charging surges are evident during pedal releases.

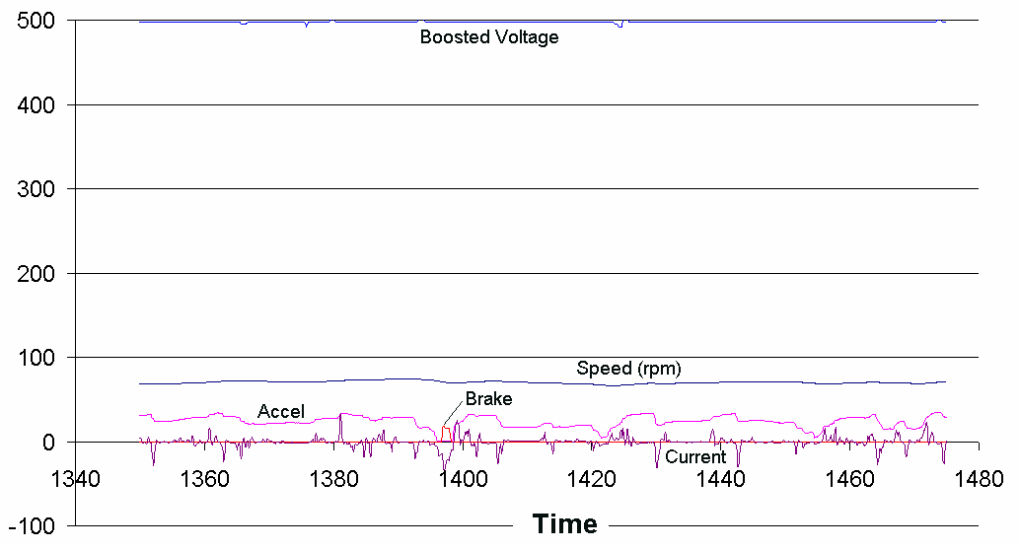

Fig. A-7. Drive-cycle plot chosen to illustrate a 70 mph sustained speed.

APPENDIX B
PRIUS PERFORMANCE-MAPPING DATA

Full design envelope testing of the operation of the 2004 Prius subsystems was described in Section 3.3. Section 3.3.3 provided efficiency-contour maps of the motor, inverter, and combined motor/inverter. This appendix provides the test data used to derive the contours and other summary data. Figure B.1 shows the actual speed-torque combinations at which all the data sets were recorded.

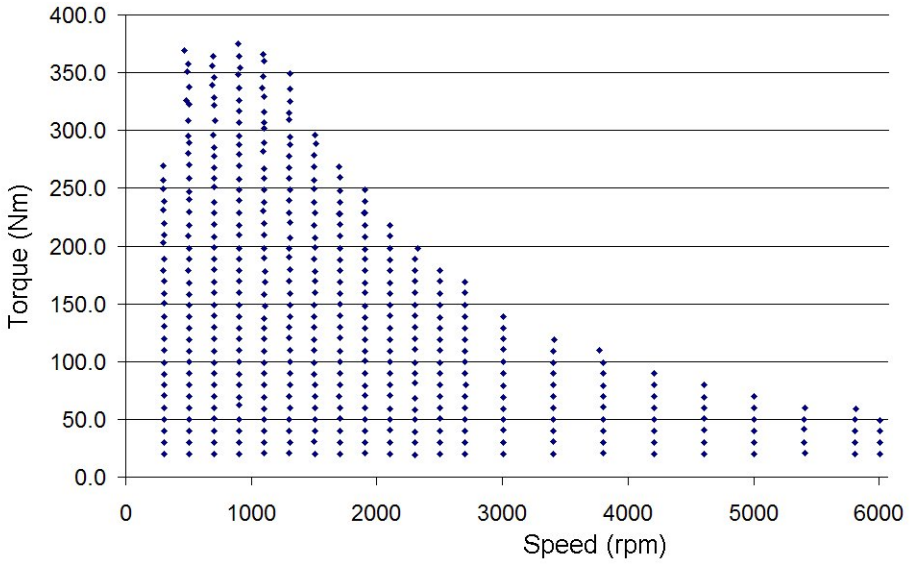

Fig. B.1. Speed-torque combinations at which data sets were obtained.

A selected portion of the mechanical, operational, electrical, and thermal data was prepared for presentation in this report. Table B-1 provides a selective sample of the most basic and significant measurements for characterizing the performance of the motor and inverter subsystems. To save on required space for the table, most of the thermal data was excluded and three-phase voltages and currents were averaged. Each row of data in the table is the average of generally 5–10 data sets; this averaging serves to eliminate data scatter, effects of noise, etc.

The table is sorted by increasing values of speed and then by increasing values of torque. The table is not arranged in the order by which the data was obtained. The three power columns provide the dc input to the inverter, the mechanical shaft power, and the three-phase power output from the inverter. The three efficiency columns provide the inverter, motor, and combined inverter-motor efficiencies. The two dc columns provide the inverter's dc power supply voltages and current levels. The two three-phase columns provide the inverter output voltages and currents averaged over the three phases.

The last column provides the stator temperature from one of three stator TCs that was embedded between two stator windings. This particular TC agreed closely with the other two at low temperatures, but during high temperature excursions provided the highest temperature reading (often higher than the other two by 5–15°C). This TC was located in the upper left region of the stator when viewing it with the motor casing end cap removed and with the three-phase terminals at the upper right. The other two TCs were located in the upper right and lower right. Even if data from all three TCs were provided, it would be of limited use since the actual temperatures were largely dependant on how long the motor had operated at a given load level before the data was obtained. Especially at low speeds and high shaft-load levels, data had to be obtained as quickly as possible while stator temperatures were rapidly climbing.

Table B-1. Mechanical, operational, electrical, and thermal data from the Prius performance-mapping test

Motor Conditions		Power (W)			Efficiency			dc Input to Inverter (rms)		Three-Phase Average from Inverter (rms)		Thermal (°C)
Speed (rpm)	Torque (Nm)	dc	Mech.	ac	Inverter	Motor	Total	V	I	V	I	Stator winding
297	269.7	15145	8398	13572	0.896	0.619	0.555	498.1	46.72	212.3	129.8	192.9
300	202.6	9665	6372	8522	0.882	0.748	0.660	498.2	28.57	211.3	97.8	69.9
300	249.2	13338	7838	11938	0.895	0.657	0.588	498.1	40.92	212.3	121.1	149.9
301	257.1	14086	8118	12647	0.898	0.642	0.576	498.1	44.21	212.2	123.1	172.1
302	179.2	8893	5685	8034	0.903	0.708	0.639	504.0	21.32	108.0	87.3	163.2
302	231.4	12120	7324	10778	0.889	0.680	0.604	498.2	38.13	212.4	114.1	108.0
303	20.2	891	642	769	0.863	0.836	0.721	503.9	3.68	81.7	14.8	58.6
303	30.2	1295	960	1123	0.867	0.855	0.741	504.1	4.29	82.7	19.9	91.2
303	59.8	2544	1903	2257	0.887	0.843	0.748	504.0	6.67	89.1	33.7	85.5
303	109.5	4810	3487	4342	0.903	0.803	0.725	504.1	11.51	99.1	54.9	99.6
303	119.4	5337	3802	4827	0.904	0.788	0.712	504.1	13.01	101.1	59.2	106.9
303	150.2	6978	4773	6318	0.905	0.756	0.684	504.1	16.57	104.7	73.0	124.5
303	169.4	8142	5391	7374	0.906	0.731	0.662	504.1	19.38	107.0	82.1	141.8
303	188.4	9664	5998	8770	0.907	0.684	0.621	504.0	23.32	110.4	92.9	179.9
303	209.2	10499	6638	9246	0.881	0.718	0.632	498.3	31.91	211.9	103.7	88.5
303	219.4	10976	6978	9772	0.890	0.714	0.636	498.2	34.96	211.6	105.9	76.8
304	40.0	1696	1272	1491	0.879	0.853	0.750	504.0	4.97	83.8	24.7	85.8
304	50.2	2138	1600	1895	0.887	0.844	0.748	504.0	5.81	86.6	29.5	85.1
304	71.0	3021	2266	2707	0.896	0.837	0.750	504.0	7.70	92.0	38.5	87.4
304	89.1	3846	2842	3463	0.901	0.821	0.739	504.0	9.26	95.9	46.1	94.5
304	158.5	7547	5054	6828	0.905	0.740	0.670	504.1	18.15	105.8	77.2	131.9
304	238.4	12556	7594	11218	0.893	0.677	0.605	498.1	37.98	211.9	114.0	134.5
305	80.0	3443	2557	3088	0.897	0.828	0.743	504.0	8.52	93.2	42.5	92.0
305	130.3	5875	4163	5305	0.903	0.785	0.709	504.1	14.10	102.3	63.8	111.5
305	138.8	6400	4442	5786	0.904	0.768	0.694	504.1	15.45	104.2	68.5	114.9
306	99.3	4309	3184	3878	0.900	0.821	0.739	504.0	10.42	97.7	50.4	96.2
468	369.3	26103	18140	25848	0.990	0.702	0.695	504.9	124.49	224.1	189.2	162.7

Table B-1. Mechanical, operational, electrical, and thermal data from the Prius performance-mapping test (cont'd)

Motor Conditions		Power (W)			Efficiency			dc Input to Inverter (rms)		Three-Phase Average from Inverter (rms)		Thermal (°C)
Speed (rpm)	Torque (Nm)	dc	Mech.	ac	Inverter	Motor	Total	V	I	V	I	Stator winding
485	325.9	24527	16585	23082	0.941	0.719	0.676	504.5	83.46	220.1	160.8	103.5
492	351.3	27133	18113	26483	0.976	0.684	0.668	504.4	109.10	222.1	180.7	140.2
497	357.5	27471	18613	27186	0.990	0.685	0.678	504.5	122.60	223.9	185.3	195.7
499	280.3	20250	14669	18914	0.934	0.776	0.724	499.8	43.51	215.9	134.2	64.3
500	308.2	24962	16161	22956	0.920	0.704	0.647	499.9	68.27	217.5	154.1	129.1
501	178.5	12653	9379	11821	0.934	0.794	0.741	504.0	27.60	128.9	86.8	165.8
501	208.6	15604	10963	14566	0.933	0.753	0.703	504.0	35.14	133.7	103.7	164.9
501	295.0	22465	15478	20946	0.932	0.739	0.689	500.0	50.40	216.6	143.8	86.4
502	70.0	4517	3686	4205	0.931	0.877	0.816	504.1	10.35	109.0	38.2	78.2
502	79.6	5171	4190	4818	0.932	0.870	0.810	504.1	11.68	111.3	42.4	82.1
502	188.8	13772	9936	12886	0.936	0.771	0.721	503.9	30.56	131.1	93.0	179.7
502	229.6	16078	12074	14966	0.931	0.807	0.751	500.9	38.27	215.8	108.2	78.4
502	289.0	21650	15219	20207	0.933	0.753	0.703	499.8	47.47	216.4	142.2	73.5
503	20.2	1363	1067	1235	0.906	0.864	0.783	504.1	4.37	95.2	14.7	69.9
503	30.2	1974	1592	1805	0.915	0.882	0.807	504.2	5.40	97.1	20.0	71.4
503	49.9	3224	2634	2973	0.922	0.886	0.817	504.1	7.94	104.5	29.4	73.5
503	60.0	3867	3165	3585	0.927	0.883	0.818	504.2	9.02	106.8	33.9	75.0
503	108.9	7141	5738	6679	0.935	0.859	0.804	504.1	15.75	116.9	54.7	91.9
503	119.0	7873	6275	7356	0.934	0.853	0.797	504.1	17.20	119.6	59.0	101.1
503	128.5	8543	6777	7976	0.934	0.850	0.793	504.1	18.52	121.0	62.9	108.8
503	148.8	10091	7848	9435	0.935	0.832	0.778	504.0	22.01	124.4	72.2	125.6
503	240.6	17418	12686	16243	0.933	0.781	0.728	501.0	41.59	215.9	114.1	107.7
503	247.0	18231	13011	16990	0.932	0.766	0.714	500.9	41.99	215.8	119.1	127.5
503	258.9	19811	13653	18417	0.930	0.741	0.689	500.9	45.16	215.7	128.7	149.9
503	337.3	27384	17782	26561	0.970	0.670	0.649	504.6	99.60	221.6	171.9	157.1
504	40.1	2590	2118	2382	0.920	0.889	0.818	504.2	6.65	101.8	24.8	72.7
504	89.7	5843	4740	5443	0.931	0.871	0.811	504.1	13.06	113.3	46.6	86.4
504	157.6	10809	8330	10116	0.936	0.824	0.771	504.0	23.72	125.9	76.5	144.7

Table B-1. Mechanical, operational, electrical, and thermal data from the Prius performance-mapping test (cont'd)

Motor Conditions		Power (W)			Efficiency			dc Input to Inverter (rms)		Three-Phase Average from Inverter (rms)		Thermal (°C)
Speed (rpm)	Torque (Nm)	dc	Mech.	ac	Inverter	Motor	Total	V	I	V	I	Stator winding
505	99.5	6497	5265	6063	0.933	0.868	0.810	504.1	14.41	115.2	50.7	88.7
505	139.1	9385	7362	8773	0.935	0.839	0.784	504.1	20.48	123.4	67.9	121.2
505	197.8	14406	10463	13439	0.933	0.779	0.726	504.0	32.16	131.9	97.5	141.9
505	218.3	16576	11555	15453	0.932	0.748	0.697	504.0	38.60	135.1	108.5	193.2
505	270.5	21825	14308	20275	0.929	0.706	0.656	500.9	50.60	216.1	138.6	179.2
507	167.7	11775	8906	11007	0.935	0.809	0.756	504.0	25.60	127.6	81.9	153.9
508	323.0	25911	17217	24456	0.944	0.704	0.664	503.8	87.13	220.5	161.6	106.3
687	339.2	31671	24435	31265	0.987	0.782	0.771	504.8	116.87	226.6	175.6	146.1
692	356.0	34568	25823	34121	0.987	0.757	0.747	504.8	121.40	226.6	187.2	174.7
693	364.5	36181	26458	35628	0.985	0.744	0.732	504.7	122.88	227.2	190.7	170.7
697	296.2	28979	21639	27697	0.956	0.781	0.747	504.7	87.73	225.0	147.0	102.5
700	346.1	34669	25394	34218	0.987	0.742	0.733	504.7	119.59	227.2	181.3	192.7
701	129.6	11491	9523	10920	0.950	0.872	0.829	503.8	24.29	141.3	64.4	117.6
701	159.8	14625	11741	13933	0.953	0.843	0.803	503.7	30.62	145.6	78.8	142.8
701	198.7	18807	14595	17853	0.949	0.818	0.776	503.7	39.76	148.6	96.7	159.8
701	237.7	22779	17455	21585	0.948	0.809	0.766	500.8	50.58	220.1	115.4	153.2
702	40.0	3502	2944	3284	0.938	0.896	0.841	504.0	8.30	116.2	25.1	97.8
702	59.6	5162	4385	4875	0.944	0.900	0.850	503.9	11.43	122.9	33.9	95.8
702	228.8	21717	16822	20561	0.947	0.818	0.775	500.9	47.99	220.2	110.1	137.9
702	321.4	33383	23650	32317	0.968	0.732	0.709	504.6	97.87	225.8	166.2	183.3
703	20.2	1811	1487	1684	0.930	0.883	0.821	504.0	5.11	106.4	14.8	106.4
703	30.2	2661	2224	2487	0.935	0.894	0.836	504.0	6.74	112.3	20.2	99.6
703	179.8	16779	13252	15953	0.951	0.831	0.790	503.7	35.65	146.6	87.6	167.8
703	188.4	17604	13878	16703	0.949	0.831	0.788	503.7	37.15	146.6	91.5	141.6
703	251.0	24627	18486	23296	0.946	0.794	0.751	500.8	55.28	220.5	122.9	171.0
703	258.7	25752	19064	24363	0.946	0.783	0.740	500.8	57.09	220.5	128.2	187.0
703	267.7	26635	19719	25165	0.945	0.784	0.740	500.7	60.15	220.8	134.3	131.7
703	277.5	28555	20458	26962	0.944	0.759	0.716	500.7	65.24	221.3	140.8	170.1

Table B-1. Mechanical, operational, electrical, and thermal data from the Prius performance-mapping test (cont'd)

Motor Conditions		Power (W)			Efficiency			dc Input to Inverter (rms)		Three-Phase Average from Inverter (rms)		Thermal (°C)
Speed (rpm)	Torque (Nm)	dc	Mech.	ac	Inverter	Motor	Total	V	I	V	I	Stator winding
703	328.2	33845	24169	33147	0.979	0.729	0.714	504.5	104.44	225.9	167.6	206.8
704	79.4	6892	5856	6537	0.949	0.896	0.850	503.9	14.93	128.6	42.4	97.6
704	89.7	7844	6612	7451	0.950	0.887	0.843	503.9	16.73	130.6	46.9	101.5
704	119.6	10616	8820	10082	0.950	0.875	0.831	503.8	22.34	138.6	59.9	114.9
704	139.6	12392	10302	11771	0.950	0.875	0.831	503.8	25.84	142.0	68.4	123.1
704	149.0	13430	10988	12746	0.949	0.862	0.818	503.7	28.11	144.7	73.5	135.4
704	169.2	15468	12473	14690	0.950	0.849	0.806	503.7	32.70	147.9	83.0	148.2
704	218.9	21520	16157	20390	0.947	0.792	0.751	503.8	46.18	154.5	109.4	189.3
704	285.5	27426	21048	25919	0.945	0.812	0.767	504.7	74.47	224.0	140.0	51.7
705	50.5	4375	3728	4118	0.941	0.905	0.852	503.9	9.94	119.8	29.9	96.5
705	69.8	6051	5155	5735	0.948	0.899	0.852	503.9	13.20	125.8	38.4	96.9
705	99.0	8768	7312	8315	0.948	0.880	0.834	503.8	18.72	133.2	51.1	104.6
705	108.8	9605	8042	9110	0.949	0.883	0.837	503.8	20.18	136.5	55.2	109.2
705	208.0	19804	15371	18757	0.947	0.820	0.776	503.7	41.86	150.7	101.1	173.6
715	308.2	30100	23087	29611	0.984	0.780	0.767	504.7	108.79	226.3	158.6	141.9
892	348.1	39620	32546	39205	0.990	0.830	0.822	503.5	124.88	231.0	182.5	186.8
892	374.8	40929	35011	40418	0.988	0.866	0.856	501.2	127.04	229.8	191.4	98.7
900	139.2	15423	13128	14796	0.959	0.887	0.851	503.7	31.89	158.4	68.0	120.1
900	257.9	30836	24315	29442	0.955	0.826	0.789	500.6	67.56	224.9	128.0	133.5
901	148.8	16878	14048	16102	0.954	0.872	0.832	503.6	34.99	162.0	74.0	125.2
901	188.5	21684	17803	20794	0.959	0.856	0.821	503.7	45.21	167.0	92.7	163.7
901	337.1	40151	31813	39408	0.981	0.808	0.793	503.5	112.79	229.6	174.3	128.3
902	99.9	10922	9441	10472	0.959	0.902	0.864	503.8	22.98	150.6	51.0	101.1
902	169.4	19483	16008	18672	0.958	0.857	0.822	503.6	40.30	165.4	84.3	142.4
902	217.8	25331	20579	24284	0.959	0.847	0.812	500.8	54.49	224.2	105.9	130.9
902	228.8	26915	21627	25765	0.957	0.839	0.804	500.8	58.37	224.5	111.7	154.5
902	239.4	28435	22623	27205	0.957	0.832	0.796	500.7	61.09	224.6	117.7	174.0
902	279.1	34960	26375	33370	0.955	0.790	0.754	500.6	79.43	226.1	142.1	194.0

Table B-1. Mechanical, operational, electrical, and thermal data from the Prius performance-mapping test (cont'd)

Motor Conditions		Power (W)			Efficiency			dc Input to Inverter (rms)		Three-Phase Average from Inverter (rms)		Thermal (°C)
Speed (rpm)	Torque (Nm)	dc	Mech.	ac	Inverter	Motor	Total	V	I	V	I	Stator winding
902	288.1	36287	27229	34531	0.952	0.789	0.750	500.6	85.00	226.4	149.1	160.9
903	20.2	2321	1908	2181	0.940	0.875	0.822	503.9	5.96	122.2	15.0	105.8
903	29.8	3326	2821	3156	0.949	0.894	0.848	503.9	7.81	125.3	20.1	100.4
903	40.0	4415	3787	4205	0.952	0.901	0.858	503.8	9.95	131.5	25.2	99.0
903	50.1	5459	4735	5228	0.958	0.906	0.867	503.8	11.94	136.7	29.8	97.2
903	62.6	6679	5925	6390	0.957	0.927	0.887	503.8	14.46	137.9	34.8	96.7
903	178.4	20501	16874	19647	0.958	0.859	0.823	503.5	43.01	165.3	87.3	154.0
903	248.4	29760	23502	28456	0.956	0.826	0.790	500.7	65.77	225.3	121.7	190.3
903	269.9	32824	25520	31324	0.954	0.815	0.778	500.6	72.43	225.4	135.4	161.5
903	306.8	36776	29046	35760	0.972	0.812	0.790	503.4	99.81	229.0	153.3	103.0
904	128.8	14315	12195	13774	0.962	0.885	0.852	503.7	29.48	157.9	64.3	114.7
904	295.2	34547	27962	33127	0.959	0.844	0.809	503.3	85.64	227.8	143.8	43.5
904	325.9	41078	30861	39863	0.970	0.774	0.751	503.4	103.61	229.0	165.4	184.4
905	69.4	7571	6581	7218	0.953	0.912	0.869	503.8	16.25	143.2	38.2	97.0
905	79.9	8679	7579	8337	0.961	0.909	0.873	503.7	18.27	146.4	42.8	97.8
905	89.4	9718	8474	9339	0.961	0.907	0.872	503.7	20.28	146.7	46.7	99.6
905	109.5	11967	10384	11532	0.964	0.901	0.868	503.7	24.86	152.9	55.2	104.5
905	159.4	18004	15109	17302	0.961	0.873	0.839	503.6	37.25	162.4	78.3	132.5
905	197.8	23301	18768	22336	0.959	0.840	0.806	503.6	48.57	168.9	98.5	172.3
905	317.0	38709	30076	37727	0.975	0.797	0.777	503.4	102.53	229.2	159.0	142.9
906	120.1	13340	11398	12795	0.959	0.891	0.854	503.7	27.62	156.8	60.6	109.4
906	209.6	24763	19898	23717	0.958	0.839	0.804	503.5	51.61	170.7	104.9	186.2
906	364.6	43683	34608	42998	0.984	0.805	0.793	503.9	126.14	231.3	190.9	150.5
913	353.9	43617	33848	42934	0.984	0.789	0.777	503.7	123.41	230.8	188.6	156.1
1089	337.0	46589	38446	45849	0.984	0.839	0.825	501.1	122.72	233.3	175.4	148.0
1096	230.0	30727	26416	29650	0.965	0.891	0.860	500.4	64.96	228.3	107.8	86.4
1096	366.3	51279	42077	50509	0.985	0.833	0.821	501.7	134.30	234.4	191.3	192.0
1097	282.1	39656	32413	38151	0.962	0.850	0.818	500.3	87.29	230.4	137.3	194.4

Table B-1. Mechanical, operational, electrical, and thermal data from the Prius performance-mapping test (cont'd)

Motor Conditions		Power (W)			Efficiency			dc Input to Inverter (rms)		Three-Phase Average from Inverter (rms)		Thermal (°C)
Speed (rpm)	Torque (Nm)	dc	Mech.	ac	Inverter	Motor	Total	V	I	V	I	Stator winding
1097	346.4	47779	39817	47151	0.987	0.845	0.834	501.2	132.09	234.5	183.7	206.0
1100	359.7	48612	41456	47925	0.986	0.865	0.853	501.8	131.03	233.6	188.4	130.6
1101	267.3	38166	30817	36774	0.964	0.838	0.807	500.3	85.33	230.1	131.8	181.1
1102	119.6	15652	13804	15138	0.967	0.912	0.882	503.6	32.12	169.3	59.0	88.9
1102	237.6	32303	27430	31158	0.965	0.880	0.849	500.4	68.76	228.6	112.7	100.4
1102	258.3	36100	29820	34786	0.964	0.857	0.826	500.3	78.55	229.2	125.3	132.4
1102	307.2	43249	35478	42288	0.978	0.839	0.820	501.3	108.06	232.2	154.1	108.7
1103	158.3	21161	18281	20443	0.966	0.894	0.864	503.6	43.35	177.7	77.4	138.3
1103	248.9	34232	28766	32994	0.964	0.872	0.840	500.4	73.76	229.0	119.1	114.7
1103	289.8	42243	33478	40658	0.962	0.823	0.793	500.2	96.10	231.4	145.6	172.2
1103	329.6	46775	38095	45983	0.983	0.829	0.815	501.3	121.10	233.3	170.7	187.0
1104	20.4	2827	2356	2686	0.950	0.877	0.834	503.8	6.98	135.4	14.7	69.3
1104	30.3	4101	3505	3923	0.957	0.893	0.855	503.8	9.41	137.9	20.1	68.7
1104	40.1	5367	4644	5144	0.958	0.903	0.865	503.8	11.91	142.8	25.0	68.9
1104	50.1	6603	5794	6380	0.966	0.908	0.877	503.8	14.09	150.9	29.6	69.8
1104	59.4	7766	6867	7493	0.965	0.917	0.884	503.7	16.50	149.4	33.7	70.6
1104	69.2	9115	8009	8784	0.964	0.912	0.879	503.7	19.26	155.7	37.8	72.1
1104	79.6	10407	9205	10074	0.968	0.914	0.884	503.6	21.72	161.5	42.3	73.7
1104	89.5	11671	10352	11298	0.968	0.916	0.887	503.6	24.25	160.7	46.3	78.0
1104	128.7	16848	14886	16279	0.966	0.914	0.884	503.7	34.77	173.3	63.2	94.6
1104	198.0	27227	22899	26285	0.965	0.871	0.841	503.4	56.33	184.9	97.7	166.0
1104	209.4	29563	24211	28504	0.964	0.849	0.819	503.4	61.99	188.1	105.7	177.0
1104	316.1	45409	36566	44559	0.981	0.821	0.805	501.2	115.20	233.2	163.5	148.5
1105	99.2	13016	11481	12566	0.965	0.914	0.882	503.6	26.96	163.9	50.4	81.7
1105	109.3	14242	12660	13759	0.966	0.920	0.889	503.6	29.39	166.5	54.4	84.2
1105	137.1	18169	15882	17544	0.966	0.905	0.874	503.6	37.40	172.3	66.6	100.9
1105	189.5	25876	21932	24954	0.964	0.879	0.848	503.4	53.31	182.9	93.0	157.2
1105	219.2	30816	25364	29675	0.963	0.855	0.823	503.3	64.65	189.3	110.1	194.1

Table B-1. Mechanical, operational, electrical, and thermal data from the Prius performance-mapping test (cont'd)

Motor Conditions		Power (W)			Efficiency			dc Input to Inverter (rms)		Three-Phase Average from Inverter (rms)		Thermal (°C)
Speed (rpm)	Torque (Nm)	dc	Mech.	ac	Inverter	Motor	Total	V	I	V	I	Stator winding
1105	301.5	42211	34896	41051	0.972	0.850	0.827	501.3	103.54	231.7	149.7	77.4
1106	148.4	19669	17190	19050	0.969	0.902	0.874	503.7	40.29	175.2	72.4	133.0
1107	168.6	22889	19556	22134	0.967	0.884	0.854	503.5	47.28	179.6	82.4	143.3
1107	177.9	24365	20624	23479	0.964	0.878	0.846	503.5	50.89	182.7	88.3	147.2
1297	258.9	41788	35178	40505	0.969	0.868	0.842	500.3	90.82	233.6	127.3	147.6
1299	169.4	26456	23044	25581	0.967	0.901	0.871	503.8	53.91	193.8	82.2	127.1
1301	120.2	18186	16385	17847	0.981	0.918	0.901	503.6	37.24	183.3	59.3	94.0
1301	309.3	50326	42142	49358	0.981	0.854	0.837	501.7	118.33	235.5	156.7	137.4
1302	228.9	36584	31234	35512	0.971	0.880	0.854	500.4	77.18	232.8	111.5	135.1
1302	267.8	43640	36535	42307	0.969	0.864	0.837	500.3	96.18	233.8	132.9	165.7
1302	278.1	45978	37933	44558	0.969	0.851	0.825	500.2	101.45	234.3	140.0	189.3
1302	315.0	53418	42960	52405	0.981	0.820	0.804	501.7	122.76	235.8	167.4	183.7
1303	20.4	3309	2784	3131	0.946	0.889	0.842	503.8	7.83	141.7	14.7	81.9
1303	49.8	7725	6804	7442	0.963	0.914	0.881	503.9	16.40	159.0	29.5	77.1
1303	69.6	10757	9497	10362	0.963	0.916	0.883	503.7	22.47	166.1	38.2	78.4
1303	130.0	20076	17740	19415	0.967	0.914	0.884	503.6	41.10	185.6	64.0	102.9
1303	197.8	31327	26991	30440	0.972	0.887	0.862	503.1	64.67	199.5	96.9	160.0
1304	40.0	6283	5458	6013	0.957	0.908	0.869	503.6	13.79	156.8	25.0	77.1
1304	190.2	30090	25990	29113	0.968	0.893	0.864	503.4	61.77	198.0	93.0	152.2
1304	239.2	38559	32678	37413	0.970	0.873	0.848	500.4	82.29	233.9	116.9	154.7
1305	29.9	4754	4082	4552	0.958	0.897	0.859	503.8	10.53	148.1	20.0	78.0
1305	80.1	12318	10959	11914	0.967	0.920	0.890	503.9	25.62	173.1	42.6	79.4
1305	100.1	15407	13686	14859	0.964	0.921	0.888	503.6	31.75	178.4	50.9	86.2
1305	139.2	21509	19036	21050	0.979	0.904	0.885	503.3	44.12	187.5	68.4	107.7
1305	149.3	22877	20413	22184	0.970	0.920	0.892	503.5	46.56	189.5	72.1	114.7
1305	220.3	35875	30131	34810	0.970	0.866	0.840	503.0	75.37	204.5	111.0	189.1
1305	294.5	48046	40260	46711	0.972	0.862	0.838	501.8	107.86	235.1	148.1	87.8
1305	325.5	53902	44488	52914	0.982	0.841	0.825	501.5	125.52	235.4	174.5	117.5

Table B-1. Mechanical, operational, electrical, and thermal data from the Prius performance-mapping test (cont'd)

Motor Conditions		Power (W)			Efficiency			dc Input to Inverter (rms)		Three-Phase Average from Inverter (rms)		Thermal (°C)
Speed (rpm)	Torque (Nm)	dc	Mech.	ac	Inverter	Motor	Total	V	I	V	I	Stator winding
1305	335.7	55954	45889	55029	0.983	0.834	0.820	501.5	131.62	235.9	183.4	180.2
1306	59.9	9200	8194	8943	0.972	0.916	0.891	503.7	19.32	162.6	34.0	77.6
1306	89.6	13623	12260	13255	0.973	0.925	0.900	503.2	28.20	176.1	46.5	83.0
1306	158.7	24629	21705	23974	0.973	0.905	0.881	503.3	50.43	193.2	77.6	118.1
1306	179.8	28280	24599	27389	0.969	0.898	0.870	503.5	58.05	196.1	87.7	143.4
1306	248.9	39613	34045	38442	0.970	0.886	0.859	500.4	85.45	234.3	120.9	114.6
1307	110.1	16815	15072	16281	0.968	0.926	0.896	503.7	34.44	181.2	55.1	90.4
1307	207.4	33340	28402	32418	0.972	0.876	0.852	503.0	69.69	202.7	104.3	173.6
1307	349.3	55774	47827	54916	0.985	0.872	0.858	501.7	134.65	236.5	186.2	124.0
1312	288.0	48430	39567	46928	0.969	0.843	0.817	500.2	105.68	236.5	147.3	186.6
1500	88.9	15502	13965	15087	0.973	0.926	0.901	504.3	31.70	186.5	46.0	71.5
1501	99.1	17272	15580	16828	0.974	0.926	0.902	504.4	35.26	191.9	50.5	78.1
1502	218.0	39882	34306	38900	0.975	0.882	0.860	504.0	80.99	219.1	110.4	174.4
1502	237.9	43408	37430	42373	0.976	0.883	0.862	500.2	90.42	237.1	116.8	122.0
1502	249.7	45221	39301	44128	0.976	0.891	0.869	500.2	94.61	237.4	122.1	141.1
1502	257.2	47121	40473	45947	0.975	0.881	0.859	500.2	98.14	237.7	127.1	161.9
1502	278.6	51887	43838	50573	0.975	0.867	0.845	500.1	110.28	238.9	141.0	142.4
1503	30.6	5533	4824	5349	0.967	0.902	0.872	504.4	12.16	159.0	20.2	58.9
1503	109.4	19067	17221	18565	0.974	0.928	0.903	504.5	38.83	193.2	54.5	81.6
1503	119.2	20760	18765	20248	0.975	0.927	0.904	504.6	42.08	195.3	58.7	84.5
1503	129.7	22668	20422	22102	0.975	0.924	0.901	504.4	46.05	201.1	63.8	87.7
1503	138.9	24391	21863	23722	0.973	0.922	0.896	504.5	49.30	200.5	67.5	94.0
1503	148.9	26079	23452	25426	0.975	0.922	0.899	504.4	52.66	203.3	71.8	99.2
1503	188.9	33580	29735	32766	0.976	0.908	0.886	504.3	67.82	211.4	91.4	128.5

Table B-1. Mechanical, operational, electrical, and thermal data from the Prius performance-mapping test (cont'd)

Motor Conditions		Power (W)			Efficiency			dc Input to Inverter (rms)		Three-Phase Average from Inverter (rms)		Thermal (°C)
Speed (rpm)	Torque (Nm)	dc	Mech.	ac	Inverter	Motor	Total	V	I	V	I	Stator winding
1503	268.7	50187	42318	48931	0.975	0.865	0.843	500.1	105.47	238.3	134.8	185.7
1504	20.3	3794	3199	3637	0.958	0.880	0.843	504.6	8.80	152.3	14.6	57.8
1504	49.9	8771	7859	8529	0.972	0.921	0.896	504.4	18.47	176.5	29.6	61.4
1504	69.4	12185	10940	11850	0.973	0.923	0.898	504.5	25.22	180.0	37.8	67.9
1504	159.3	28049	25101	27356	0.975	0.918	0.895	504.4	56.72	207.2	77.2	105.7
1504	177.7	31455	27995	30681	0.975	0.912	0.890	504.4	63.51	208.6	85.2	121.3
1504	228.7	42051	36035	41021	0.975	0.878	0.857	503.9	85.30	218.2	113.5	191.0
1504	295.8	55755	46601	54131	0.971	0.861	0.836	500.0	133.40	230.3	153.5	201.1
1505	40.2	7198	6343	6972	0.969	0.910	0.881	504.4	15.40	169.3	25.0	59.8
1505	60.2	10633	9497	10319	0.970	0.920	0.893	504.5	22.25	174.3	34.0	64.4
1505	169.4	29842	26712	29126	0.976	0.917	0.895	504.3	60.28	207.5	81.8	110.9
1505	206.8	37395	32605	36515	0.976	0.893	0.872	504.0	75.72	215.1	101.2	164.5
1506	198.9	35915	31375	35039	0.976	0.895	0.874	504.1	72.71	215.3	98.6	141.1
1507	79.6	13945	12571	13542	0.971	0.928	0.901	504.5	28.55	187.8	42.5	68.7
1512	288.8	53954	45737	52403	0.971	0.873	0.848	500.0	120.66	234.7	147.2	148.0
1701	228.0	46043	40622	45119	0.980	0.900	0.882	500.1	94.13	240.2	112.5	125.4
1702	69.8	13845	12445	13487	0.974	0.923	0.899	504.5	28.34	188.2	38.6	90.1
1702	268.5	55479	47866	54376	0.980	0.881	0.863	500.0	112.82	241.4	135.5	197.9
1703	19.9	4173	3556	4022	0.964	0.884	0.852	504.6	9.46	160.6	14.6	107.9
1703	50.3	10026	8983	9751	0.973	0.921	0.896	504.4	20.78	173.1	30.6	91.7
1703	60.1	11862	10731	11587	0.977	0.926	0.905	504.4	24.42	183.9	34.3	90.4
1703	79.7	15714	14223	15358	0.977	0.926	0.905	504.2	32.06	192.5	42.7	90.3
1703	99.5	19646	17762	19226	0.979	0.924	0.904	504.3	39.85	202.9	51.3	92.0
1703	158.9	31306	28347	30698	0.981	0.923	0.905	504.1	63.06	218.2	76.9	117.4
1703	247.8	50830	44200	49777	0.979	0.888	0.870	500.1	104.10	240.8	124.3	164.3
1704	40.0	8053	7146	7806	0.969	0.915	0.887	504.5	16.96	169.5	25.5	95.3
1704	129.5	25413	23110	24879	0.979	0.929	0.909	504.2	51.26	207.7	63.4	100.8
1704	139.9	27480	24968	26904	0.979	0.928	0.909	504.2	55.26	210.9	68.0	107.0

Table B-1. Mechanical, operational, electrical, and thermal data from the Prius performance-mapping test (cont'd)

Motor Conditions		Power (W)			Efficiency			dc Input to Inverter (rms)		Three-Phase Average from Inverter (rms)		Thermal (°C)
Speed (rpm)	Torque (Nm)	dc	Mech.	ac	Inverter	Motor	Total	V	I	V	I	Stator winding
1704	149.4	29565	26658	28960	0.980	0.921	0.902	504.1	59.47	212.9	72.4	112.3
1704	168.7	33465	30112	32763	0.979	0.919	0.900	504.0	67.32	215.5	81.0	126.0
1704	178.6	35573	31876	34878	0.980	0.914	0.896	504.0	71.53	218.7	86.0	134.7
1704	197.6	39572	35273	38830	0.981	0.908	0.891	503.9	79.94	224.5	95.7	155.4
1704	238.0	48651	42484	47657	0.980	0.891	0.873	500.1	99.41	240.6	118.7	144.5
1705	30.3	6141	5407	5959	0.970	0.907	0.881	504.6	13.19	161.5	20.8	98.7
1705	90.1	17884	16093	17491	0.978	0.920	0.900	504.3	36.33	200.3	47.4	90.6
1705	109.3	21533	19524	21042	0.977	0.928	0.907	504.3	43.49	202.2	55.1	96.9
1705	218.5	44372	39019	43546	0.981	0.896	0.879	503.8	89.72	230.9	107.9	177.3
1705	227.8	46617	40677	45685	0.980	0.890	0.873	503.8	93.79	229.0	111.7	192.0
1705	259.7	53594	46384	52495	0.979	0.884	0.866	500.0	109.53	241.7	130.9	183.4
1706	120.2	23751	21480	23229	0.978	0.925	0.904	504.2	47.89	208.5	59.9	98.4
1706	188.2	37702	33642	37002	0.981	0.909	0.892	504.0	75.96	223.3	91.3	149.7
1707	208.4	42159	37278	41335	0.980	0.902	0.884	503.9	84.96	226.3	101.5	171.1
1900	229.0	51348	45578	50442	0.982	0.904	0.888	500.0	104.20	242.1	118.3	144.5
1902	40.0	8972	7973	8723	0.972	0.914	0.889	504.3	18.76	172.7	26.5	61.8
1902	109.1	23774	21724	23315	0.981	0.932	0.914	504.1	47.96	212.4	54.7	90.1
1903	30.0	6834	5990	6618	0.968	0.905	0.877	504.3	14.61	166.5	21.6	60.8
1903	70.4	15451	14033	15098	0.977	0.929	0.908	504.2	31.55	198.1	38.4	70.5
1903	79.0	17322	15749	16934	0.978	0.930	0.909	504.2	35.29	192.6	43.5	74.2
1903	89.6	19621	17870	19183	0.978	0.932	0.911	504.2	39.89	194.1	48.8	77.1
1904	59.6	13158	11883	12865	0.978	0.924	0.903	504.2	26.96	188.8	34.3	69.6
1904	119.2	25992	23765	25542	0.983	0.930	0.914	504.0	52.44	219.3	59.1	92.8
1904	129.1	27939	25748	27430	0.982	0.939	0.922	504.1	56.24	219.4	62.9	100.7
1904	167.8	36829	33477	36215	0.983	0.924	0.909	503.9	74.60	228.6	81.1	131.8
1904	178.8	39346	35663	38709	0.984	0.921	0.906	503.8	79.41	231.6	86.2	141.2
1904	208.1	46503	41502	45726	0.983	0.908	0.892	503.9	93.46	231.3	102.0	167.6
1904	238.3	54123	47518	53193	0.983	0.893	0.878	499.9	109.81	242.6	124.3	170.8

Table B-1. Mechanical, operational, electrical, and thermal data from the Prius performance-mapping test (cont'd)

Motor Conditions		Power (W)			Efficiency			dc Input to Inverter (rms)		Three-Phase Average from Inverter (rms)		Thermal (°C)
Speed (rpm)	Torque (Nm)	dc	Mech.	ac	Inverter	Motor	Total	V	I	V	I	Stator winding
1904	249.0	57109	49658	56146	0.983	0.885	0.870	499.9	115.74	241.2	130.4	193.8
1905	20.6	4796	4113	4615	0.962	0.891	0.858	504.4	10.55	159.5	16.7	60.3
1905	148.4	32323	29610	31805	0.984	0.931	0.916	504.1	65.28	225.0	71.8	119.7
1905	159.4	34891	31803	34335	0.984	0.926	0.912	503.9	70.62	229.3	77.1	124.4
1905	197.2	43791	39343	43045	0.983	0.914	0.898	504.0	88.21	230.3	95.9	159.0
1905	218.1	49006	43538	48200	0.984	0.903	0.888	503.7	98.55	232.9	107.4	177.5
1905	228.6	51714	45611	50837	0.983	0.897	0.882	503.6	103.82	232.3	114.3	190.3
1906	50.1	11149	10003	10832	0.972	0.923	0.897	504.2	22.98	173.9	32.3	63.2
1906	100.4	21850	20046	21422	0.980	0.936	0.918	504.1	44.17	209.3	51.0	86.0
1906	138.4	30119	27633	29597	0.983	0.934	0.917	504.1	60.57	222.1	67.3	113.4
1906	189.0	41874	37730	41171	0.983	0.916	0.901	503.9	84.33	230.2	91.5	152.4
2102	217.8	54387	47946	53434	0.982	0.897	0.882	503.5	109.03	233.1	117.1	180.7
2103	79.5	19025	17510	18683	0.982	0.937	0.920	504.1	38.64	211.8	42.2	76.2
2103	119.0	28546	26216	28095	0.984	0.933	0.918	504.0	57.57	224.4	59.3	90.4
2104	29.6	7399	6520	7219	0.976	0.903	0.881	504.3	15.73	179.4	20.3	70.9
2104	40.4	10026	8908	9755	0.973	0.913	0.889	504.5	20.89	186.4	25.8	71.0
2104	70.4	17106	15513	16666	0.974	0.931	0.907	504.4	34.83	204.5	38.8	74.7
2104	90.0	21659	19832	21238	0.981	0.934	0.916	504.4	43.82	220.7	46.7	79.5
2104	99.7	23997	21975	23540	0.981	0.934	0.916	504.0	48.45	220.6	50.8	82.1
2104	129.3	30821	28496	30311	0.983	0.940	0.925	504.2	61.98	227.4	63.3	93.6
2104	198.1	48496	43661	47740	0.984	0.915	0.900	503.7	97.16	233.4	100.5	140.7
2105	139.4	33132	30730	32620	0.985	0.942	0.928	503.6	66.83	227.7	67.9	97.1
2105	148.8	35864	32804	35303	0.984	0.929	0.915	504.1	72.18	227.9	73.4	103.7
2105	158.7	38106	34993	37546	0.985	0.932	0.918	503.9	76.52	231.2	77.3	111.5
2105	168.2	40548	37081	39959	0.985	0.928	0.915	503.8	81.51	232.0	82.5	118.6
2105	178.6	43223	39378	42566	0.985	0.925	0.911	503.7	86.81	233.0	88.0	127.6
2106	20.4	5251	4494	5112	0.974	0.879	0.856	504.4	11.54	177.9	14.8	71.3
2106	49.7	12075	10955	11786	0.976	0.929	0.907	504.4	24.81	192.5	29.8	71.7

Table B-1. Mechanical, operational, electrical, and thermal data from the Prius performance-mapping test (cont'd)

Motor Conditions		Power (W)			Efficiency			dc Input to Inverter (rms)		Three-Phase Average from Inverter (rms)		Thermal (°C)
Speed (rpm)	Torque (Nm)	dc	Mech.	ac	Inverter	Motor	Total	V	I	V	I	Stator winding
2106	59.4	14448	13100	14210	0.984	0.922	0.907	504.5	29.55	202.2	34.0	72.4
2106	109.3	26090	24114	25682	0.984	0.939	0.924	504.1	52.83	224.5	54.7	86.7
2106	187.8	45739	41427	45026	0.984	0.920	0.906	503.7	91.83	231.9	94.8	126.0
2106	208.4	51326	45955	50499	0.984	0.910	0.895	503.6	102.90	234.5	106.3	155.9
2302	129.9	33763	31326	33411	0.990	0.938	0.928	496.5	69.10	241.2	66.2	88.3
2302	139.4	36593	33620	36189	0.989	0.929	0.919	496.5	75.02	240.6	73.4	96.7
2303	29.8	8047	7195	7902	0.982	0.910	0.894	496.7	17.56	231.8	19.7	46.8
2303	58.2	15255	14042	15079	0.988	0.931	0.920	496.7	31.77	238.9	33.3	57.3
2303	89.4	23158	21571	22906	0.989	0.942	0.931	496.6	47.59	240.2	46.2	67.3
2303	110.8	28530	26730	28142	0.986	0.950	0.937	496.3	58.41	240.3	55.8	73.0
2303	149.1	39151	35972	38645	0.987	0.931	0.919	496.2	80.13	241.1	78.6	105.2
2303	159.5	42021	38469	41509	0.988	0.927	0.915	496.2	85.86	241.4	84.7	114.7
2303	169.8	44918	40959	44357	0.988	0.923	0.912	496.1	91.57	240.4	90.4	124.7
2303	188.6	51287	45490	50545	0.986	0.900	0.887	496.1	104.48	240.4	109.1	186.7
2304	19.0	5247	4594	5151	0.982	0.892	0.876	496.7	12.10	227.6	14.0	44.9
2304	39.4	10484	9519	10314	0.984	0.923	0.908	496.7	22.46	235.5	24.9	49.2
2304	68.2	17905	16467	17701	0.989	0.930	0.920	496.7	37.31	240.2	38.5	63.3
2304	99.2	25733	23947	25448	0.989	0.941	0.931	496.7	52.60	240.7	50.4	72.3
2304	119.5	31024	28841	30696	0.989	0.940	0.930	496.7	63.49	240.9	60.8	81.2
2304	178.8	48004	43149	47300	0.985	0.912	0.899	496.5	97.83	241.6	100.3	151.7
2305	49.7	13101	11993	12892	0.984	0.930	0.916	496.6	27.47	239.1	30.5	51.7
2305	81.2	21082	19605	20817	0.987	0.942	0.930	496.7	43.40	240.6	42.7	62.7
2329	197.7	53735	48209	53010	0.987	0.909	0.897	496.3	110.22	238.3	114.1	197.6
2502	119.3	34123	31262	33698	0.988	0.928	0.916	496.6	70.40	239.1	69.2	108.0
2503	89.9	25463	23567	25187	0.989	0.936	0.926	496.6	52.55	238.6	50.5	95.9
2503	109.4	31161	28679	30813	0.989	0.931	0.920	496.6	64.37	239.5	61.6	102.0
2503	138.3	40100	36255	39560	0.987	0.916	0.904	496.6	82.48	239.3	85.2	126.0
2504	20.2	6033	5285	5939	0.984	0.890	0.876	497.0	13.39	229.7	15.2	119.8

Table B-1. Mechanical, operational, electrical, and thermal data from the Prius performance-mapping test (cont'd)

Motor Conditions		Power (W)			Efficiency			dc Input to Inverter (rms)		Three-Phase Average from Inverter (rms)		Thermal (°C)
Speed (rpm)	Torque (Nm)	dc	Mech.	ac	Inverter	Motor	Total	V	I	V	I	Stator winding
2504	30.2	8820	7907	8667	0.983	0.912	0.896	496.9	19.11	234.4	20.8	111.2
2504	39.8	11532	10452	11349	0.984	0.921	0.906	497.0	24.33	238.9	26.3	106.4
2504	50.3	14379	13195	14197	0.987	0.929	0.918	496.9	29.85	239.2	30.3	102.4
2504	60.0	17109	15745	16869	0.986	0.933	0.920	497.0	35.37	237.7	34.9	92.9
2504	69.6	19733	18247	19506	0.988	0.935	0.925	496.7	40.82	237.7	39.8	93.0
2504	79.7	22558	20915	22315	0.989	0.937	0.927	496.8	46.59	238.2	45.1	94.0
2504	99.4	28116	26057	27773	0.988	0.938	0.927	496.7	57.90	238.7	55.9	98.1
2504	129.2	37241	33890	36773	0.987	0.922	0.910	496.4	76.10	238.9	77.2	118.8
2504	149.0	43382	39081	42745	0.985	0.914	0.901	496.5	88.83	239.9	93.2	134.6
2504	159.0	46987	41695	46243	0.984	0.902	0.887	496.5	95.83	240.4	101.9	148.1
2505	169.6	50293	44504	49521	0.985	0.899	0.885	496.3	102.65	240.8	110.0	163.5
2505	178.7	53754	46888	52857	0.983	0.887	0.872	496.2	109.40	240.4	118.7	184.4
2703	89.7	27580	25399	27277	0.989	0.931	0.921	496.7	57.11	238.6	53.9	99.8
2703	99.7	30721	28240	30381	0.989	0.930	0.919	496.7	63.71	239.6	59.8	102.4
2703	109.2	33630	30899	33261	0.989	0.929	0.919	496.6	69.41	240.2	65.2	105.5
2703	119.1	36841	33730	36429	0.989	0.926	0.916	496.5	75.97	240.6	73.0	112.8
2703	128.8	40243	36479	39768	0.988	0.917	0.906	496.8	82.99	240.8	81.5	122.4
2704	20.2	6591	5731	6511	0.988	0.880	0.869	497.0	14.58	232.1	15.4	107.4
2704	30.3	9539	8572	9423	0.988	0.910	0.899	497.0	20.43	237.2	20.9	102.9
2704	40.3	12445	11412	12285	0.987	0.929	0.917	497.1	25.98	237.6	25.5	98.8
2704	49.9	15517	14145	15310	0.987	0.924	0.912	496.7	32.22	238.2	30.6	96.8
2704	59.6	18282	16892	18145	0.992	0.931	0.924	496.9	37.78	238.5	35.7	95.5
2704	69.8	21358	19761	21133	0.989	0.935	0.925	497.0	44.20	239.1	41.0	95.4
2704	138.9	43658	39338	43025	0.985	0.914	0.901	496.5	89.54	240.5	91.8	135.5
2704	148.8	47309	42135	46646	0.986	0.903	0.891	496.5	96.98	240.7	102.9	146.0
2704	159.5	51170	45168	50486	0.987	0.895	0.883	496.2	104.89	239.4	110.7	164.2
2704	169.2	54925	47915	54152	0.986	0.885	0.872	496.3	115.48	238.6	121.5	180.8
2705	79.5	24385	22530	24084	0.988	0.935	0.924	496.6	50.44	239.4	46.4	96.2

Table B-1. Mechanical, operational, electrical, and thermal data from the Prius performance-mapping test (cont'd)

Motor Conditions		Power (W)			Efficiency			dc Input to Inverter (rms)		Three-Phase Average from Inverter (rms)		Thermal (°C)
Speed (rpm)	Torque (Nm)	dc	Mech.	ac	Inverter	Motor	Total	V	I	V	I	Stator winding
3003	79.4	27104	24966	26897	0.992	0.928	0.921	496.5	56.11	240.2	50.0	99.5
3003	110.3	38169	34697	37779	0.990	0.918	0.909	496.6	78.90	240.6	74.3	120.6
3004	20.3	7354	6390	7281	0.990	0.878	0.869	497.1	16.13	235.3	15.5	105.5
3004	30.1	10676	9481	10574	0.990	0.897	0.888	497.1	22.53	236.4	21.4	100.9
3004	40.5	13990	12735	13820	0.988	0.922	0.910	496.9	29.04	237.4	27.0	98.4
3004	50.0	17241	15732	17077	0.990	0.921	0.913	496.9	35.71	238.4	32.7	97.3
3004	59.5	20437	18707	20247	0.991	0.924	0.915	497.0	42.31	238.8	38.4	96.9
3004	69.1	23541	21755	23334	0.991	0.932	0.924	496.7	48.93	239.4	43.8	97.4
3004	89.9	30775	28296	30479	0.990	0.928	0.919	496.5	63.86	240.1	57.8	104.4
3004	119.5	41719	37598	41203	0.988	0.913	0.901	496.7	86.13	241.0	84.7	129.4
3004	128.9	45493	40563	44856	0.986	0.904	0.892	496.4	93.52	240.7	95.7	138.7
3005	99.6	34111	31341	33737	0.989	0.929	0.919	496.7	70.08	240.9	63.3	109.5
3005	139.0	49554	43738	48894	0.987	0.895	0.883	496.3	102.34	238.9	106.6	154.6
3403	50.1	19571	17874	19375	0.990	0.923	0.913	497.1	40.31	238.8	35.9	97.4
3403	89.9	35413	32037	34975	0.988	0.916	0.905	496.7	72.82	239.7	69.0	110.0
3403	109.3	44010	38953	43429	0.987	0.897	0.885	496.4	90.01	240.6	91.2	128.8
3404	20.1	8197	7180	8122	0.991	0.885	0.877	497.2	17.58	235.0	17.0	106.9
3404	30.4	12007	10849	11895	0.991	0.912	0.904	497.3	25.09	236.3	23.6	100.4
3404	40.0	15631	14243	15498	0.992	0.919	0.911	497.1	32.38	237.7	29.6	98.2
3404	69.9	27239	24911	27008	0.992	0.922	0.915	496.9	56.12	239.7	50.1	99.7
3404	79.6	31217	28387	30908	0.990	0.918	0.909	496.6	64.26	239.8	58.3	105.3
3404	99.3	39436	35392	38955	0.988	0.909	0.897	496.6	81.04	239.9	80.0	120.2
3405	59.9	23347	21372	23199	0.994	0.921	0.915	497.0	48.08	240.2	42.0	97.6
3409	119.2	48236	42556	47675	0.988	0.893	0.882	496.2	99.82	237.9	100.4	140.8
3772	109.4	49553	43223	49133	0.992	0.880	0.872	499.0	105.18	236.4	101.0	164.9
3803	79.2	35399	31558	34967	0.988	0.903	0.892	499.2	72.26	239.3	70.8	112.2
3804	40.1	17816	15962	17626	0.989	0.906	0.896	499.6	36.60	238.6	33.9	75.6
3804	49.8	22185	19843	21879	0.986	0.907	0.894	499.5	45.43	236.3	44.7	78.8

Table B-1. Mechanical, operational, electrical, and thermal data from the Prius performance-mapping test (cont'd)

Motor Conditions		Power (W)			Efficiency			dc Input to Inverter (rms)		Three-Phase Average from Inverter (rms)		Thermal (°C)
Speed (rpm)	Torque (Nm)	dc	Mech.	ac	Inverter	Motor	Total	V	I	V	I	Stator winding
3804	60.4	26877	24059	26482	0.985	0.908	0.895	499.5	55.17	235.6	55.8	84.8
3804	69.7	30798	27789	30509	0.991	0.911	0.902	499.2	62.71	240.2	57.2	100.5
3804	89.5	40491	35655	39939	0.986	0.893	0.881	499.1	82.36	240.5	84.9	125.4
3804	98.6	45021	39291	44410	0.986	0.885	0.873	499.0	91.37	241.0	95.6	140.2
3805	20.4	9393	8130	9314	0.992	0.873	0.865	499.7	19.87	240.7	17.1	75.1
3805	30.2	13564	12034	13446	0.991	0.895	0.887	499.5	28.05	241.4	23.7	73.9
4204	30.1	15204	13254	14982	0.985	0.885	0.872	499.5	31.38	235.7	32.1	101.8
4204	40.2	20108	17721	19851	0.987	0.893	0.881	499.4	41.26	238.0	38.6	101.2
4204	50.3	24912	22139	24640	0.989	0.899	0.889	499.6	50.80	238.4	47.4	102.9
4204	59.8	29538	26338	29244	0.990	0.901	0.892	499.5	60.11	239.2	55.9	106.6
4204	69.6	34577	30664	34191	0.989	0.897	0.887	499.3	70.21	239.9	67.2	117.4
4204	79.7	39838	35087	39361	0.988	0.891	0.881	499.5	80.70	241.0	78.3	128.1
4204	89.4	45559	39365	45041	0.989	0.874	0.864	499.2	92.67	239.1	95.2	159.6
4205	20.2	10564	8884	10434	0.988	0.852	0.841	499.7	22.13	239.0	21.1	107.5
4604	30.0	16922	14463	16719	0.988	0.865	0.855	499.8	34.92	235.1	37.1	90.8
4604	40.4	22559	19499	22216	0.985	0.878	0.864	499.5	46.27	234.1	48.7	95.6
4604	50.4	28080	24293	27647	0.985	0.879	0.865	499.4	57.51	234.9	60.3	102.2
4604	69.4	38080	33450	37710	0.990	0.887	0.878	499.2	77.08	240.8	72.2	120.6
4605	20.2	11911	9732	11725	0.984	0.830	0.817	499.9	24.87	237.8	25.9	89.7
4605	60.1	32733	28996	32421	0.990	0.894	0.886	499.4	66.37	240.4	60.8	109.0
4606	79.7	44257	38452	43813	0.990	0.878	0.869	499.2	89.65	239.4	87.5	145.1
5003	40.1	24083	21005	23878	0.991	0.880	0.872	499.5	49.05	240.3	43.6	99.8
5004	50.1	30195	26252	29885	0.990	0.878	0.869	499.5	61.35	238.9	57.6	106.3
5004	59.8	36053	31347	35657	0.989	0.879	0.870	499.4	73.17	239.7	71.1	113.7
5005	30.0	18344	15734	18176	0.991	0.866	0.858	500.0	37.68	238.0	37.0	92.6
5005	69.9	43252	36650	42753	0.988	0.857	0.847	499.4	87.96	239.4	91.8	118.7
5006	20.0	12716	10495	12552	0.987	0.836	0.826	500.0	26.43	240.8	25.6	92.3
5402	41.3	26956	23349	26685	0.990	0.875	0.866	499.7	54.73	240.3	48.7	96.7

Table B-1. Mechanical, operational, electrical, and thermal data from the Prius performance-mapping test (cont'd)

Motor Conditions		Power (W)			Efficiency			dc Input to Inverter (rms)		Three-Phase Average from Inverter (rms)		Thermal (°C)
Speed (rpm)	Torque (Nm)	dc	Mech.	ac	Inverter	Motor	Total	V	I	V	I	Stator winding
5403	49.8	32495	28169	32208	0.991	0.875	0.867	499.6	65.98	239.9	60.2	104.9
5404	30.3	20222	17157	20042	0.991	0.856	0.848	499.8	41.37	242.1	35.0	97.3
5405	20.7	14455	11699	14305	0.990	0.818	0.809	499.9	29.88	238.9	31.0	98.2
5406	59.9	39575	33884	39198	0.990	0.864	0.856	499.5	80.18	241.4	77.5	119.8
5804	29.6	21854	17979	21522	0.985	0.835	0.823	499.7	44.97	234.3	47.6	107.9
5804	40.0	28447	24311	28190	0.991	0.862	0.855	499.7	57.90	238.8	53.8	111.9
5805	20.1	15197	12198	15050	0.990	0.811	0.803	499.9	31.49	240.9	30.8	108.3
5805	50.0	35466	30397	35120	0.990	0.866	0.857	499.6	71.92	240.3	67.8	120.5
5815	59.4	41730	36187	41341	0.991	0.875	0.867	499.5	85.71	237.2	78.1	150.8
6004	30.1	22279	18951	22050	0.990	0.859	0.851	499.7	45.48	239.5	42.4	97.5
6005	20.3	15604	12781	15440	0.990	0.828	0.819	500.1	32.10	241.8	31.0	93.4
6005	40.1	29403	25214	29093	0.989	0.867	0.858	499.7	59.79	239.6	53.9	102.9
6005	49.4	36322	31044	36006	0.991	0.862	0.855	499.6	73.60	240.7	68.2	117.0

DISTRIBUTION

Internal

1. D. J. Adams
2. C. W. Ayers
3. M. A. Brown
4. T. A. Burress
5. K. P. Gambrell
6. L. D. Marlino
6. M. Olszewski
7. R. H. Staunton
8. Laboratory Records

External

9. J. N. Chiasson, The Universisty of Tennessee-Knoxville, ECE Department, Knoxville, Tennessee 37996.
10. T. Q. Duong, U.S. Department of Energy, Forrestal Building/EE2G, 1000 Independence Avenue, S.W., Washington, D.C. 20585.
11. R. R. Fessler, BIZTEK Consulting, Inc., 820 Roslyn Place, Evanston, Illinois 60201-1724.
12. K. Fiegenschuh, Ford Motor Company, Scientific Research Laboratory, 1505 Commerce Drive, North, Dearborn, Michigan 48120-1261.
13. V. Garg, Ford Motor Company, 15050 Commerce Drive, North, Dearborn, Michigan 48120-1261.
14. E. Jih, Ford Motor Company, Scientific Research Laboratory, 1505 Commerce Drive, North, Dearborn, Michigan 48120-1261.
15. A. Lee, Daimler Chrysler, CIMS 484-08-06, 800 Chrysler Drive, Auburn Hills, Michigan 48326-2757.
16. F. Liang, Ford Motor Company, Scientific Research Laboratory, 2101 Village Road, MD1170, Rm. 2331/SRL, Dearborn, Michigan 48121.
17. M. W. Lloyd, Energetics, Inc., 7164 Columbia Gateway Drive, Columbia, Maryland 21046.
18. M. Mehall, Ford Motor Company, Scientific Research Laboratory, 2101 Village Road, MD-2247, Rm. 3317, Dearborn, Michigan 48124-2053.
19. N. M. Olds, United States Council for Automotive Research, nolds@uscar.org.
20. J. Rogers, Chemical and Environmental Sciences Laboratory, GM R&D Center, 30500 Mound Road, Warren, Michigan 48090-9055.
21. S. A. Rogers, U.S. Department of Energy, Forrestal Building/EE2G, 1000 Independence Avenue, S.W., Washington, D.C. 20585.
22. G. S. Smith, General Motors Advanced Technology Center, 3050 Lomita Boulevard, Torrance, California 90505.
23. E. J. Wall, U.S. Department of Energy, Forrestal Building/EE2G, 1000 Independence Avenue, S.W., Washington, D.C. 20585.
24. B. Welchko, General Motors Advanced Technology Center, 3050 Lomita Boulevard, Torrance, California 90505.
25. P. G. Yoshida, U.S. Department of Energy, Forrestal Building/EE2G, 1000 Independence Avenue, S.W., Washington, D.C. 20585.